ENGINEERING RESEARCH INSTITUTE
UNIVERSITY OF MICHIGAN
ANN ARBOR

THE SHOCK TUBE AS AN INSTRUMENT FOR THE INVESTIGATION OF TRANSONIC AND SUPERSONIC FLOW PATTERNS

A Report on Work Done under Office of Naval Research
Contract N6-ONR-232 between April, 1947, and June, 1949

BY

F. W. GEIGER

C. W. MAUTZ

WITH AN ADDENDUM BY

R. N. HOLLYER, JR.

* *

SUPERVISED BY

OTTO LAPORTE

Project M720-4

U. S. NAVY DEPARTMENT OFFICE OF NAVAL RESEARCH
CONTRACT NO. N6-ONR-232, TASK ORDER NO. IV
WASHINGTON, D. C.

FOREWORD

The shock tube project which is summarized in this report, was started in April, 1947 under the supervision of L. G. Smith and is, since August, 1948, being continued under the supervision of the writer.

It is believed that the present work is of value both to the physicist and to the engineer. It establishes, for the first time, the shock tube as an instrument for the investigation of flow patterns, indeed as an instrument which can compete with the wind tunnel. The circumstances under which the one or the other installation is of superior value are explained in the report. At any rate the considerable usefulness of the shock tube is demonstrated here, and this is confirmed by the fact that new shock tubes are being constructed in many laboratories in this country.

It is intended to continue this research program at least for another year.

O. L.

TABLE OF CONTENTS

	Page
FOREWORD	ii
CHAPTER I INTRODUCTION AND THEORY	1
1. The Use of the Shock Tube in the Study of Supersonic Phenomena	1
2. The Flow Field Produced by a Plane Shock	3
3. The Process Following the Rupture of the Diaphragm	7
a. Expansion into Vacuum	7
b. Expansion into a Second Gas	11
4. Reflections at the Ends of the Tube	18
a. The Reflected Shock	18
b. The Reflection of the Rarefaction at the End of the Compression Chamber	19
5. Duration of Uniform Flow	24
CHAPTER II DESCRIPTION AND OPERATION OF THE APPARATUS	31
1. General Description of the Apparatus	31
2. Method of Photography	32
3. The Shock Tube	34
4. The Diaphragm	36
5. The Plunger	37
6. The Measurement of the Pressures	39
7. The Firing Operation	39
8. The Vacuum Connections	41
9. The Light Screens	43
10. The Photographic Lens	48

11. The Windows 49

12. The Mounting of the Models 49

CHAPTER III ELECTRONIC EQUIPMENT (by R. N. Hollyer, Jr.) 52

1. Introduction 52

2. Light Screens and Phototube Amplifiers 56

3. The Gate Circuit 58

4. Pulse Source and Counter 61

5. Delay Circuit 62

6. The Spark Unit 64

CHAPTER IV THE FLOW IN THE SHOCK TUBE 67

1. The Initial Pressure Ratio Versus the Pressure Ratio Across the Shock 68

2. The Flow Calibration 74
   a. The Method 74
   b. Measurement of the Shock Wave Angle 78
   c. The Wedge 79
   d. Determination of Predicted Mach Number 80
   e. Determination of γ 81
   f. Flow in the Hot Air Ahead of the Contact Surface 81
   g. Flow in the Cold Air Behind the Contact Surface 84

3. The Relation Between the Uniformity of the Flow and the Contact Surface 88

4. The Bursting Diaphragm and the Formation of the Tube Shock 91
   a. Inhomogeneity of the Flow Near the Burst Diaphragm 92
   b. Discussion of the Possible Failure of the Timing System Because of Incompletely Formed Shock Waves 103

CHAPTER V AERODYNAMIC TESTS IN THE SHOCK TUBE 107

1. Introduction 107

2. The Detached Shock Wave 110

3. Starting Vortices and a Shock Wave-Boundary Layer Interaction in Supersonic Flow 117

4. Transonic Flow About a Symmetrical Double Wedge Airfoil 121
   a. Zero Angle of Attack 124
   b. 6-Degree Angle of Attack 128
   c. 8-Degree Angle of Attack 137

5. The Choking of a Duct in Initially Supersonic Flow 147

6. Higher Mach Number Flow in Gases Other than Air 154

CONCLUSIONS 160

Chapter I 160

Chapter IV 160

Chapter V 160

TABLES 162

APPENDICES 173

APPENDIX I DERIVATION OF THE RANKINE-HUGONIOT RELATION FOR AN IDEAL GAS 174

APPENDIX II DERIVATION OF PRANDTL'S RELATION $v_o v_1 = a^{*2}$ 178

APPENDIX III DERIVATION OF THE FORMULAE FOR THE SPEED OF A SHOCK OF PRESSURE RATIO ξ , PROCEEDING INTO A STATIONARY GAS, AND FOR THE FLOW SPEED BEHIND THE SHOCK 180

APPENDIX IV DERIVATION OF THE EXPRESSION FOR THE MACH NUMBER OF THE FLOW BEHIND A SHOCK WAVE WHICH MOVES INTO A STATIONARY MEDIUM 183

APPENDIX V DERIVATION OF THE EXPRESSION FOR THE MACH NUMBER IN THE FLOW BEHIND THE CONTACT SURFACE IN THE SHOCK TUBE, WHEN AIR IS USED IN BOTH CHAMBERS 184

APPENDIX VI DERIVATION OF THE EXPRESSION FOR THE SPEED OF THE REFLECTED SHOCK FRONT 186

LIST OF FIGURES

		Page
1.	Mach Number versus ξ	6
2.	Initial Pressure Distribution for Expansion into Vacuum	7
3.	Propagation Velocity of Pressure Distribution	9
4.	Pressure Distribution at Various Times after Burst	10
5.	Initial Pressure Ratio Required to Produce a Shock of Strength ξ	13
6.	Motion Produced by Bursting Diaphragm	16
7.	Reflections and Interactions of Waves in the Shock Tube with $\xi = 0.2$	23
8.	Paths of C, R and F in x-t Plane	26
9.	Theoretical Time of Arrival of the Various Disturbances in the Test Section	29
10.	Theoretical Duration of Uniform Flow	30
11.	The Shock Tube	34
12.	The Shock Tube	35
13.	The Plunger	38
14.	The Vacuum Connections	42
15.	Diagram of Light Screens	45
16.	The Light Screens	47
17.	Method of Mounting the Windows	50
18.	Test Section with 5-Degree Wedge Mounted	51
19.	Block Diagram for Velocity Measurement	53

20. Block Diagram for Photography 55

21. Circuit of Phototube and Amplifier 57

22. The Gate Circuit 59

23. The Delay Circuit 63

24. The Spark Gap 65

25. The Relations between M, ξ and T 69

26. p_o/p_2 versus ξ for Air-Air 70

27. p_o/p_2 versus ξ for Helium-Air 71

28. Shock Wave Attached to a Wedge 75

29. Variation of Apparent Mach Number with Time 82

30. Variation of Apparent Mach Number with Time 83

31. Experimental Duration of Uniform Flow for Helium-Air 85

32. Mach Number of the Flow in the Cold Air 87

33. Arrival of Contact Surface 89

34. The Glass Section in Place 93

35-37. The Bursting Diaphragm 95

38-41. The Formation of the Primary Shock Wave 98

42-43. The Formation of the Primary Shock Wave for Helium-Air 104

44. Models Used in Detached Bow Wave Study 111

45. Combinations of M, d and A Observed 112

46. Typical Plate of Detached Bow Wave 113

47. Detachment versus Time, 45-Degree Wedge 114

48. Detachment versus Time, 30-Degree Wedge 115

49-52. Photographs: 5-Degree Wedge, M = 1.15, Angle of Attack = 2.5° 119

53-56. Photographs: 5-Degree Wedge, M = 1.15, Angle of Attack = 0° 122

57. Photographs: 10-Percent Double Wedge, M = 0.70, Angle of Attack = 0° 125

58-61. Photographs: 10-Percent Double Wedge, M = 0.79, Angle of Attack = 0° 126

62-64. Photographs: 10-Percent Double Wedge, M = 0.90, Angle of Attack = 0° 129

65. Photographs: 10-Percent Double Wedge, M = 0.90, Angle of Attack = 6° 132

66-71. Photographs: 10-Percent Double Wedge, M = 0.79, Angle of Attack = 6° 133

72-73. Photographs: 10-Percent Double Wedge, M = 1.00, Angle of Attack = 6° 136

74-75. Photographs: 10-Percent Double Wedge, M = 1.30, Angle of Attack = 6° 138

76-79. Photographs: 10-Percent Double Wedge, M = 0.60, Angle of Attack = 8° 139

80-84. Photographs: 10-Percent Double Wedge, M = 0.70, Angle of Attack = 8° 141

85-90. Photographs: 10-Percent Double Wedge, M = 0.79, Angle of Attack = 8° 144

91-99. Photographs: Choking of a Duct, M = 1.16 148

100-101. Photographs: Helium-Carbon Tetrachloride, 5-Degree Wedge 156

102-103. Photographs: Helium-Carbon Tetrachloride, 45-Degree Wedge 157

104-105. Photographs: Helium-Freon-12, 45-Degree Wedge 159

CHAPTER I

INTRODUCTION AND THEORY

1. The Use of the Shock Tube in the Study of Supersonic Phenomena

The study of shock waves in gases is facilitated by the use of the shock tube, which consists in essence of a rigid tube, divided into two sections by a gas-tight diaphragm which may be caused to rupture, allowing a difference of the pressures in the two sections to be suddenly equalized. The use of the shock tube began with Vieille[1], who demonstrated that the bursting of the diaphragm was followed by a pressure wave moving with a velocity greater than that of sound into the expansion chamber, or low-pressure section of the tube.

Little was done toward the study of the pressure waves released when a diaphragm burst until Payman and Shepherd[2] conducted a set of experiments in which copper-foil diaphragms were used to sustain high pressures in the compression chamber of their tube.

---

[1]Vieille, Paul, "Sur Les Discontinuites Produites par la Detent Brusque de Gas Comprimes," Comptes Rendus 129, 1228-1230 (1899).

[2]Payman, W., "The Detonation Wave in Gaseous Mixtures and the Predetonation Period," Proceedings of the Royal Society A-120, 90-109; and Payman, W. and Shepherd, W. F. C., "Explosion Waves and Shock Waves VI. The Disturbance Produced by Bursting Diaphragms with Compressed Air," Proceedings of the Royal Society A-186, 293-321 (1946).

In 1943 Reynolds[1] used a shock tube to produce shock waves of known strength for the calibration of piezo-electric pressure gauges which were to be used in blast-wave measurements.

In 1945 Smith[2] made an extensive study of the reflection of shock waves (using the shock tube which was later used in the work described in this report), in which the shock was allowed to fall on an inclined steel plate, special attention being given to the conditions for the onset of Mach reflection[3].

At the time of this writing, Bleakney[4] and his co-workers at Princeton are continuing the study of Mach reflection, using a shock tube equipped with a Mach-Zehnder interferometer.

This report is concerned with an investigation of the transonic and supersonic flow behind the shock wave rather than with a study of the shock wave itself. The investigation was motivated by the anticipation that the flow fields produced in the shock tube might render the instrument useful in aerodynamic research, as a kind of intermittent wind tunnel.

The shock tube thus employed has both advantages and disadvantages with respect to the wind tunnel. An obvious disadvantage is that the maximum Mach number obtainable in air is limited to some value less

---

[1]Reynolds, George T., A Preliminary Study of Plane Shock Waves Formed by Bursting Diaphragms in a Tube, OSRD Report No. 1519, June, 1943.

[2]Smith, Lincoln G., Photographic Investigation of the Reflection of Plane Shocks in Air, OSRD Report No. 6271, November, 1945.

[3]See, e.g., Courant, R. and Friedrichs, K. O., Supersonic Flow and Shock Waves, Interscience, New York, 1948.

[4]Physical Review 75, 1294-5 (1949), and 76, 323-4 (1949).

than 1.89 (see Section 2 below). Other disadvantages arise from the duration of the operating periods: lack of time for the establishment of a close approximation to a desired steady flow in certain cases, and the evident difficulty of measuring forces and torques on models.

On the other hand, a considerable advantage arises from the fact that the flow at a particular station in the tube starts practically instantaneously. Although the starting process is a special one, it allows certain well-known steady flow patterns to be studied in a process of formation. Such studies can be expected to yield fundamental information regarding the phenomena involved. Another advantage is that the initial Mach number may be set at any value in the range available, merely by adjusting the ratio of the pressures in the two chambers before firing. In particular, the Mach number may be set arbitrarily close to unity.

The remainder of this chapter will be devoted to a theoretical discussion of the flow fields produced in the shock tube, in which the diaphragm is assumed to burst instantaneously (theory of the ideal shock tube). Chapter II will be a description of the apparatus, except for the electronic circuits, which will be described in Chapter III. In Chapter IV the flow fields in the actual tube will be discussed and compared with the theoretical predictions of the present chapter, and in Chapter V will be given the results of certain aerodynamic tests with models. The derivation of some of the formulae are given in the appendices.

2. The Flow Field Produced by a Plane Shock

The pressures, p_o and p_1, and the corresponding flow speeds, v_o and v_1, on either side of a shock wave are related by the Rankine-Hugoniot

relation

$$\frac{V_o}{V_1} = \frac{\frac{\gamma+1}{\gamma-1} + \frac{p_o}{p_1}}{1 + \frac{\gamma+1}{\gamma-1}\frac{p_o}{p_1}} \quad , \tag{1}$$

where v_o and v_1 are measured with respect to the shock, and γ is the ratio of specific heats of the gas. In the case of a shock wave proceeding into a stationary gas, if the shock speed is denoted by U and the speed of the flow by u, an obvious transformation of Equation (1) gives

$$\frac{U}{U-u} = \frac{\frac{\gamma+1}{\gamma-1} + \frac{p_o}{p_1}}{1 + \frac{\gamma+1}{\gamma-1}\frac{p_o}{p_1}} \quad , \tag{2}$$

where p_o is the pressure in the stationary medium, and p_1 is the pressure behind the shock wave. Adopting the notation $\xi \equiv p_o/p_1, (0 < \xi < 1)$; $\mu \equiv (\gamma + 1)/(\gamma - 1)$; Equation (2) becomes

$$\frac{U}{U-u} = \frac{\mu + \xi}{1 + \mu\xi} \tag{3}$$

(Appendix I). The relation between the shock speed, U, and the pressure ratio, ξ, is (Appendix III)

$$U = a_0 \sqrt{\frac{\mu + \xi}{(\mu+1)\xi}} \tag{4}$$

Equations (3) and (4) and the expression for the ratio of the sound speeds a_0 and a_1 are combined in Appendix IV to give

$$M = \frac{u}{a_1} = \frac{(\mu-1)(1-\xi)}{\sqrt{(\mu+1)(1+\mu\xi)}} , \tag{5}$$

where M is the Mach number of the flow. If the ratio of specific heats is taken to be 7/5, which is very nearly true for air, Equation (5) becomes

$$M = \frac{5(1-\xi)}{\sqrt{7(1+6\xi)}} . \tag{6}$$

This relation is plotted in Figure 1. From the figure it can be seen that for any value of ξ less than 0.207, the flow will be supersonic. As ξ approaches zero, both u, the flow speed, and a_1, the sound speed, diverge; but their ratio approaches the limit $5/\sqrt{7} \cong 1.89$. It will be shown later, however, that ξ cannot be made arbitrarily small in the shock tube.

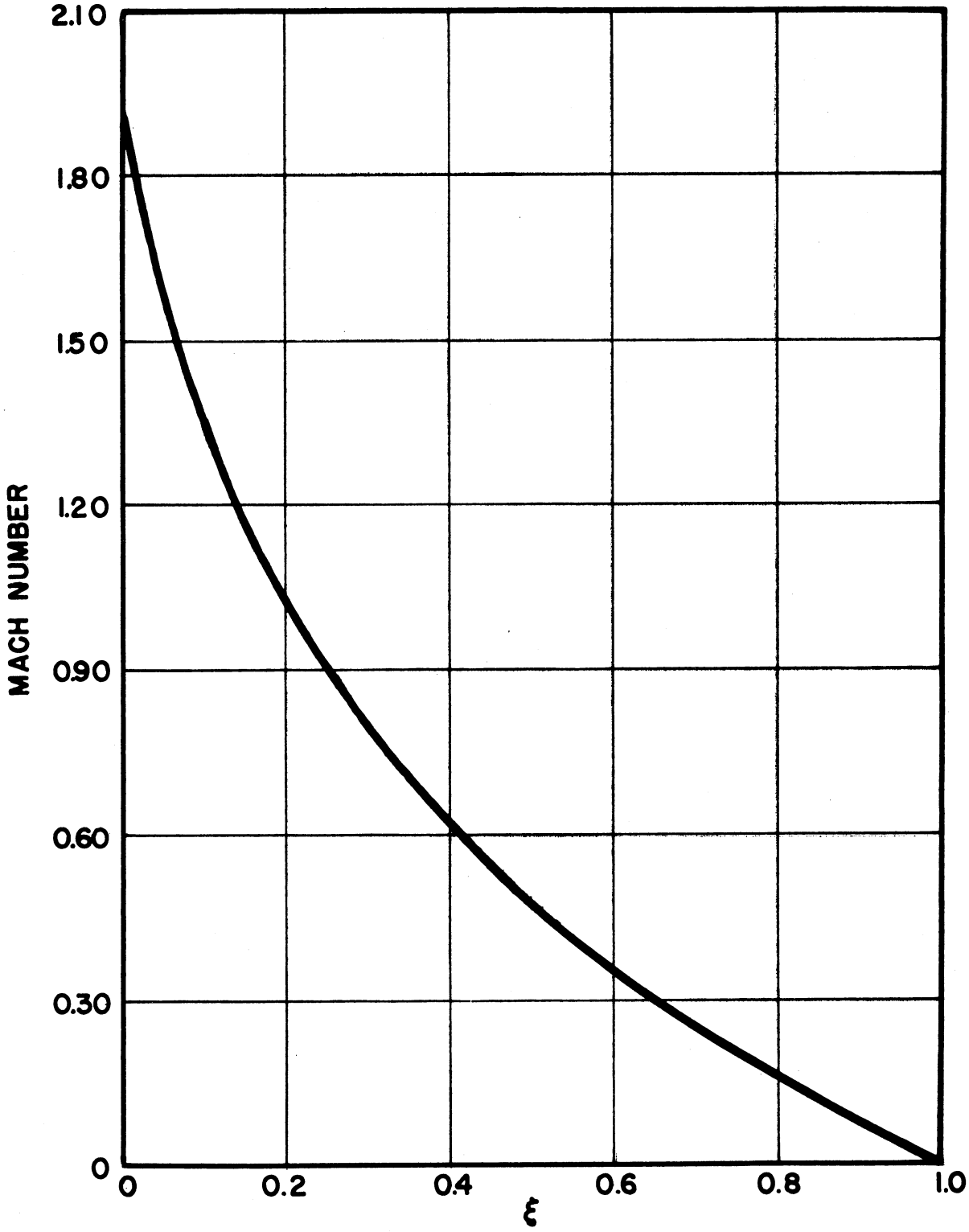

Figure 1
Mach Number Versus ξ

3. The Process Following the Rupture of the Diaphragm

In the analysis of the process following the rupture of the diaphragm, the assumptions are made that the diaphragm is a plane barrier which disappears instantaneously, and that the gases in the compression and expansion chambers obey the ideal gas law.

It will be seen that, in general, a shock wave will proceed into the expansion chamber, and that a rarefaction will proceed into the compression chamber. The pressure, gas velocity, and Mach number at various places along the tube will be investigated, with particular attention given to the sequence of events at some fixed point in the expansion chamber which may be thought of as the place where flow patterns are to be studied.

The events in the tube will be described in terms of x and t, with the origin of x at the position of the diaphragm, and with the compression chamber on the left, extending in the negative x-direction. The time t = 0 will be taken at the time of rupture of the diaphragm. The initial pressures in the expansion and compression chambers will be denoted by p_0 and p_2, respectively.

a. Expansion into Vacuum: In the special case in which the expansion chamber is completely evacuated, $p_0 = 0$, the pressure distribution at time t = 0 is that shown in Figure 2. After the diaphragm has ruptured, a rarefaction will travel to the left into the compression chamber, and will

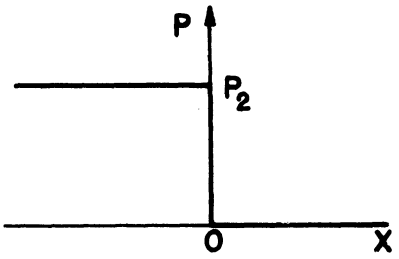

Figure 2
Initial Pressure Distribution
for Expansion into a Vacuum

impart a velocity, u, to the gas over which it has passed, given by the well-known relation

$$u = \int_{\rho}^{\rho_0} \sqrt{\frac{dp}{d\rho}}\ \frac{d\rho}{\rho} \quad . \tag{7}$$

Using the gas law for an ideal adiabatic expansion, $p/p_2 = (\rho/\rho_2)^{\gamma}$, this becomes

$$u = \frac{2a_0}{\gamma-1}\left[1 - \left(\frac{p}{p_2}\right)^{\frac{\gamma-1}{2\gamma}}\right], \tag{8}$$

a function of p alone, which in turn is a function of x and t.

A point which moves in such a manner that it remains in that part of the tube where the pressure is some given value, say p, will move to the left with respect to the fluid at the local sound speed, a(p), given by

$$a(p) = \sqrt{\frac{dp}{d\rho}} = a_0\left(\frac{p}{p_2}\right)^{\frac{\gamma-1}{2\gamma}}, \tag{9}$$

and at the same time will be swept to the right with the flow speed, u(p).

Thus the speed of propagation, s, of any such point will be given by

$$s(p) = u - a = a_0 \left[\frac{2}{\gamma - 1} - \frac{\gamma + 1}{\gamma - 1} \left(\frac{p}{p_2} \right)^{\frac{\gamma - 1}{2\gamma}} \right]. \tag{10}$$

Writing $\mu = (\gamma + 1)/(\gamma - 1)$, this becomes

$$s = a_0 \left[(\mu - 1) - \mu \left(\frac{p}{p_2} \right)^{\frac{1}{\mu + 1}} \right]. \tag{11}$$

For a gas such as air, $\mu = 6$, and (11) becomes

$$s = a_0 \left[5 - 6 \left(\frac{p}{p_2} \right)^{\frac{1}{7}} \right]. \tag{12}$$

This velocity curve is plotted with s/a_0 as abscissa vs. p as ordinate in Figure 3. Since each point of the vertical part of the p vs. x curve of Figure 2 begins at x = 0, t = 0, with the velocity s(p), the position, x(p,t), of a point where the

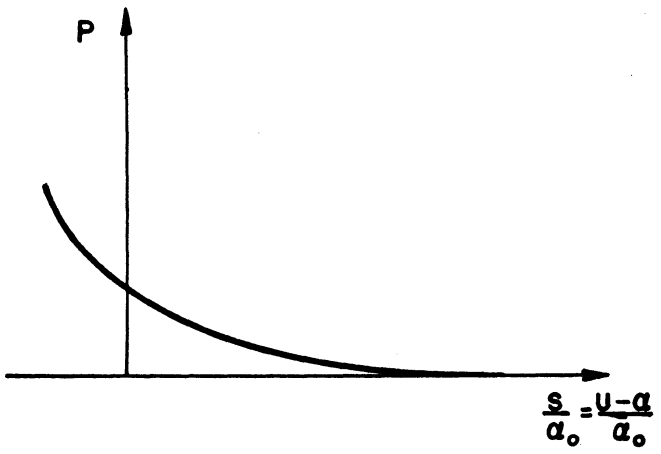

Figure 3
Propagation Velocity of
Pressure Distribution

pressure is p is given by

$$x(p,t) = s(p)\cdot t \ , \tag{13}$$

and p may be expressed as a function of x and t, for, from Equation (11),

$$\frac{p}{p_2} = \left[\frac{\mu-1}{\mu} - \frac{s}{\mu a_0} \right]^{\mu+1} = \left[\frac{\mu-1}{\mu} - \frac{x/t}{\mu a_0} \right]^{\mu+1}, \tag{14}$$

when $t > 0$; $-a_0 t < x < (\mu - 1)a_0 t$.

In Figure 4 are plotted the pressure distributions for air (μ=6) corresponding to the times t = 0, 1, 2, and 3.

It is interesting to note that there is a value of pressure, p_k, for which s(p) is zero, given by

$$p_K = p_2 \left(\frac{\mu-1}{\mu} \right)^{\mu+1}. \tag{15}$$

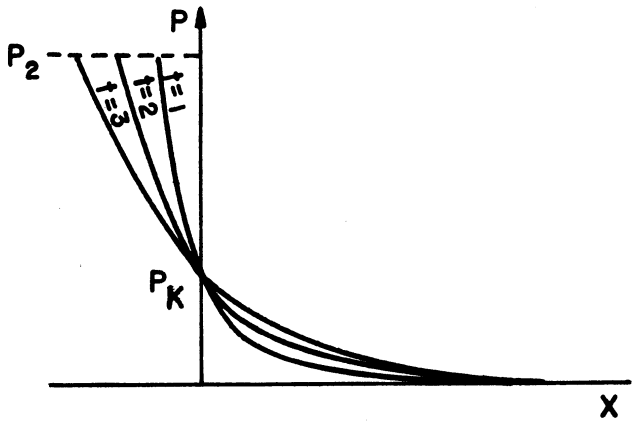

Figure 4
Pressure Distribution
at Various Times after Burst

The pressure at x = 0 acquires this value instantly, and remains constant at this value until it is disturbed by the arrival of a reflection from one end or the other of the tube.

Since the Mach number, u/a, is $\gtrless$ 1 according to whether (u-a) $\gtrless$ 0, the flow will be supersonic in the expansion chamber, sonic at x = 0, and subsonic in the compression chamber.

b. Expansion into a Second Gas: If a second gas, at pressure p_o ($p_o < p_2$) fills the expansion chamber there is a value of pressure, p_1, intermediate between p_2 and p_o, for which

1) A shock wave, raising the pressure from p_o to p_1 in the expansion chamber, imparts to the gas in the expansion chamber a velocity u_1, and

2) A rarefaction wave, reducing the pressure in the compression chamber from p_2 to p_1, imparts the same velocity, u_1, to the gas in the compression chamber.

The velocity, u_{1S}, imparted to the gas in the expansion chamber by the shock wave is given by

$$u_{1S} = a_{oE} \frac{(\mu_E - 1)(1 - \frac{p_o}{p})}{\sqrt{(\mu_E + 1)\frac{p_o}{p}(\mu_E + \frac{p_o}{p})}} \qquad (16)$$

(see Equation III-6 in Appendix III), and the velocity u_{1R} imparted to the gas in the compression chamber by the rarefaction is given by Equation (8), or

$$u_{1R} = a_{oc}(\mu_c - 1)\left[1 - \left(\frac{p}{p_2}\right)^{\frac{1}{\mu_c + 1}}\right], \qquad (17)$$

where a_o is the sound speed in the undisturbed gas, $\mu = (\gamma + 1)/(\gamma - 1)$ as before, and the subscripts C and E refer to the gases originally in the compression and expansion chambers, respectively.

Applying the boundary condition that $u(p) = u_{1S}(p) = u_{1R}(p)$, the relation between p_2, p_1 and p_o which results is

$$\frac{p_o}{p_2} = \xi \left[1 - \frac{a_{oE}}{a_{oC}} \frac{\mu_E - 1}{\mu_C - 1} \frac{1 - \xi}{\sqrt{(\mu_E + 1)\xi(\mu_E + \xi)}} \right]^{\mu_C + 1}. \qquad (18)$$

Equation (18) is the most important equation governing the operation of the shock tube, as it gives the pressure which must be initially set in order to produce a shock of given strength.

If the same gas is used in each chamber, Equation (18) reduces to

$$\frac{p_o}{p_2} = \xi \left[1 - \frac{1 - \xi}{\sqrt{(\mu + 1)\xi(\mu + \xi)}} \right]^{\mu + 1}, \qquad (19)$$

and for air, with $\mu = 6$,

$$\frac{p_o}{p_2} = \xi \left[1 - \frac{1 - \xi}{\sqrt{7\xi(6 + \xi)}} \right]^{7}. \qquad (20)$$

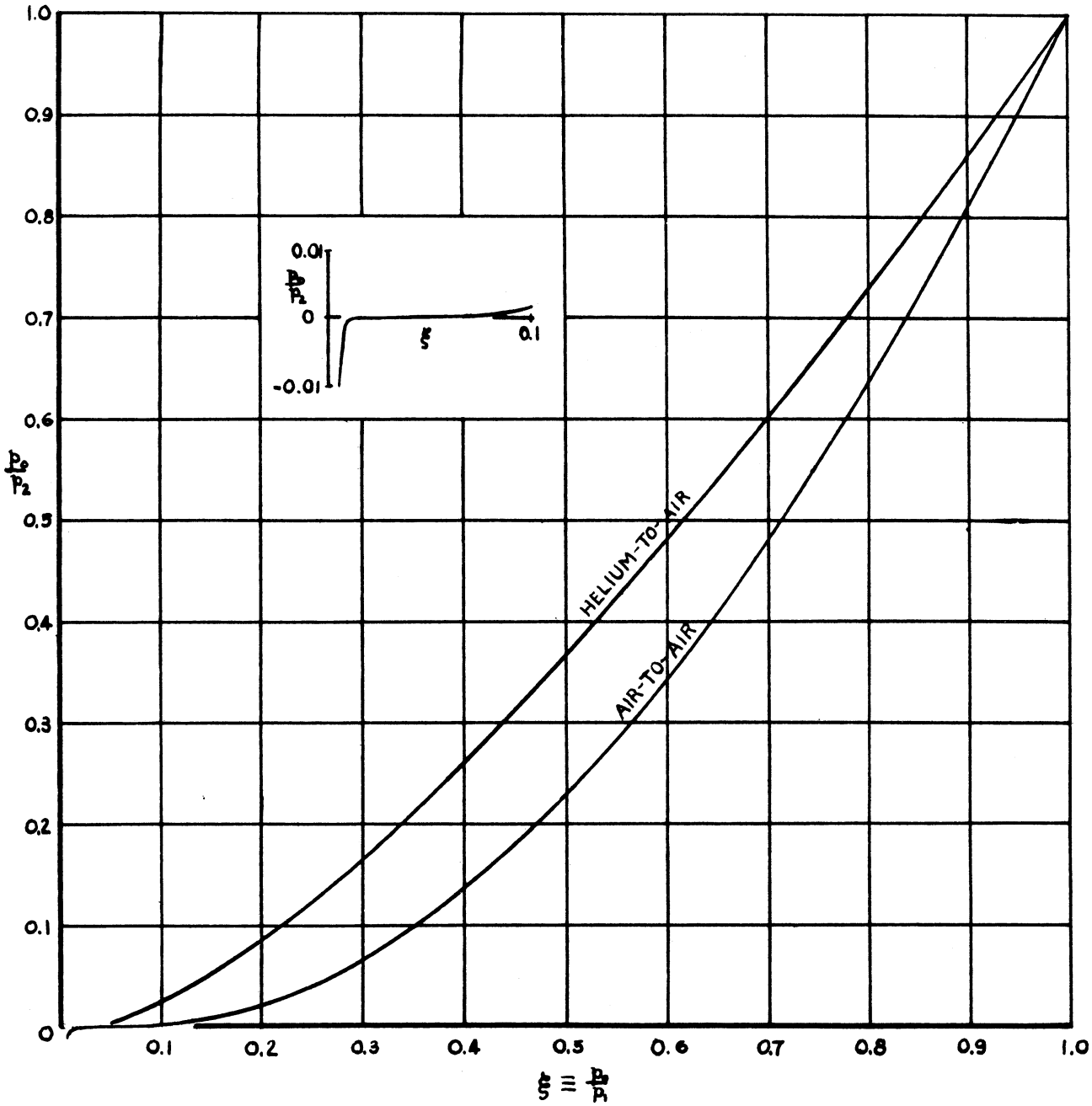

Figure 5

Initial pressure ratio required to produce a shock of strength ξ.

Equation (19) was obtained by Dr. A. H. Taub for the report of Reynolds[1].

Equation (20) is plotted in Figure 5 ("air-to-air") and also in Figure 5 is plotted a graph of Equation (18), in which the gas in the compression chamber is taken to be helium, with air in the expansion chamber. The values required for this are $\mu_C = 4$ and $a_{oE}/a_{oC} = 0.3420$, so that for helium-to-air

$$\frac{p_o}{p_2} = \xi \left[1 - 0.5701 \frac{1 - \xi}{\sqrt{7\xi(6 + \xi)}} \right]^5. \qquad (21)$$

Equations (20) and (21) may be looked upon as implicit equations defining ξ as a function of p_o/p_2. It is interesting to note the behavior of ξ in the neighborhood $p_o/p_2 = 0$. This is shown in the insert of Figure 5 for the case of air-to-air, where it is seen that ξ has a value of 0.0227 when p_o/p_2 is zero. The corresponding value for helium-to-air is 0.0077. No physical meaning can be attached to the portion of the curve for which p_o/p_2 is negative. This brings out the impossibility of producing a shock in the shock tube with ξ arbitrarily close to zero, which can be understood from the following physical reasoning: The flow speed behind the shock wave goes to infinity as ξ goes to zero, and in the shock tube there is a finite maximum flow speed obtainable from the compression chamber gas, namely $(\mu_C - 1)\, a_{oC}$.

---

[1] loc. cit. ante, p. 2.

The fact that the curve for helium-to-air lies above that for air-to-air means that, with p_2 fixed, a shock of given strength can be produced with a higher value of p_o when helium is used in the compression chamber. This fact is of considerable practical importance (see Paragraph 7 of Chapter II).

It is necessary now to reconsider the pressure distribution in the tube following the rupture of the diaphragm (see Figure 6). The shock front is a discontinuity in pressure which travels at high speed into the expansion chamber. Following the shock front, and moving with the speed of the flow behind the shock wave, is the contact surface, which is an interface between the gases which were originally on either side of the diaphragm. Even if the same gas is used in each chamber, this contact surface is a discontinuity surface, since the gas ahead of it has been compressed and heated, while the gas behind it has been expanded and cooled. The pressure will have the value p_1 on both sides of the interface, the discontinuity being in the values of temperature and density. The shock front and the contact surface are represented by the points S and C, respectively, in Figure 6.

The rarefaction wave will have the same shape that it does in the expansion into a vacuum, except that its descent will terminate abruptly at the value p_1. The extremities of the rarefaction wave are labeled R and F in Figure 6. The Point R will be referred to as the head of the rarefaction, and the point F, as its foot. It is important to notice that the foot of the rarefaction moves to the left, with respect to the contact surface, with speed a_{1C}, the sound speed corresponding to the pressure p_1 in the compression chamber gas. The region between F and C is thus a region

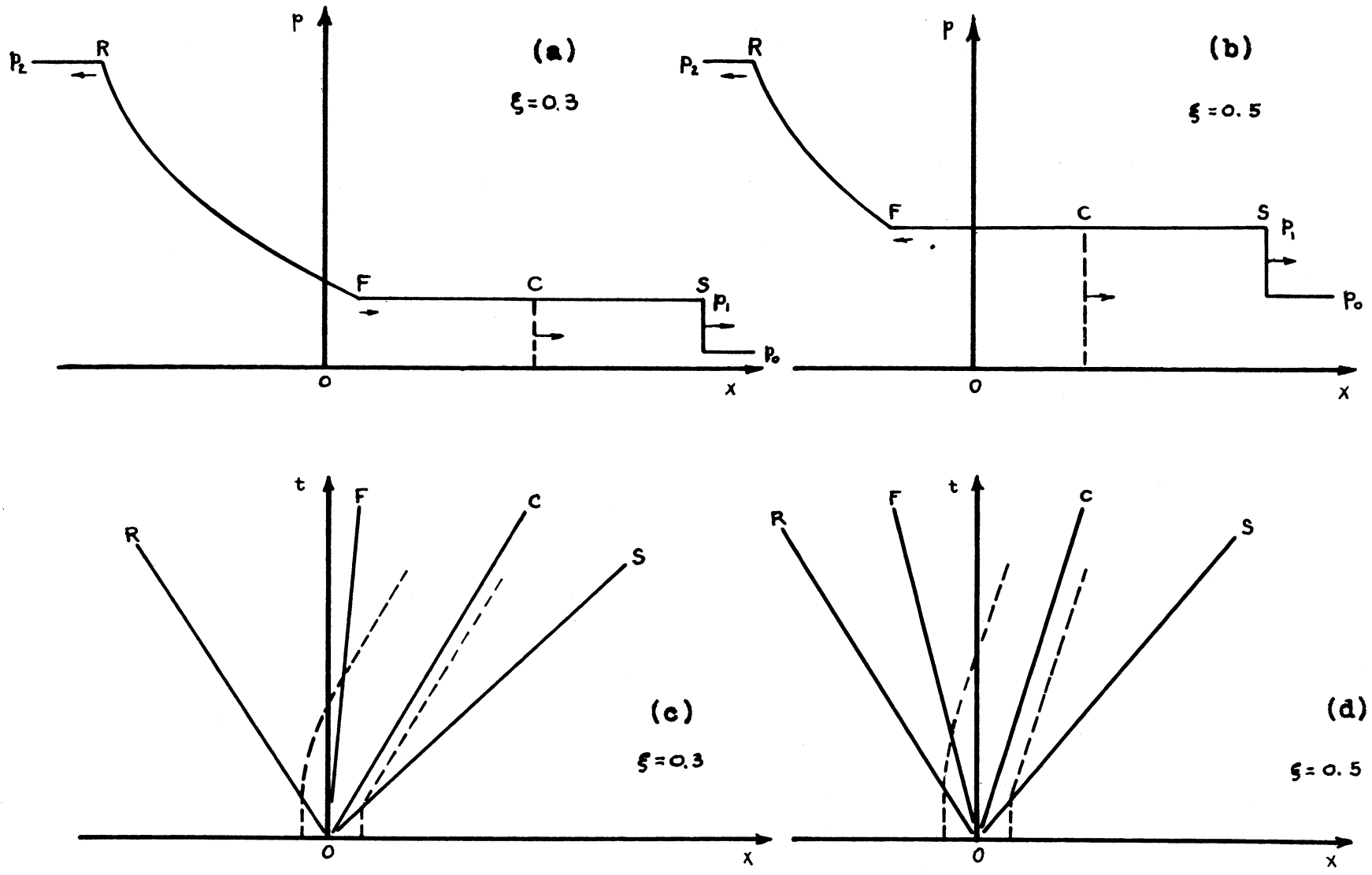

Figure 6

Motion produced by bursting diaphragm.
Dotted lines in (c) and (d) are particle paths.

of uniform flow in the cooled compression chamber gas, and the gas in this region will be referred to as the "cold" gas.

In Part a of this section it was shown that the flow speed in the compression chamber gas will equal the local sound speed if the pressure falls to a critical pressure p_k (see Equation 15), and will exceed the local sound speed if the pressure falls below this value. Therefore the point F may move to the left, remain stationary or move to the right, depending upon whether p_1 is greater than, equal to, or less than, the value p_k. This behavior may be summarized, along with that of the Mach number of the flow in the cold gas, as follows:

p_1	$> p_k$	$= p_k$	$< p_k$
F	←	0	→
M_{1C}	< 1	$= 1$	> 1

Figures 6 (a) and (b) show the pressure distributions when $p_1 < p_k$ and $p_1 > p_k$, respectively. In Figures 6(c) and (d), the motion of the points S, C, F and R are represented in the x-t plane for the two cases. Two particle paths are shown by dotted lines in each of these x-t diagrams. The behavior of these particle paths brings out the difference in the manner in which the gases originally occupying the separate chambers are accelerated, the expansion chamber gas undergoing an abrupt change in velocity along the line S, and the compression chamber gas undergoing a gradual one, in the angular region between the lines R and F.

The problem in the shallow water theory of surface waves which is analogous to this (that of a dam which bursts suddenly into a flooded valley) has been extensively treated by Stoker[1].

4. Reflections at the Ends of the Tube

a. The Reflected Shock: J. von Neumann[2] has shown that if a shock wave of pressure ratio ξ suffers "head-on" reflection from a rigid wall, the pressure ratio ξ', of the reflected shock (defined again as the ratio of the pressure ahead of the shock front to that behind it) is given by

$$\xi' = \frac{1 + \mu\xi}{\mu + 2 - \xi} . \tag{22}$$

The velocity, U', of this shock with respect to the wall (the end of the expansion chamber) is then given by

$$U' = a_o \frac{2 + (\mu - 1)\xi}{\sqrt{(\mu+1)\xi(\mu+\xi)}} , \tag{23}$$

where a_o is the sound speed in the undisturbed gas. For air, with μ = 6, (23) becomes

---

[1] Stoker, J.J., "The Formation of Breakers and Bores," Communications on Applied Mathematics, 1, No. 1, 1-87 (1948).

[2] von Neumann, John, Progress Report on the Theory of Shock Waves, OSRD Report No. 1140 (1943).

$$U' = a_0 \frac{2+5\xi}{\sqrt{7\xi(6+\xi)}} . \qquad (24)$$

(See Appendix VI for the derivations of these).

It may be of interest to consider the rather extreme temperatures which are produced by the processes in the tube. The gas in the compression chamber is cooled by adiabatic expansion to the temperature T_{1C}, say, and the gas in the expansion chamber is heated by the shock to the temperature T_{1E} and then is heated further to the temperature T' by the reflected shock. The following table illustrates a few representative values of these temperatures, calculated on the basis that T_o, the initial temperature, is 300° K.

ξ	T_{1C} air-air	T_{1C} He-air	T_{1E}	T'
0.05	36° K.	118° K.	1290° K.	2640° K.
0.10	95	170	786	1500
0.15	133	197	612	1110
0.20	159	214	532	915

b. The Reflection of the Rarefaction at the End of the Compression Chamber: The head of the rarefaction wave, "R" in Figure 6, will travel to the end of the compression chamber, where it will be reflected. After reflection it will move to the right, with respect to the fluid, at the local sound speed, and will eventually overtake the shock front, if

the expansion chamber is long enough. The flow speed and sound speed are obtainable as functions of x and t at all points ahead of the reflected rarefaction, and hence it is possible to find the path of the point R in the x-t plane.

The paths of the points R, F, C and S (Figure 6) are already known in the region of the x-t plane which is unaffected by the reflected waves, since these points start from the origin and move with constant velocities which are known.

The speed of the head of the reflected rarefaction, R, will be the sum of the local flow speed and the local sound speed, and will not be constant until R has overtaken F. From the time R is reflected to the time it overtakes F, its speed is given by

$$\frac{dx_R}{dt} = u_R + a_R = a_{oc}\left[(\mu_c - 1) - (\mu_c - 2)\left(\frac{p_R}{p_2}\right)^{\frac{1}{\mu_c + 1}}\right], \tag{25}$$

where p_R denotes $p(x_R, t)$ (see Equations 8 and 9). From Equation (14), this is

$$\frac{dx_R}{dt} = a_{oc}\left[(\mu_c - 1) - (\mu_c - 2)\left(\frac{\mu_c - 1}{\mu_c} - \frac{x_R/t}{\mu_c a_{oc}}\right)\right] \tag{26}$$

$$= a_{oc}\left[\frac{2(\mu_c - 1)}{\mu_c} + \frac{\mu_c - 2}{\mu_c}\frac{x_R}{\mu_c a_{oc} t}\right].$$

Letting $A = a_{oc}2(\mu_c - 1)/\mu_c$ and $B = (\mu_c - 2)/\mu_c$, Equation (26)

takes the form

$$\frac{dx_R}{dt} = A + B\frac{x_R}{t} \quad ,$$

a homogeneous first order differential equation of degree zero, the general solution of which is

$$t = C\left[A + (B-1)\frac{x_R}{t}\right]^{\frac{1}{B-1}} ,$$

where C is an arbitrary constant, to be determined by the initial condition that $x_R = -L_C$ when $t = L_C/a_{OC}$, where L_C is the length of the compression chamber. The solution then becomes

$$t = \frac{L_c}{a_{oc}}\left[\frac{\mu_c - 1}{\mu_c} - \frac{x_R}{\mu_c a_{oc}\, t}\right]^{-\frac{\mu_c}{2}} , \qquad (27)$$

or

$$x_R(t) = (\mu_c - 1)a_{oc}t - \mu_c L_c\left(\frac{a_{oc}}{L_c}\, t\right)^{\frac{\mu_c - 2}{\mu_c}} . \qquad (28)$$

This gives explicitly the path of the point R in the x-t plane, from the

point where it is reflected to the point where it crosses the path of the point F. The path of R will be straight where the flow velocity and sound speed are uniform, which is the case between the paths of F and C, and again between the paths of C and S. Since there is no discontinuity in (u + a) at F, the parts of the path of R on either side of the path of F will be tangent at the intersection.

Between the paths of F and C, the velocity of the point R is

$$u_1 + a_{1C} = a_{0E} \frac{(\mu_E - 1)(1 - \xi)}{\sqrt{(\mu_E + 1)\xi(\mu_E + \xi)}} + a_{0C} \left(\frac{p_1}{p_2}\right)^{\frac{1}{\mu_C + 1}},$$

and between the paths of C and S, the velocity of the point R is

$$u_1 + a_{1E} = a_{0E} \left[\frac{(\mu_E - 1)(1 - \xi)}{\sqrt{(\mu_E + 1)\xi(\mu_E + \xi)}} + \sqrt{\frac{1 + \mu_E \xi}{\xi(\mu_E + \xi)}} \right],$$

both of which are known constants, if ξ and the properties of the gases are given.

The paths in the x-t plane of the points R, F, C and S are plotted in Figure 7 for $\xi = 0.2$ and $\mu = 6$. The sound speed in the undisturbed medium is taken to be 0.3455 meters per millisecond, which is the accepted experimental value for air at room temperature, and the dimensions of the tube correspond to the dimensions of the one used in the laboratory (see Figure 11, Page 34). For comparison, the paths are drawn also

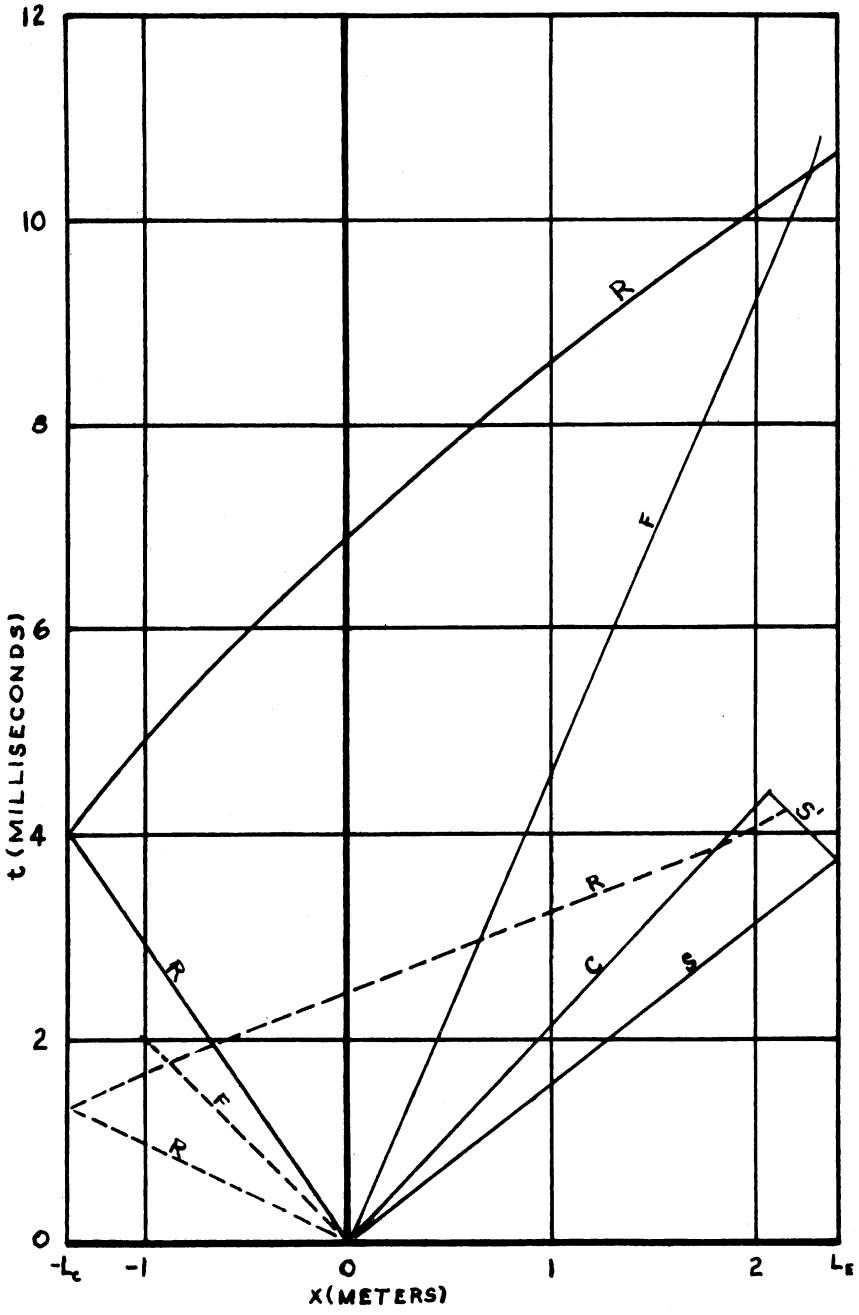

Figure 7

Reflections and interactions of waves in the shock tube with $\xi = 0.2$. The dotted curves are for helium-to-air operation.

for the case in which helium is used in the compression chamber, with $\mu_c = 4$ and $a_{oC} = 2.960\, a_{oE}$.

5. Duration of Uniform Flow

A form of presentation of these results which is of more practical interest is a graph of the time of arrival of the various disturbances at some point in the expansion chamber, plotted against .

Let

L_W = distance from the diaphragm to the test section window (meters)

L_E = length of the expansion chamber

t_{RF} = time at which R overtakes F, and similarly for t_{RC}

t_{RW} = time at which R arrives in the window, and similarly for t_{CW}, t_{FW}, etc.

X_{RF} = position where R overtakes F, and similarly for X_{RC}.

Then the times of arrival of S, C, F and S' in the window are given by

$$t_{SW} = L_W \frac{dt}{dx_s} = \frac{L_W}{a_{oE}} \sqrt{\frac{(\mu_E+1)\xi}{\mu_E+\xi}} \quad ,$$

$$t_{CW} = L_W \frac{dt}{dx_c} = \frac{L_W}{u_1} = \frac{L_W}{a_{oE}} \frac{\sqrt{(\mu_E+1)\xi(\mu_E+\xi)}}{(\mu_E-1)(1-\xi)} \quad ,$$

$$t_{FW} = \frac{L_W}{u_1 - a_{1C}} = L_W \left[a_{0E} \frac{(\mu_E - 1)(1 - \xi)}{\sqrt{(\mu_E + 1)\,\xi\,(\mu_E + \xi)}} - a_{0C} \left(\frac{p_1}{p_2} \right)^{\frac{1}{\mu_C + 1}} \right]^{-1},$$

and

$$t_{S'W} = \frac{L_E}{U} + \frac{L_E - L_W}{U'} = \frac{L_E}{a_{0E}} \sqrt{\frac{(\mu_E + 1)\,\xi}{\mu_E + \xi}} + \frac{L_E - L_W}{a_{0E}} \frac{\sqrt{(\mu_E + 1)\,\xi\,(\mu_E + \xi)}}{2 + (\mu_E - 1)\,\xi}$$

(see Equation 23). These functions have been computed and tabulated, using values of the constants appropriate for discussion of the events following air-to-air and helium-to-air shots in the tube: L_W = 1.600 meters; L_C = 1.385 meters; $L_E - L_W$ = 0.815 meters; μ_E = 6; μ_C = 6 and 4; a_{oE} = 0.3455 meters per second; a_{oC} = 0.3455 meters per second and 1.010 meters per second.

The behavior of the path of the reflected rarefaction (see Figure 7) makes it easy to compute the time of its arrival in the window, t_{RW}, once its intersection with the path of F is known.

Since $x_R(t)$ is known explicitly (Equation 28), and $x_F(t) = (u_1 - a_{1C})\,t$, or from Equations (17) and (9)

$$x_F(t) = a_{oc} \left[(\mu_c - 1) - \mu_c \left(\frac{p_1}{p_2} \right)^{\frac{1}{\mu_c + 1}} \right] t, \qquad (29)$$

t_{RF} may be obtained by setting these two expressions equal:

$$x_R(t_{RF}) = x_F(t_{RF})$$

or

$$(\mu_c - 1)\, a_{oc}\, t_{RF} - \mu L_c \left(\frac{a_{oc}}{L_c}\, t_{RF}\right)^{\frac{\mu_c - 2}{\mu_c}} = a_{oc}\left[(\mu_c - 1) - \mu_c \left(\frac{p_1}{p_2}\right)^{\frac{1}{\mu_c + 1}}\right] t_{RF}$$

$$L_c \left(\frac{a_{oc}}{L_c}\, t_{RF}\right)^{\frac{\mu_c - 2}{\mu_c}} = a_{oc} \left(\frac{p_1}{p_2}\right)^{\frac{1}{\mu_c + 1}} t_{RF}$$

$$t_{RF} = \frac{L_c}{a_{oc}} \left(\frac{p_1}{p_2}\right)^{-\frac{\mu_c}{2(\mu_c + 1)}}, \tag{30}$$

a rather simple relation, considering the complexity of the process involved.

If the paths of F and C and the path of R between them are plotted in the x-t plane, they are straight lines with the equations

$$x_F = (u - a)t$$

$$x_C = ut$$

$$x_R = (u + a)t + B$$

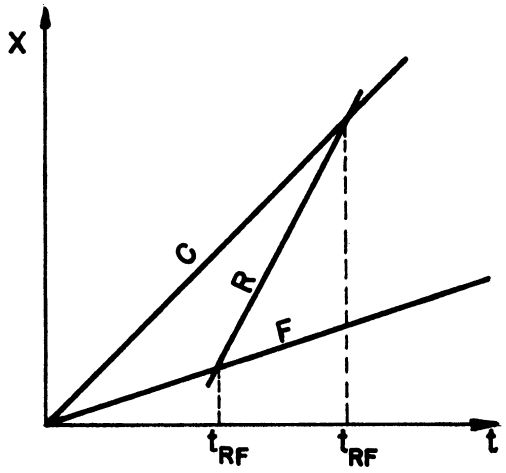

Figure 8
Paths of C, R and F in the x-t Plane

where B is a constant. (See Figure 8.) Solving for the intersections t_{RF} and t_{RC},

$$(u - a)t_{RF} = (u + a)t_{RF} + B$$

$$ut_{RC} = (u + a)t_{RC} + B$$

and subtracting the second from the first,

$$u(t_{RF} - t_{RC}) - at_{RF} = (u + a)(t_{RF} - t_{RC})$$

it follows that

$$-at_{RF} = at_{RF} - at_{RC}$$

or

$$t_{RC} = 2t_{RF} . \tag{31}$$

Over a certain range of values of ξ, the appearance in the window of the contact surface is followed by the appearance of the reflected rarefaction. For this range,

$$t_{RW} = t_{RF} + \frac{L_W - X_{RF}}{u_1 + a_{1c}} \tag{32}$$

where the second term on the right is the distance to be traveled after the intersection divided by the appropriate velocity. For higher values

of ξ, the arrival of the rarefaction precedes that of the contact surface, and in this range,

$$t_{RW} = t_{RC} + \frac{L_W - X_{RC}}{u_1 + a_{1E}} . \qquad (33)$$

The formulae now suffice to describe the succession of events in the test section. The result of the computations is given in Figure 9, from which can be determined the length of time available during which the flow is uniform. The computations were carried out to include uniform flow in the cold air which issues from the compression chamber, for while this air moves with the same speed as the hot air ahead of the contact surface the sound speed is reduced, and the Mach number may reach comparatively high values, making this portion of the flow interesting from a practical standpoint. However, when helium is used in the compression chamber, the Mach number in the cold helium is too low to be of interest, and the calculation of the time of arrival of the foot of the rarefaction wave was omitted.

In Figure 10 is plotted the length of time during which the flow in the hot air is uniform in the window, before any of the disturbances arrive. The curves labeled C, R and S' refer to the arrival of the contact surface, the reflected rarefaction and the reflected shock, respectively.

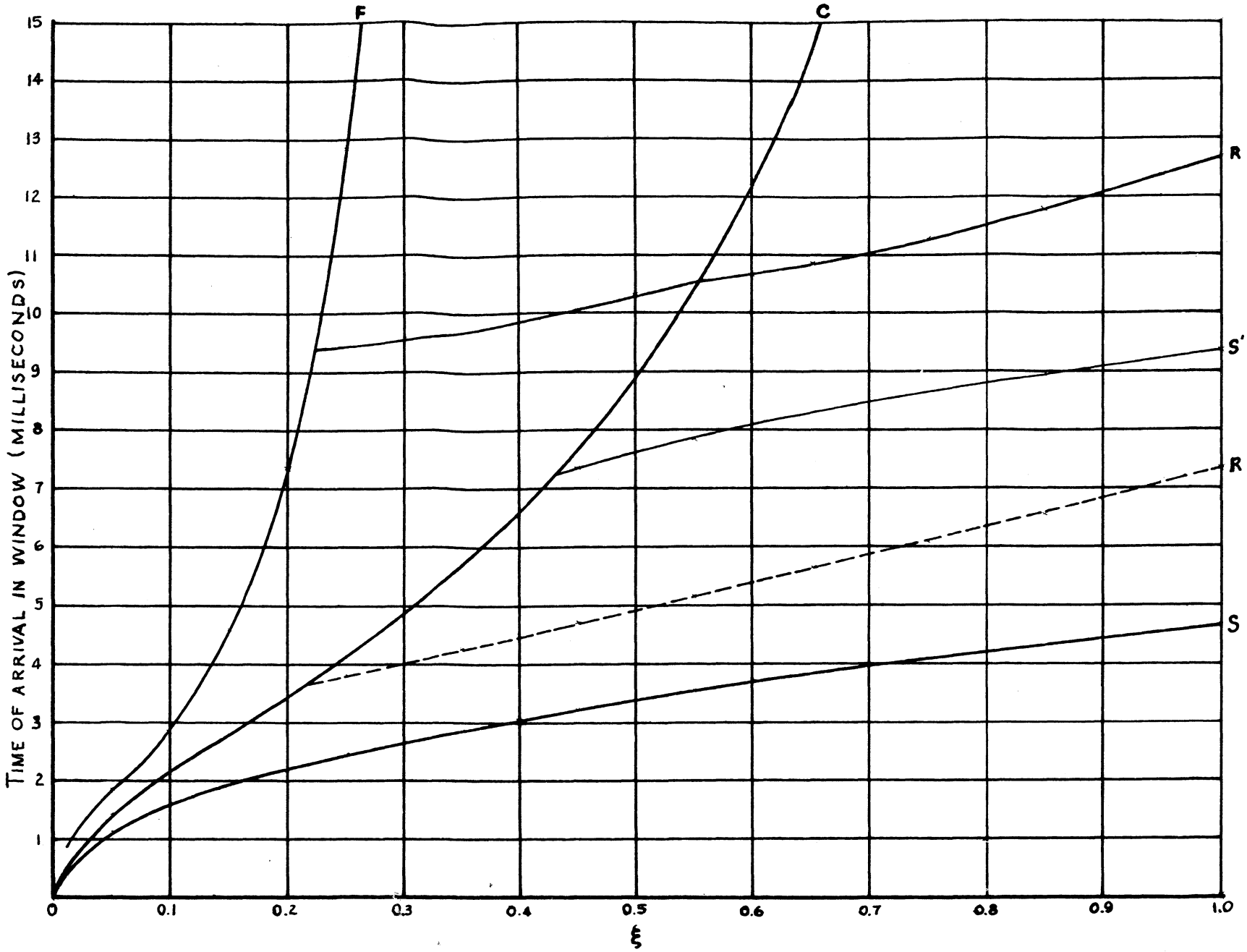

Figure 9

Theoretical time of arrival of the various disturbances in the test section. The dotted curve is for helium-to-air operation.

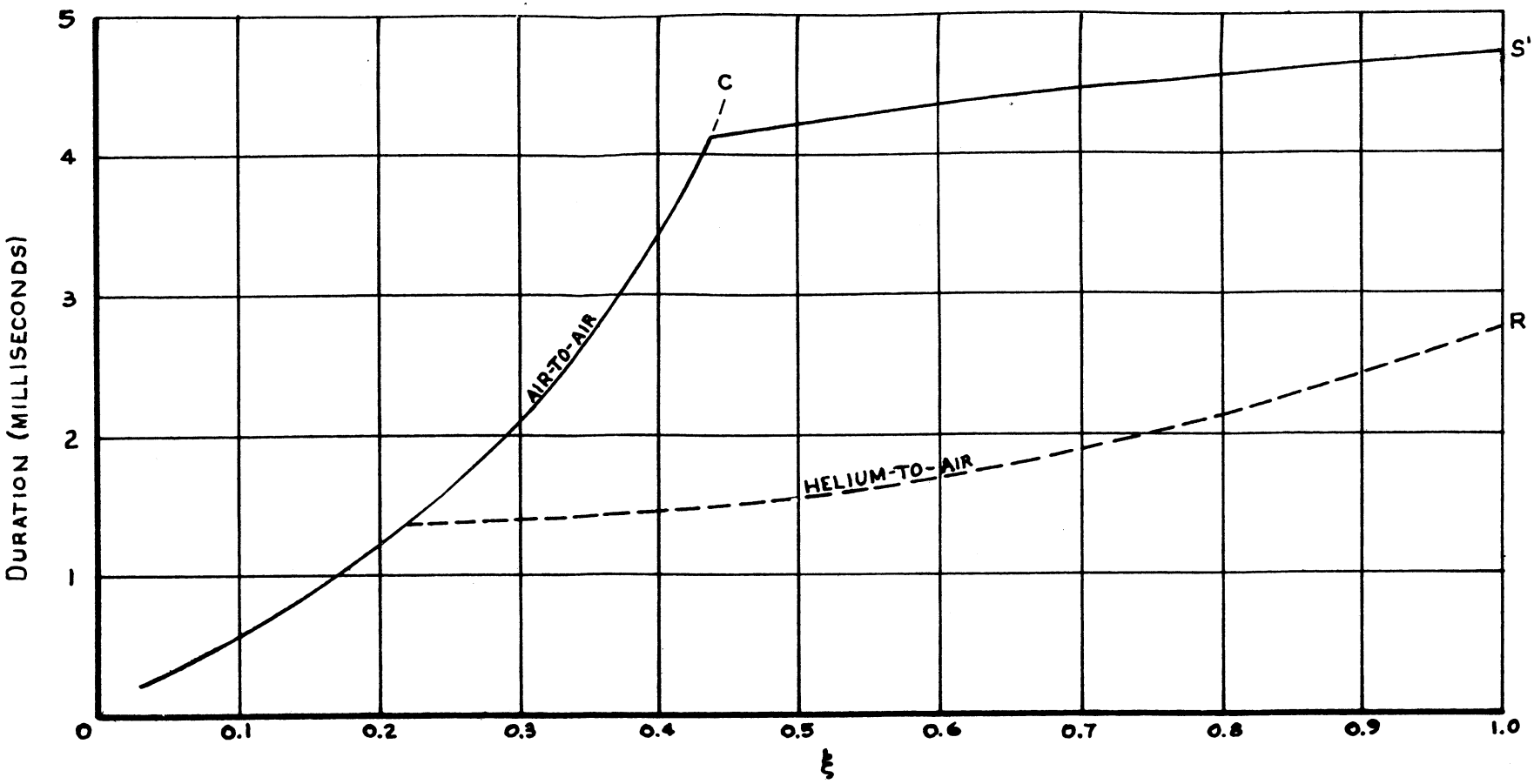

Figure 10

Theoretical duration of uniform flow following the arrival of the shock front.

CHAPTER II

DESCRIPTION AND OPERATION OF THE APPARATUS

1. General Description of the Apparatus

The shock tube used in this investigation consists essentially of a rigid tube of uniform cross-section, divided into two sections by a cellophane diaphragm. One of the sections, the compression chamber, is closed at the extreme end, so that it may be filled with gas at a pressure higher than that in the other section, the expansion chamber. When this is done, a spring-driven plunger is manually released, breaking the diaphragm, and a pressure wave travels into the expansion chamber. After travelling a short distance this pressure wave becomes a shock wave with an almost plane front, moving with nearly constant velocity.

The velocity of the shock front is determined by measuring the time between its arrival at two stations along the tube, which are a known distance apart. At each of these stations a light source and a photomultiplier tube are so arranged that the arrival of the shock front causes a brief pulse of light to fall upon the cathode of the phototube. The resulting voltage pulses are fed to an electronic

timer which records the time interval between them.

After the shock front passes the second of the stations, which will be referred to as light screens, it passes between two circular windows in the sides of the tube through which the spark-shadowgrams are taken. When it is desired to photograph the flow behind the shock wave, the first light screen is not used, and the timer is arranged to measure the interval between the arrival of the shock front at the second light screen and the flash from the spark. In this way, the "age" of the flow pattern registered on the plate can be determined, even though the shock front has passed beyond the window.

In addition to starting the timer, the voltage pulse from the second light screen starts a variable-delay circuit, which fires, or "triggers", the spark after a predetermined time. The spark is an air gap through which a capacitor can be made to discharge by the triggering action of the delay circuit.

The spark source is placed at the focal point of a large lens whose axis passes through the centers of the two circular windows, so that when the spark is fired, a burst of nearly parallel light passes through the test section, and falls on a photographic plate, making a record of the shock wave configuration.

The remainder of this chapter will be devoted to a more detailed description of the apparatus, except the electronic circuits and the spark, which will be described in Chapter III.

2. Method of Photography

The photography of shock phenomena by means of nearly parallel

light which falls directly on the photographic plate after passing through the flow field is known as the shadowgraph method. In passing through the shock tube, the light is deflected by inhomogeneities in the index of refraction of the gas, and if a shock front is present in the test section at the time the spark is fired, the light will be refracted toward the denser side of the shock front. The effect of this is to produce a line on the plate in which the photographic density is very low, and a line close to this where the density is correspondingly higher, the light which is deflected away from the former of these falling on the plate to produce the latter.

A region in which the gradient of the index of refraction is uniform will not produce any change in the photographic density on the plate, since the light which passes through such a region will be deflected as a whole. The gradient of the index of refraction is, of course, very large in the shock front, and zero, or nearly zero, on either side of it. It is this rapid change in the gradient of refractive index which enables the shock front to be photographed by the shadowgraph method.

The appearance of the shadowgram is affected by the distance of the plate from the shock front which is being photographed, since the direction of the beam of light which is refracted by the shock front makes a slight angle with the direction of the undeflected beam, and also since the undeflected beam can never be exactly parallel. In the experiments described in this report, the plates were placed

3-1/2" from the central plane of the test section, except in an endeavor to obtain schlieren photographs, which will be mentioned in the discussion of the lenses. This distance appears to be satisfactory for most purposes.

5" x 7" Eastman "Process" plates were used in nearly all of the work. They were given normal development in DK-50 developer.

3. The Shock Tube

The shock tube is made up of five flanged sections as shown in Figure 11 and Figure 12.

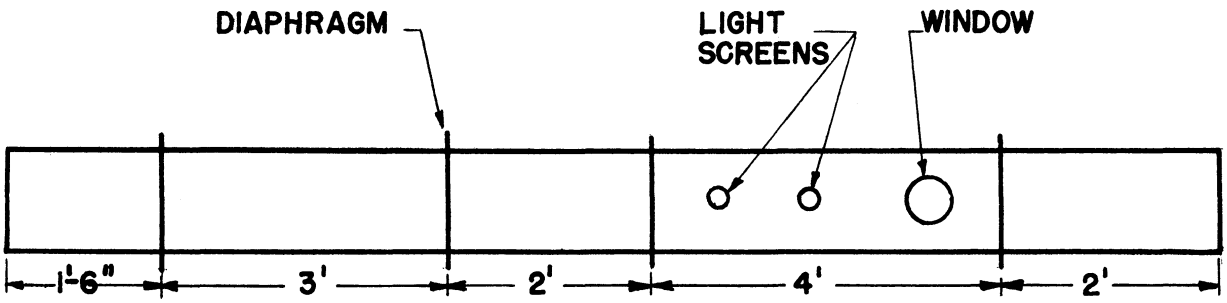

Figure 11

The Shock Tube

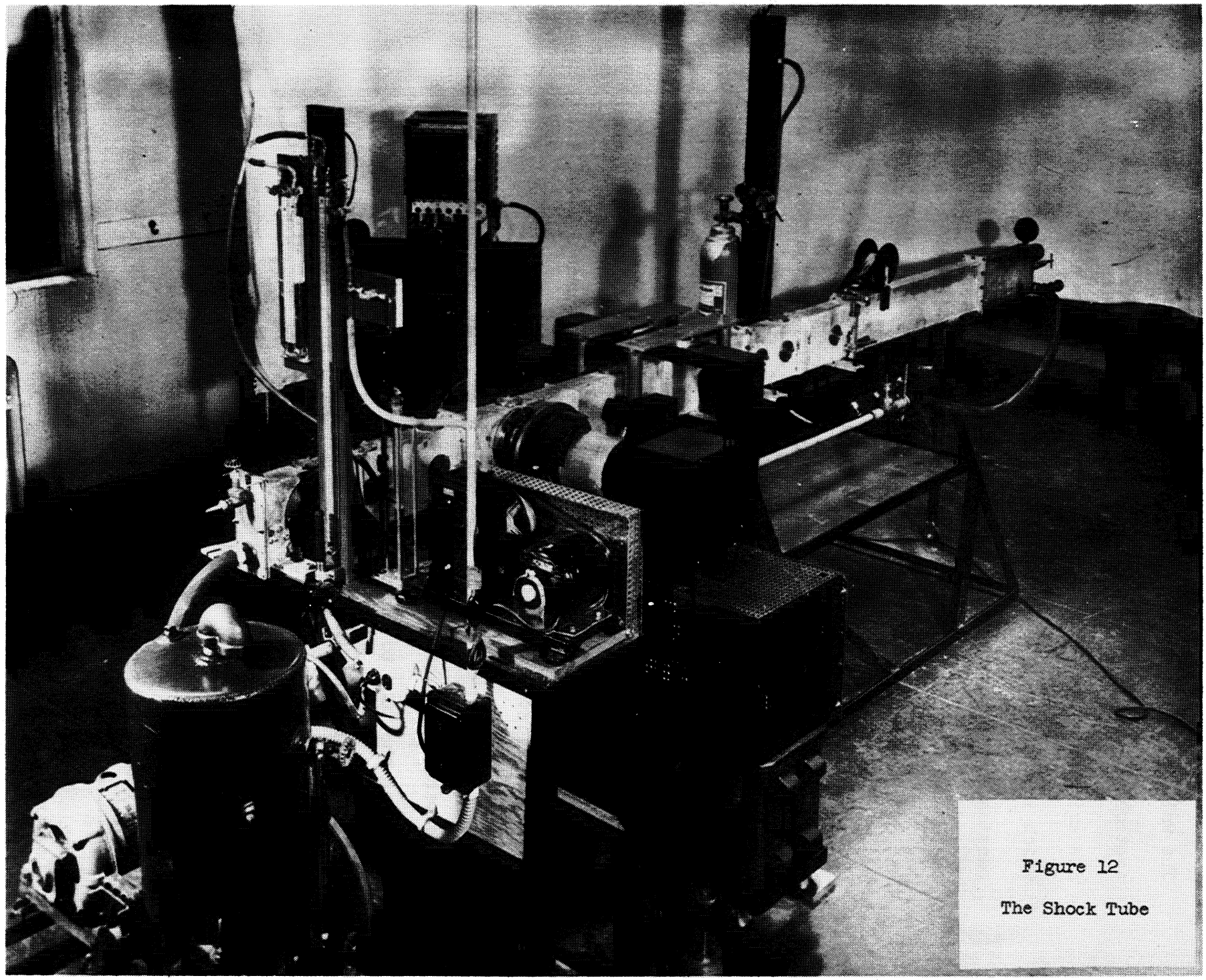

Figure 12

The Shock Tube

The walls are of 1/4-inch steel, welded at the edges, and the cross-section is 2" x 7" inside. The tube is bolted to a metal frame with its axis horizontal, the 7-inch sides vertical. The compression chamber, which is made up of the first two sections, is fastened to the expansion chamber by manually operated clamps, and is supported by a caster and a pair of hinges in such a manner that it may be swung out of the way when a new diaphragm is inserted.

At the junctions between the sections, rubber gaskets are clamped by fastening-bolts in the flanges to form vacuum seals. The gaskets between the compression and expansion chambers are soft, providing a flexible seat for the cellophane diaphragm, while the others are relatively hard, so that they will not project into the interior of the tube when the fastening-bolts are tightened. There remains a certain roughness at each joint which is undesirable, but which is difficult to avoid with a seal of the type used.

Welded to the bottom of each of the sections which make up the expansion chamber are two lengths of channel-iron. These are used to fasten the tube to the welded steel frame on which the tube rests, the bolts which pass through them being provided with nuts above and below so that the sections may readily be brought into alignment.

4. The Diaphragm

The cellophane used for the diaphragm is .002" thick, and is obtainable in long rolls[1]. It is clamped between soft rubber gaskets

---

[1] Available as "American Tobacco Company Red Zip Tape" from The Dobeckmun Company, Cleveland, Ohio. This is the material used in making the strips which facilitate the opening of cigarette packages.

which cover the flanges at the junction between the compression and expansion chambers.

A pressure difference of 18 to 20 pounds per square inch will burst the cellophane when it is clamped in the shock tube, although it can be made to sustain a difference of 25 psi for a few seconds. If a little care is used in placing it between the gaskets, it will sustain a difference of one atmosphere of pressure for practically an indefinite time, and this was taken to be the maximum difference usable in routine work. For this reason, it is necessary to evacuate the expansion chamber in order to produce shocks of sufficient strength to be useful in this work. To produce a flow of unit Mach number, for example, ξ must be approximately 1/5, and even if helium is used in the compression chamber, p_o/p_2 must be approximately 1/12. It is necessary, then, to evacuate the expansion chamber to about 1/12 atmosphere in order to obtain the required pressure ratio p_o/p_2 and remain within the usable pressure difference $p_2 - p_o$.

The mechanical properties of sheet cellophane make it admirably suited to the purpose: It is strong in tension, so that it will withstand a large difference in pressure, but once it is torn or pierced, it is very weak, and it rips into small pieces very rapidly when the tube is fired. A discussion of the bursting of the diaphragm is given in Section 4 of Chapter IV.

5. The Plunger

Sealed into the end of the compression chamber is a long spring-driven plunger which reaches almost to the diaphragm in the

"cocked" position, and which snaps forward, piercing the cellophane, when released. The sharp end of the plunger is supported by a string fastened to the upper wall of the tube. This keeps the rupture-point of the diaphragm near the axis of the tube, and also it reduces the disturbance in the flow caused by the plunger.

The plunger mechanism is shown in Figure 13, which is

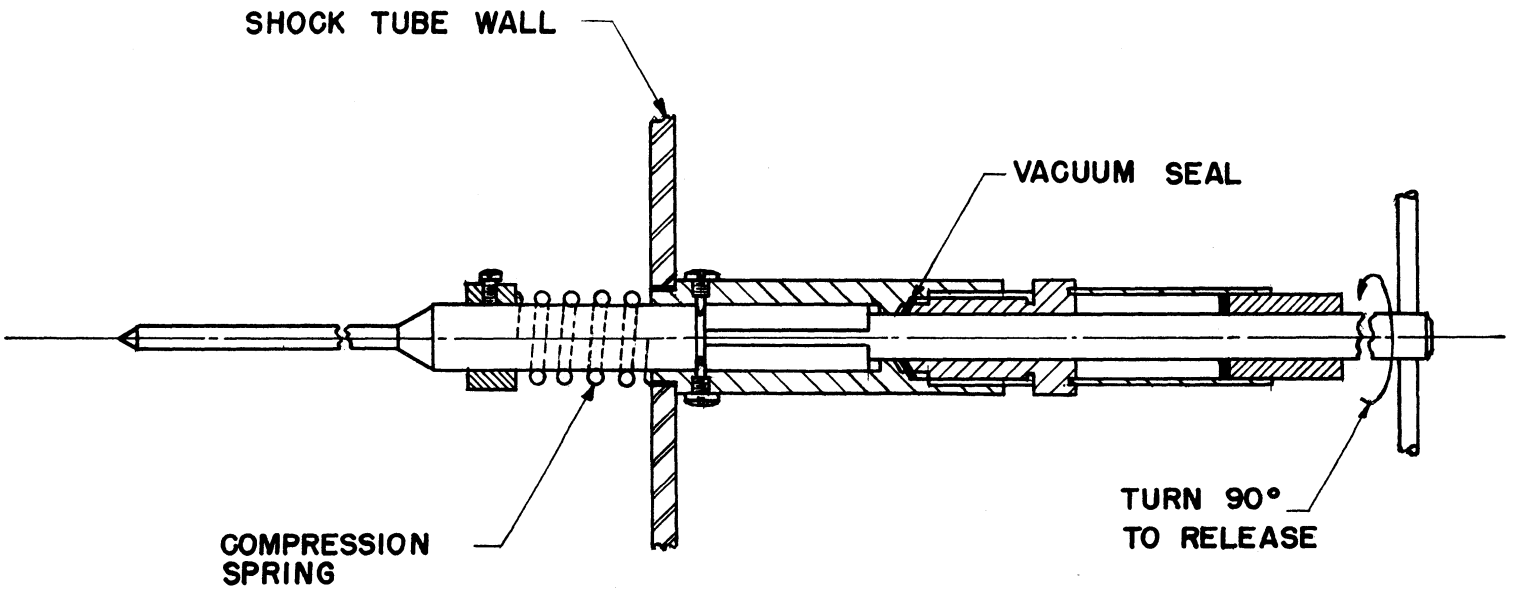

Figure 13

The Plunger

taken from the report of Smith[1].

6. The Measurement of the Pressures

The pressure in the expansion chamber is measured with an oil manometer, one side of which is kept at effectively zero pressure by means of a small vacuum pump. The range of this manometer has recently been increased from about 750 millimeters of oil to about 1500 millimeters. This is equivalent to about 100 millimeters of mercury. A large-bore mercury manometer supplements the oil manometer for measuring pressures above 100 millimeters of mercury.

A bourdon gauge indicating both pressure and vacuum is screwed into the upper wall of the compression chamber, providing a rough indication of the pressure, and a mercury manometer with one end open to the atmosphere can be connected to either the compression chamber or to the expansion chamber. In almost all the work described, the pressure in the compression chamber was set at atmospheric pressure, which could be determined accurately from a mercurial barometer on the wall.

7. The Firing Operation

The complexity of the operation of firing the tube depends upon the shock strength required. To produce weak shocks ($\xi = 0.75$ or higher) it is necessary merely to install a diaphragm, run air from the compressed air line into the compression chamber until the pressure is right, and fire. For moderately strong shocks ($\xi = 0.15$ to 0.75) it is necessary to evacuate the expansion chamber. A valve which by-

---

[1] Smith, Lincoln G., Photographic Investigation of the Reflection of Plane Shocks in Air. OSRD Report No. 6271, November, 1945.

passes the cellophane diaphragm is kept open while the tube is being exhausted, keeping tension off the diaphragm, and so avoiding the possibility of a spontaneous rupture during the time the sensitive oil manometer is opened to the expansion chamber. When the required pressure is obtained, the by-pass valve is closed, isolating the two chambers, and the compression chamber is opened to the atmosphere. After allowing some 20 seconds for the air in the compression chamber to cool to room temperature, the tube is fired.

For the strongest shocks which can be photographed in this shock tube ($\xi = 0.06$ to 0.15) it is necessary to use helium in the compression chamber. When this is done, the tube must first be relatively highly evacuated (down to, say, 1/2 millimeter of mercury) in order that the percentage of air in the compression chamber may be negligible. The valve which by-passes the diaphragm is then closed, and enough helium is admitted to the compression chamber to prevent the cellophane from being pushed back against the sharp plunger when the pressure in the expansion chamber is brought up to the required value. After the pressure in the expansion chamber is adjusted, helium is admitted into the compression chamber until the bourdon gauge shows a pressure slightly in excess of atmospheric. The chamber is then opened to the atmosphere, and when the excess pressure has disappeared, the tube is fired. Observations with a thermocouple have shown that the helium comes to room temperature so quickly that no appreciable waiting period is required.

The particles of cellophane which litter the floor of the tube are removed with a compressed air jet after every shot.

8. The Vacuum Connections

A schematic diagram of the pipe connections is given in Figure 14. The vacuum seal at the end of the expansion chamber is formed when the pressure of the atmosphere forces an end-plate against a (rectangular) ring of neoprene which projects out from the end flange. The ring is made of a length of 1/8"-square neoprene which is held by friction in a groove in the flange. The groove is 1/8" wide and 1/16" deep, and the length of the neoprene strip is such that its ends butt together.

The end plate has two openings. One of these accommodates a valve for admitting air or other gas to the expansion chamber. The other opening leads to the large vacuum pump which is used in exhausting the tube. Covering this opening is a fine wire mesh for filtering out the larger of the cellophane particles. In the vacuum line leading from the end-plate to the pump is a filter which prevents most of the dust-like particles of cellophane from reaching the pump.

The filter is made of a 10-litre wide-mouth pyrex bottle loosely filled with glass wool. As shown in Figure 14, which is a schematic layout of the pipe connections, a two-hole rubber stopper admits large-bore tubes in such manner that the gas from the tube flows through the glass wool.

All valves were made vacuum-tight by installation of Wilson seals[1].

---

[1] See Wilson, Robert R. Rev. Sci. Inst. 12, 91,(1941).

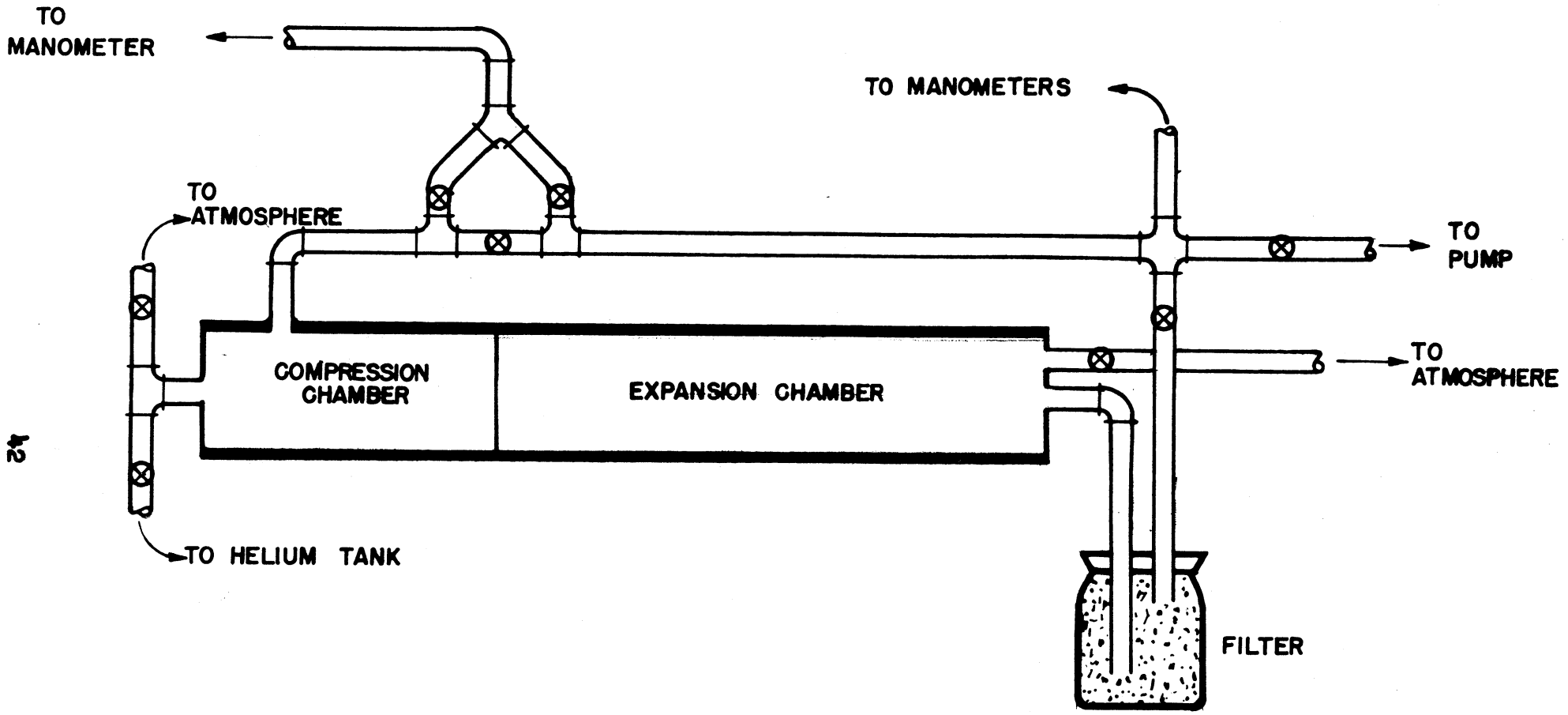

Figure 14

The Vacuum Connections.

9. The Light Screens

The change which is produced by the shock front in the optical index of refraction of the air is the quantity which the light screens depend on for their action. This change may be taken to be directly proportional to $\rho_1 - \rho_0$, the change in the density of the air, and from the Rankine-Hugoniot relation for air

$$\frac{\rho_0}{\rho_1} = \frac{1+6\xi}{6+\xi}$$

it follows that

$$\rho_1 - \rho_0 = \rho_0 \frac{5(1-\xi)}{1+6\xi}$$

which is nearly proportional to ρ_0 for low values of ξ. With p_2 fixed, low values of ρ_0 are obtained by lowering p_0, so that ρ_0, and hence $(\rho_1 - \rho_0)$ are lowered also, reducing the optical effect produced by the shock front. There is obviously a limit to the sensitivity of the light screens, and it is this limit which governs the range of shock strengths which may be observed in the tube. The advantage of the use of helium in the compression chamber arises here, for, as was pointed out in Section 3b of Chapter I, when helium is used, a higher value of p_0 may be used in producing a shock of given strength. Firing "air-to-air", the lowest value of ξ which could be observed was 0.15. The use of helium brought this down to 0.06.

The values of p_o were about the same in each case, which means that the density difference across the shock front at the limit of sensitivity of the light screens is about 50% greater when helium is used, so there must be some factor influencing this limit other than the density difference. A possibility is that the higher speed of the stronger shock makes it less effective than a simple consideration of density difference would lead one to believe. A second possibility is that the stronger shock fronts do not form properly by the time they reach the first light screen. (See Section 4b of Chapter IV.)

The optical arrangement of the light screens is shown in Figure 15. F is a straight helical filament of a 25 watt, 6-volt Westinghouse type 5-AS-11 lamp bulb. The slit, S_1, is in the focal plane of the first lens, L_1, and the second lens, L_2, forms an image on S_1 on the knife-edge, K, which is adjusted until it cuts off almost all of the light from the source. When a shock front is in the narrow beam of light which passes through the shock tube, a portion of the beam is refracted toward the high-pressure side of the shock, and so passes by the knife edge. (The shock moves from "A" to "B" in Figure 15). The lens L_3 forms an image of the central plane of the shock tube in the plane of the slit, S_2, and thus the system is a schlieren system, with the slit S_2 replacing the usual photographic plate or viewing screen. Therefore the shock front will cause a bright line of light to traverse the slit S_2 from "C" to "D". When the shock front is at some point in its travel, this line will enter the opening in S_2 and fall on the cathode surface of the photomultiplier tube P,

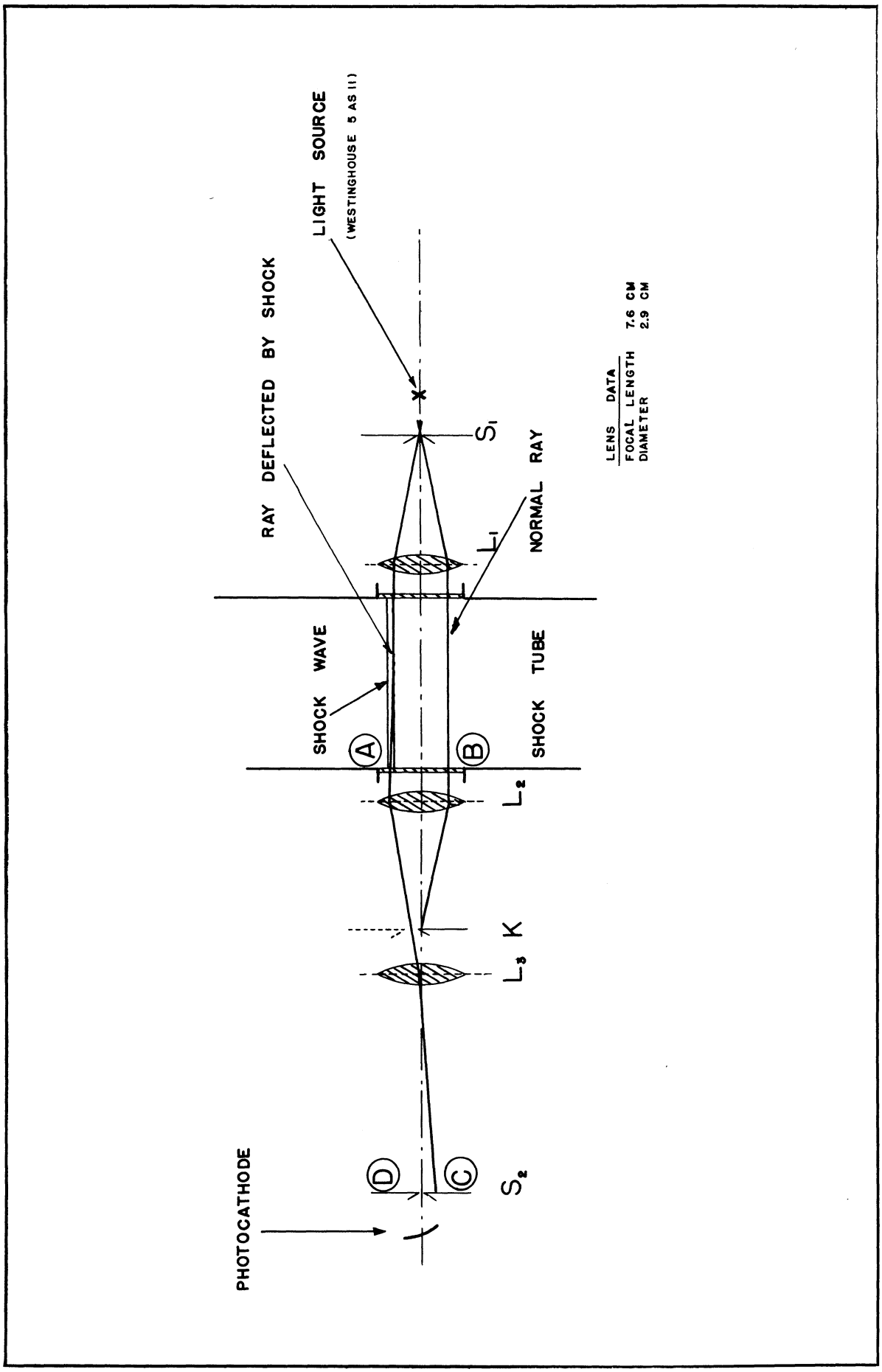

Figure 15

Diagram of Light Screens

causing the tube to produce a steep, short voltage pulse.

The design of the optical system is intended to make the "signal to noise ratio" as large as possible. The slit-leaf shown dotted at K in Figure 15 is actually in the system, its purpose being to lower the stray light (noise) level.

The lenses are achromats, L_1 and L_2 having focal lengths of 76 millimeters, and the lenses L_3, 54 millimeters. These focal lengths are uncritical, as are the slit-widths, which are all about 0.015 inch.

In order to minimize the effects of microphonics, the whole system is suspended from a rigid frame, and no part of it touches the shock tube. The system may be seen in place in Figure 12 and removed from the shock tube in Figure 16, where the light sources are on the right, and where the phototube unit has been removed from the light screen nearest the camera.

The distance between the light screens was determined by measuring the distance between two plumb-lines which passed through access ports in the upper wall of the expansion chamber and hung down through the optical path of the screens. The plumb-lines were fine silk threads, so mounted that either could be moved slowly along the tube. They were adjusted until they gave the same appearance to the eye, when viewed through the slits S_2, with the source-lamps turned on. This adjustment was a nice one, and the measurement yielded a value of 405.0 millimeters, with practical certainty in the last figure.

The phototube units are easily interchanged, so that any important difference in the delays introduced by their separate amplifiers

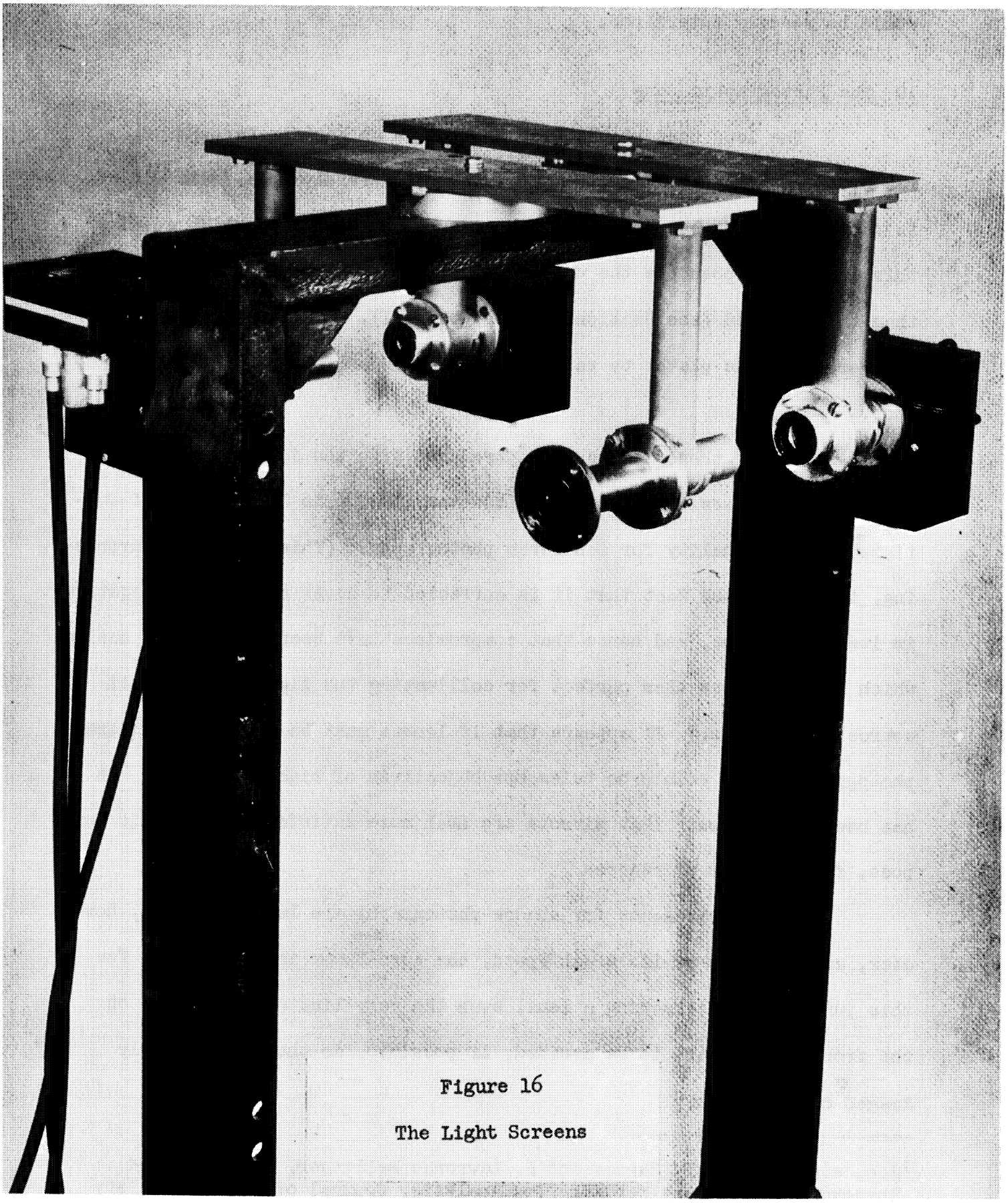

Figure 16

The Light Screens

could be readily determined.

10. The Photographic Lens

The lens used at the test section is an Eastman Aero-Ektar, f/2.5, of 12-inch focal length. It is bolted securely to a frame which is fastened to the base on which the shock tube rests. The high speed of this lens makes possible the use of an even less powerful spark source than the one used (see Section 6 of Chapter III), as it is easily possible to overexpose the plates by raising the voltage on the spark source capacitor.

Two of these lenses were purchased with the idea of using them as schlieren lenses. It was found, however, that this lens is not of sufficiently high quality for schlieren photography. (This is hardly surprising, in view of the fact that it is corrected to cover an 8" x 10" negative in its focal plane, and hence that compromises have been made in its design which leave it less than perfect for collimating the light from a small source on its axis.) It appears that if lenses must be used for schlieren photography, they should be telescope objectives of highest quality. It has been pointed out[1] that mirrors are much more satisfactory for this purpose, for a number of reasons.

The requirements for shadow-photography are less stringent, however, and, because of its great speed, the Aero-Ektar is well suited for this purpose. In selecting a lens, even the very lightest scratches on the front surface are to be avoided, if possible, as they are strongly imaged on the plate.

---

[1]See, e.g., Norman I. Barnes and S. Lawrence Bellinger, Schlieren and Shadowgraph Equipment for Air Flow Analysis, Journal of Optical Society of America, Vol. 35, No. 8, August, 1945, 497.

11. The Windows

The windows in the tube are 5-inch disks of plate glass, 1/2-inch thick, mounted flush with the inside of the shock tube walls as shown in Figure 17. Each disk is held inside a brass ring by the pressure of a compressed neoprene band, which encircles the disk, and the brass ring carries a second neoprene band which is forced against the wall of the shock tube. When the middle ring is tightened down, the neoprene band around the glass disk is highly compressed, forming an effective vacuum seal. The third ring bears directly on the face of the glass, and serves to position the glass accurately. This third ring sometimes caused the window to chip; a narrow ring of paper between the ring and the window should prevent this.

The glass for the windows was cut on the project, and an endeavor was made to avoid bubbles and scratches.

12. The Mounting of the Models

All of the models which were used were held in the shock tube by the pressure of the windows. Each model was made 1.981" wide, which is slightly less than the distance between the windows when they are in place. With a strip of gummed cloth tape fastened to each edge of a model, the fit was sufficiently snug to hold the model firmly in place. Figure 18 is a photograph of a model (the 1/4-inch, 5-degree wedge) mounted in the tube.

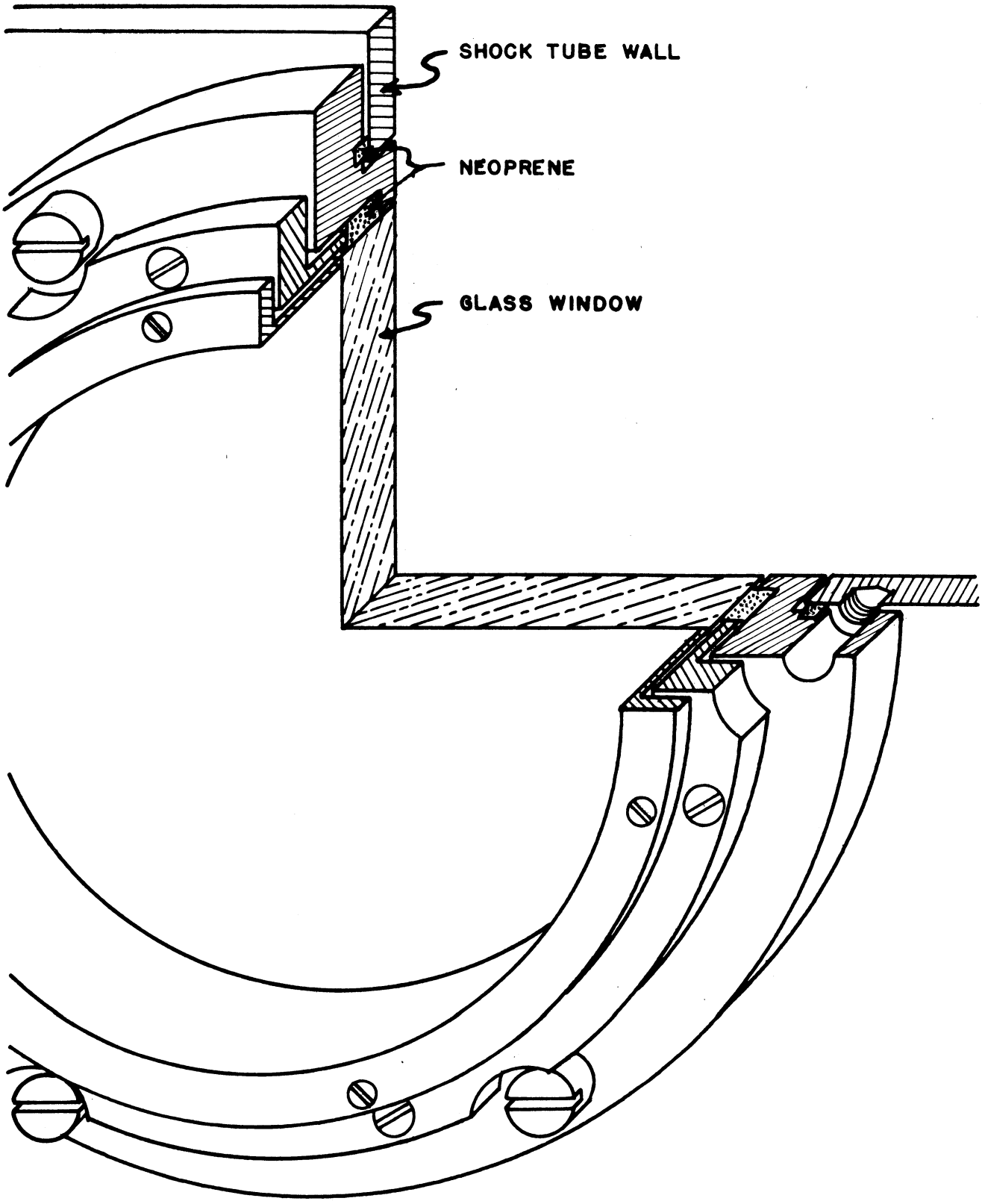

Figure 17

Method of mounting the windows.

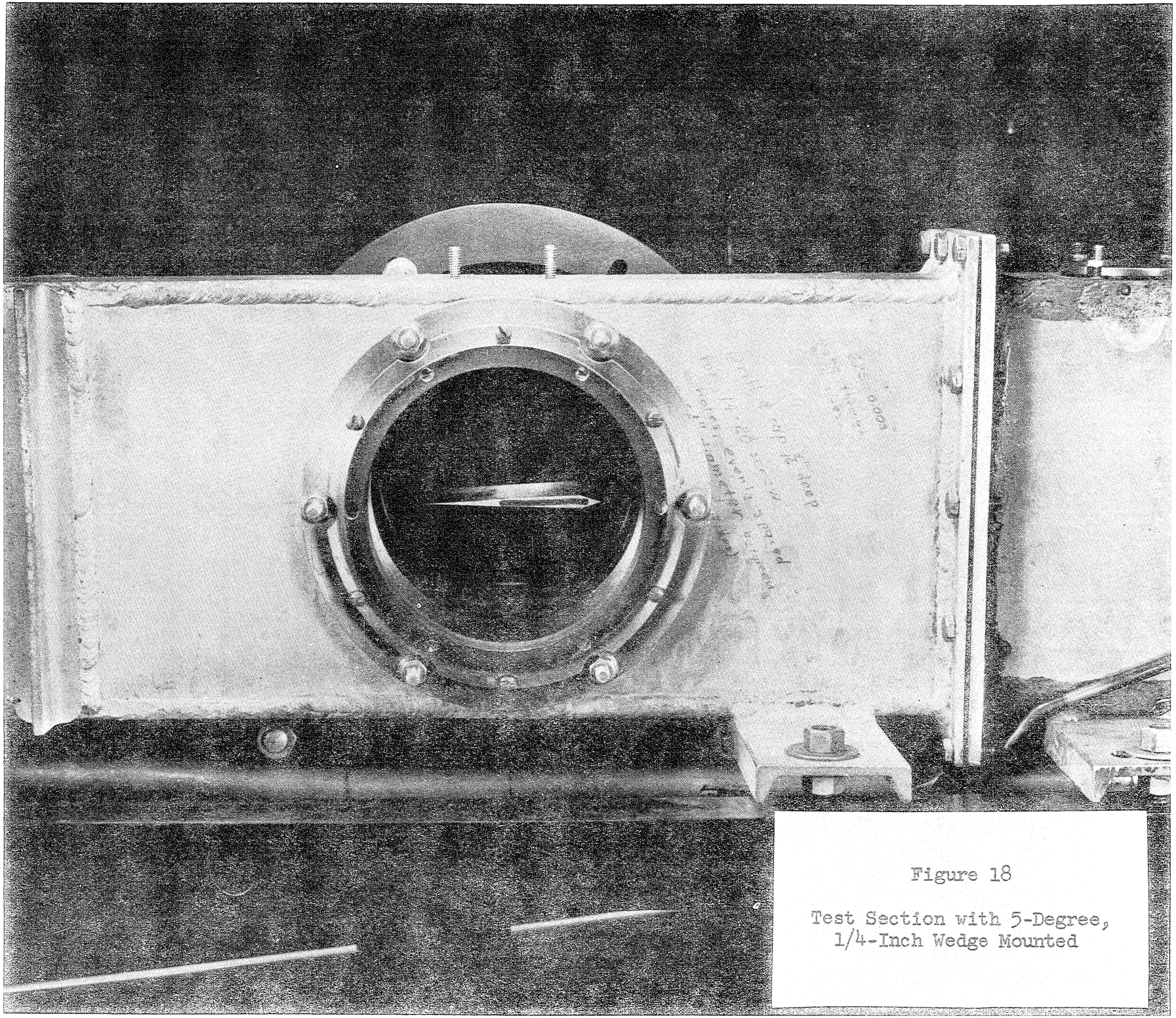

Figure 18

Test Section with 5-Degree,
1/4-Inch Wedge Mounted

CHAPTER III

ELECTRONIC EQUIPMENT

1. Introduction

The electronic equipment is designed to perform two different functions: 1) to measure the velocity of the shock wave, and 2) to control the photographic equipment discussed in the previous chapter.

The speed of the shock wave is obtained by measuring the time of passage of the disturbance between two light screens placed 405 millimeters apart. The equipment, which is shown in block diagram form in Figure 19, operates as follows:

a) A positive voltage pulse is obtained from each of the light screen amplifiers as the shock wave passes. We shall refer to these pulses as "control pulses" in this report.

b) By the first of these control pulses a "gate" circuit is opened (i.e., put into a conducting state), and the second control pulse closes this gate.

c) A generator of voltage pulses with a recurrence frequency of one megacycle is connected through the gate circuit to a scaling circuit.

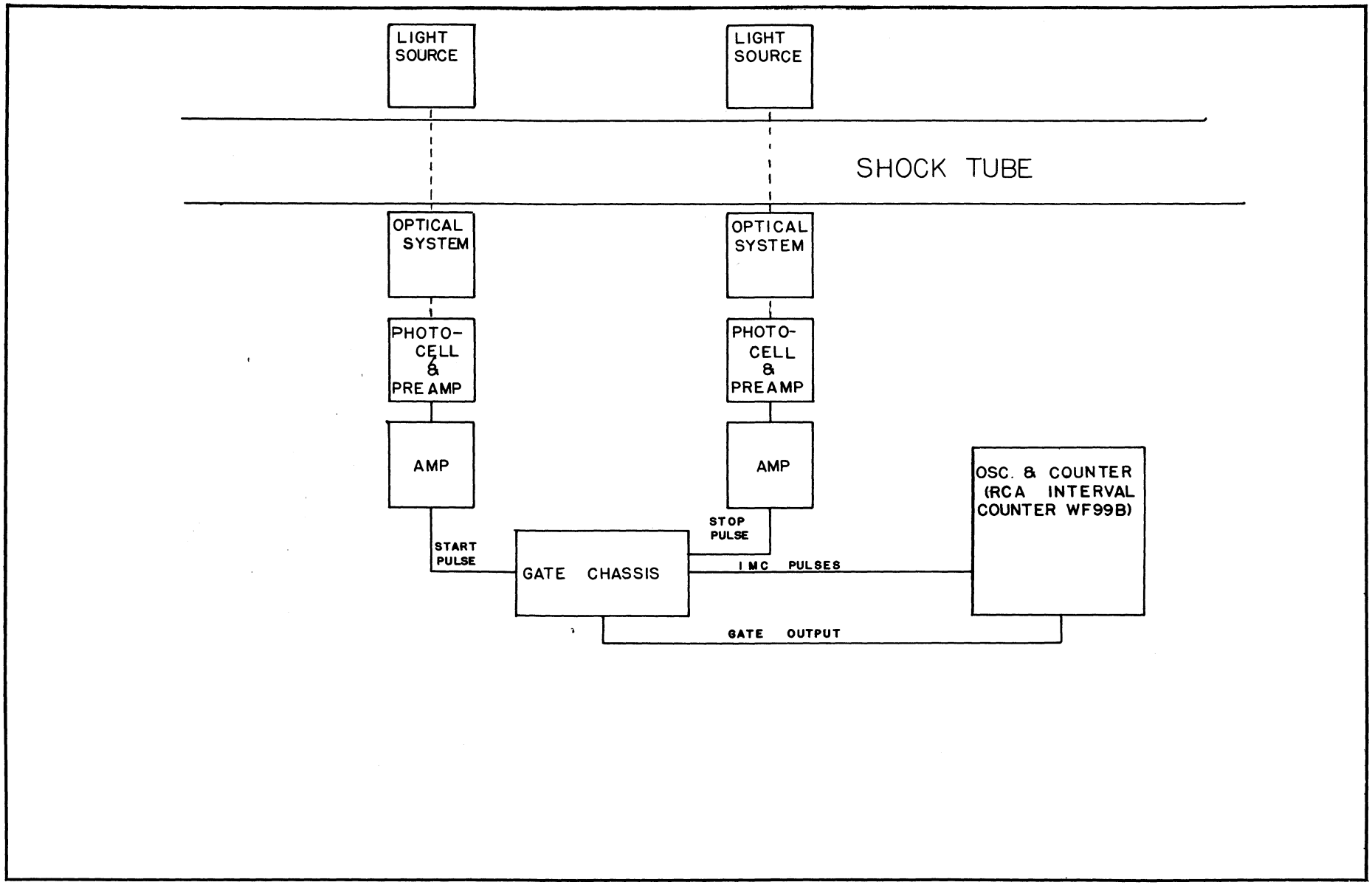

Figure 19

Block Diagram for Velocity Measurement

d) The counter circuit registers the number of pulses passed to it by the gate circuit.

e) The entire circuit is made inoperative after this count is registered to prevent further operation of the gate circuit caused by later disturbances in the flow.

f) The count registered by the counter is the time in microseconds for the passage of the shock wave between the two light screens.

The control of the photographic equipment involves two variables, 1) the duration and intensity of the spark, and 2) the time at which the spark is struck. The first of these is determined by varying the capacitance of the condenser and the voltage to which it is charged. The spark gap employed is a confined air gap which can be triggered by the application of a pulse to a "tickler" or third electrode. The equipment used to control the arrival of this pulse, and therefore the time of exposure of the photographic plate, is shown in block diagram form in Figure 20. The manner in which this control is effected and the time of the photograph recorded is as follows:

a) A control pulse is obtained from one of the light screens as the shock wave passes and opens the gate circuit.

b) In addition to the output to the scaler, the gate circuit provides a single negative pulse almost coincident with the first control pulse, which is fed to the input of a delay circuit.

c) A predetermined number of microseconds after the arrival of the control pulse, a strong current pulse appears in the output of the delay circuit.

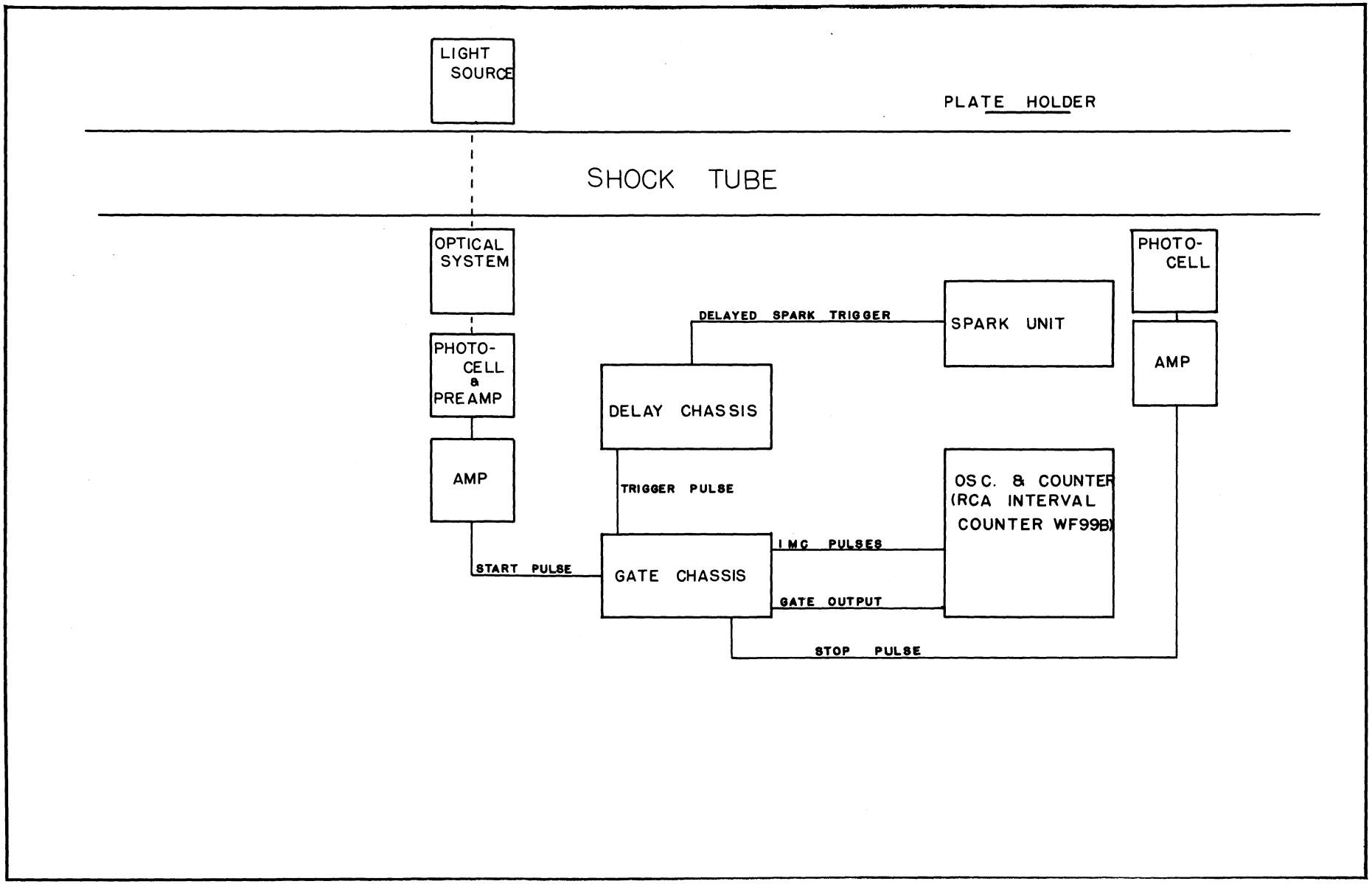

Figure 20

Block Diagram for Photography

d) This pulse is applied to the primary of an automobile ignition coil whose secondary is coupled to the third electrode of the spark gap.

e) When the spark gap fires, a control pulse is obtained from a photocell and amplifier circuit which is exposed to the light from the spark. This pulse closes the gate circuit, and thus the counter registers the time elapsed between the passage of the shock wave past the light screen and the exposure of the photographic plate.

2. Light Screens and Phototube Amplifiers

The light screens are described elsewhere in this report (Section 9, Chapter II). A circuit diagram of the phototube and amplifier unit used with the light screens is included as Figure 21. The output of the phototube, which is an RCA-931-A, is connected via a cathode follower stage to a five-stage video amplifier of standard design. The "noise control" in the fourth stage is used to bias this stage below cutoff. This control is generally set so that the background noise pulses are just removed from the amplifier output. The amplifier has a positive pulse output which is applied to Channel 1 or 2 of the gate circuit.

The photocell used to obtain a "stop" control pulse when the spark is fired is the "929". It is connected to the input of a four-stage video amplifier whose stages are identical to those in the amplifier mentioned above. The output of this amplifier is a negative pulse which is connected to Channel 3 of the gate circuit. No circuit diagram of this amplifier is included in this report.

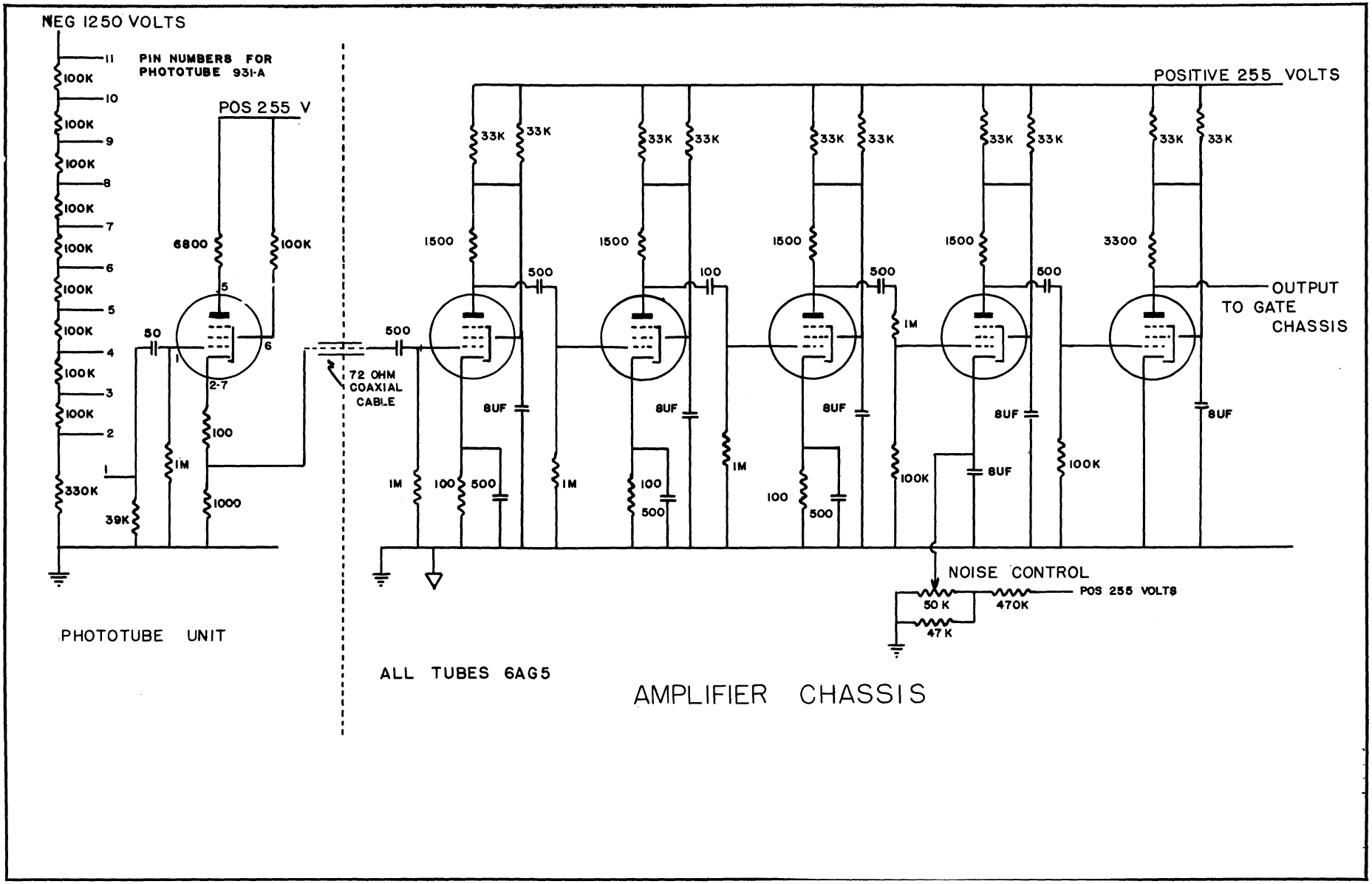

Figure 21

Circuit of Phototube and Amplifier

3. The Gate Circuit

This circuit (Figure 22) is powered by 255 volts from an external supply. A "VR 105" and a "VR 150" (tubes 1 and 7) are connected in series across the power input to make available a tap at 150 volts above ground. The pulse amplifier (tube 2) and the gate tube (tube 3) are operated with their cathodes connected to this tap and all other tubes use this tap as their plate supply. Two filament supplies are used, one for tubes 2 and 3 and one for the remainder of the tubes.

The pulse amplifier is operated normally with a slighly negative bias. The grid, which is continuously fed negative pulses with a recurrence frequency of one megacycle, is returned to the cathode through the plate load of tube 6. Until a measurement has been made, tube 6 is cut off and the pulse amplifier operates in the normal manner. But when a measurement has been completed, tube 6 conducts heavily and the pulse amplifier is cut off, thus removing all signals from the control grid of the gate tube.

The gate tube is operated with the control grid biased slightly below cutoff. The suppressor grid is connected via the "channel switch" to the plate of either tube 10 or 11. Until a control pulse is received, this grid is held about 100 volts below the cathode. The suppressor grid is lifted to the cathode potential, however, during the interval between control pulses. Since the output of the pulse amplifier is connected to the control grid, a negative pulse appears each microsecond at the plate of the gate tube during this interval. This signal is fed directly to a counter. At the end of the interval, not only is the suppressor grid returned to its cutoff position, but the input to the gate tube control grid is removed by the lowering of the pulse amplifier grid mentioned above.

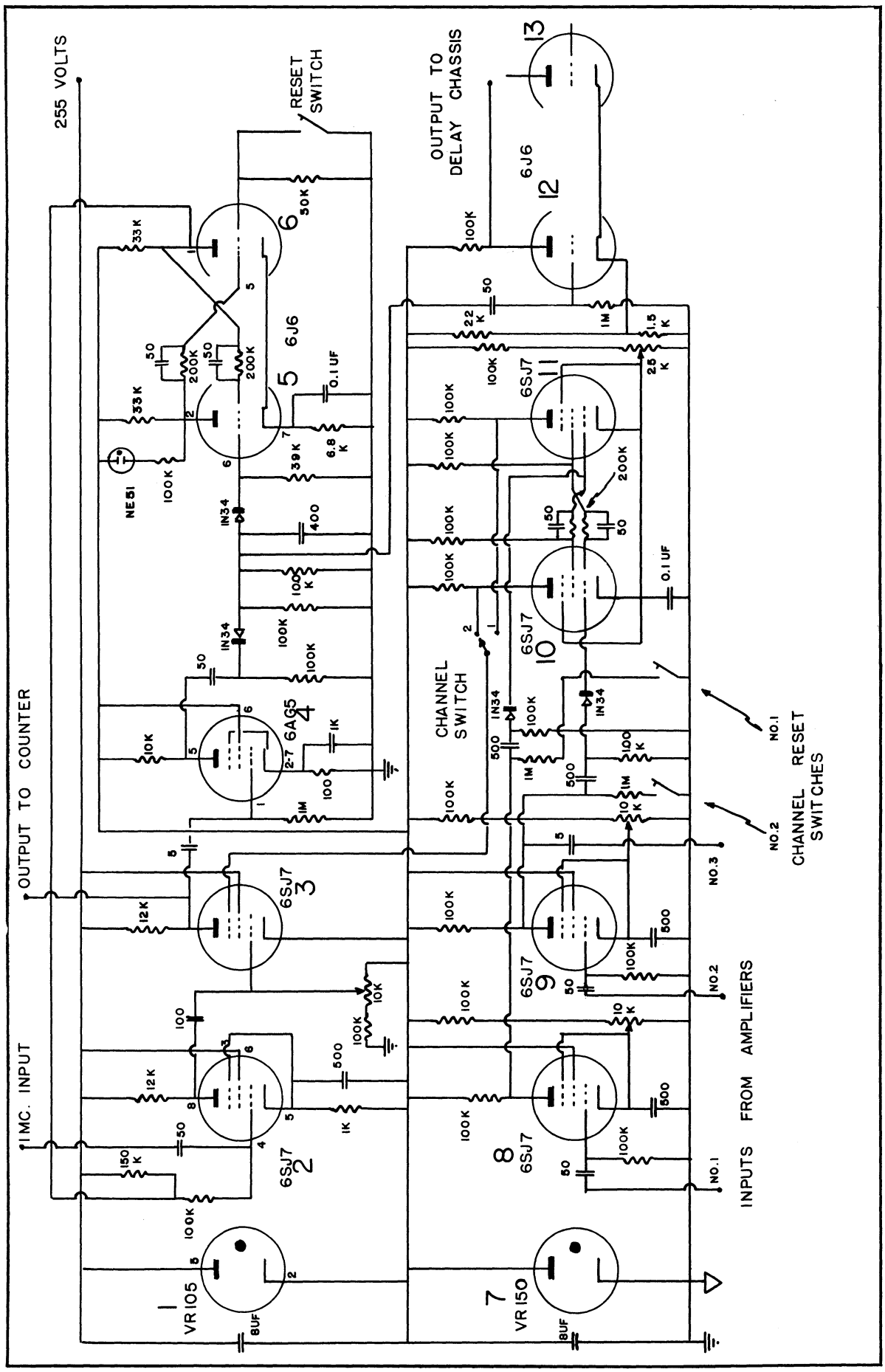

Figure 22

The Gate Circuit

Since the control grid of the gate tube is below cutoff, subsequent variations in the suppressor grid potential caused by the contact surface or cellophane do not alter the registered time.

A portion of the signal at the plate of the gate tube is coupled to the grid of tube 4, which is simply an amplifier. The amplified and inverted signal is rectified through a crystal diode. Thus we get a positive pulse whose width is roughly equal to the time interval. This pulse is used in two ways. First, it is applied to the grid of tube 12, producing at the plate of this tube a negative pulse whose leading edge is nearly coincident with the first control pulse, and which is used to trigger the delay circuit used in photographing the flow. Second, this rectified pulse is applied through another crystal diode to the grid of tube 5. The purpose of the second diode is to produce a negligible positive signal when the count is initiated and a strong (10-volt) negative pulse when at the end of the count. Tubes 5 and 6 form an Eccles-Jordan trigger pair. Normally tube 5 is conducting and tube 6 is cutoff. At the end of the count this situation is reversed. The effect of this action has already been discussed in connection with the pulse amplifier. This trigger circuit, whose state is indicated by a neon "NE 51" connected across the plate resistor of tube 5, must be reset manually before another count can be made.

The control pulses are applied directly to the grids of tubes 8 and 9. The output of each of these stages is coupled via a crystal diode to the control grid of tubes 10 and 11, respectively. Input number three is connected through a small condenser to the plate of tube 9. Tubes 10 and 11 form a rather special type of trigger circuit which is a variation of the Eccles-Jordan type in which the feedback is from screen grid to

control grid instead of from plate to control grid. The suppressor grid of tube 3 is connected to the plate of either tube 10 or 11. By using the screen grid as a signal electrode in this manner the effect of the capacitance to ground of the channel switch and the suppressor grid of the gate tube on the operation of the trigger pair is minimized.

If the suppressor grid of the gate tube is connected to the plate of tube 10, the "start" control pulse must be applied through Channel 2 and the "stop" control pulse must be applied through Channel 1. If the suppressor grid is connected to the plate of tube 11, the "start" control pulse must be applied through Channel 1 and the "stop" control pulse must be applied through either Channel 2 or 3. Channel 3 is used only when we stop on a signal from the photographic spark. This switching serves a useful purpose in that it allows us to interchange the entire start and stop systems, including photocells. Thus we can easily check the identity of our systems. We can, therefore, assure ourselves that the only systematic errors which can occur in our time measurements have their source in the gate stage, the counter, or in our megacycle pulse source. These last two can be checked independently. The maximum systematic error which can be introduced by the gate tube itself is of the order of one microsecond. There is, of course, a random error of plus or minus one microsecond, since this instrument measures in integer microseconds.

The "channel reset switches" are used to reset tubes 10 and 11 and are useful for test purposes.

4. Pulse Source and Counter

For the source of one-megacycle pulses and for the scaler we employ stages of an RCA Time Interval Counter (WF-99-B). The characteristics

of the gate circuit included in this equipment are such that we cannot use it in our measurements. The operation of the counter is not entirely satisfactory, and we are at present constructing a counter of our own design to replace it. The counter under construction consists of nine Higinbotham[1] scales of two stages preceded by four pentode scales of two stages, a total of thirteen, which will allow a registered maximum count of 8191.

5. Delay Circuit

A circuit diagram of the delay circuit is included as Figure 23 of this report. Tubes 1 and 2 form a trigger pair whose sole function is to provide a strong and reproducible negative pulse to the actual delay stage. The delay stage is a single-shot multivibrator circuit composed of tubes 3 and 4. When a negative pulse is applied to the input a rectangular negative pulse is formed at the plate of tube 4. The width of this pulse is determined by the time constant of the coupling circuit between this plate and the grid of tube 3. This pulse is differentiated and applied to the grid of tube 5, a thyratron normally biased below cutoff. Thus the thyratron is fired at the trailing edge of the pulse and provides a low impedance path to ground for the positive terminal of the 18-microfarad capacitor connected in series with the output terminal of the delay circuit.

The start and stop outputs and the jack to the external spark control which appear in the circuit diagram are used for test purposes. The reset switch is used to reset the trigger pair formed by tubes 1 and 2 so that tube 1 is conducting and tube 2 is cut off.

---

[1]Higinbotham, W. A., Gallagher, J. and Sands, M., "Model 200 Pulse Counter," Review of Scientific Instruments, 18, 706-714 (1947).

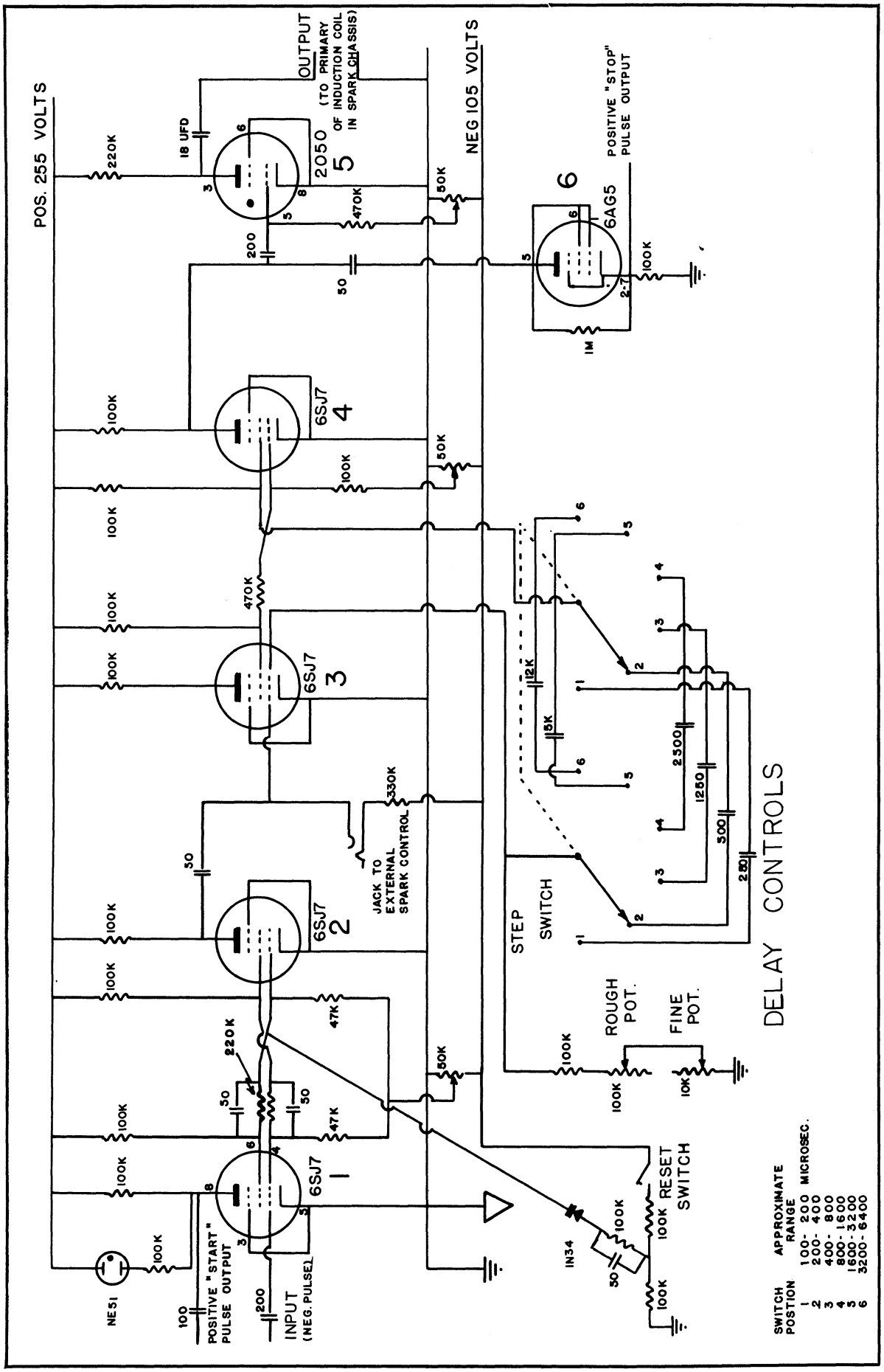

Figure 23

The Delay Circuit

The delay introduced by this circuit varies from 100 to 6000 microseconds and can be reproduced to within one microsecond at the lower limit and to within five microseconds at the upper limit.

6. The Spark Unit

A sketch of the three-electrode air spark gap which provides illumination for photography is included as Figure 24 of this report. The cathode of the gap is merely a tungsten-tipped bolt and the anode is a 3/32-inch sheet of aluminum drilled with an 0.040-inch hole. This hole is slightly enlarged on the side of the anode facing the cathode in order that the system will emit a wide enough cone of light to fill completely the collimating lens. A block of mycalex, drilled out as indicated in the figure, is mounted between the cathode and anode. A number 60 drill hole is cut into the mycalex block in such a manner that it intercepts the anode-cathode hole at right angles at a point midway between the anode and cathode. The "tickler" or third electrode, a piece of ordinary hookup wire, is inserted into this whole and coupled via a 100-kilo-ohm damping resistor to the secondary of an automobile ignition coil.

The choice of operating voltage of the main gap determines the dimensions of the mycalex block. Note in the figure that the block is drilled out to admit the cathode. The depth of this cut should be such that the voltage normally used is about 80 percent of the breakdown voltage of the main gap. The third electrode is adjusted for maximum reproducibility of the spark delay. Poor adjustment of this electrode or the use of an improperly low voltage with a given mycalex block will cause erratic additional delays as large as 100 microseconds, apparently due to

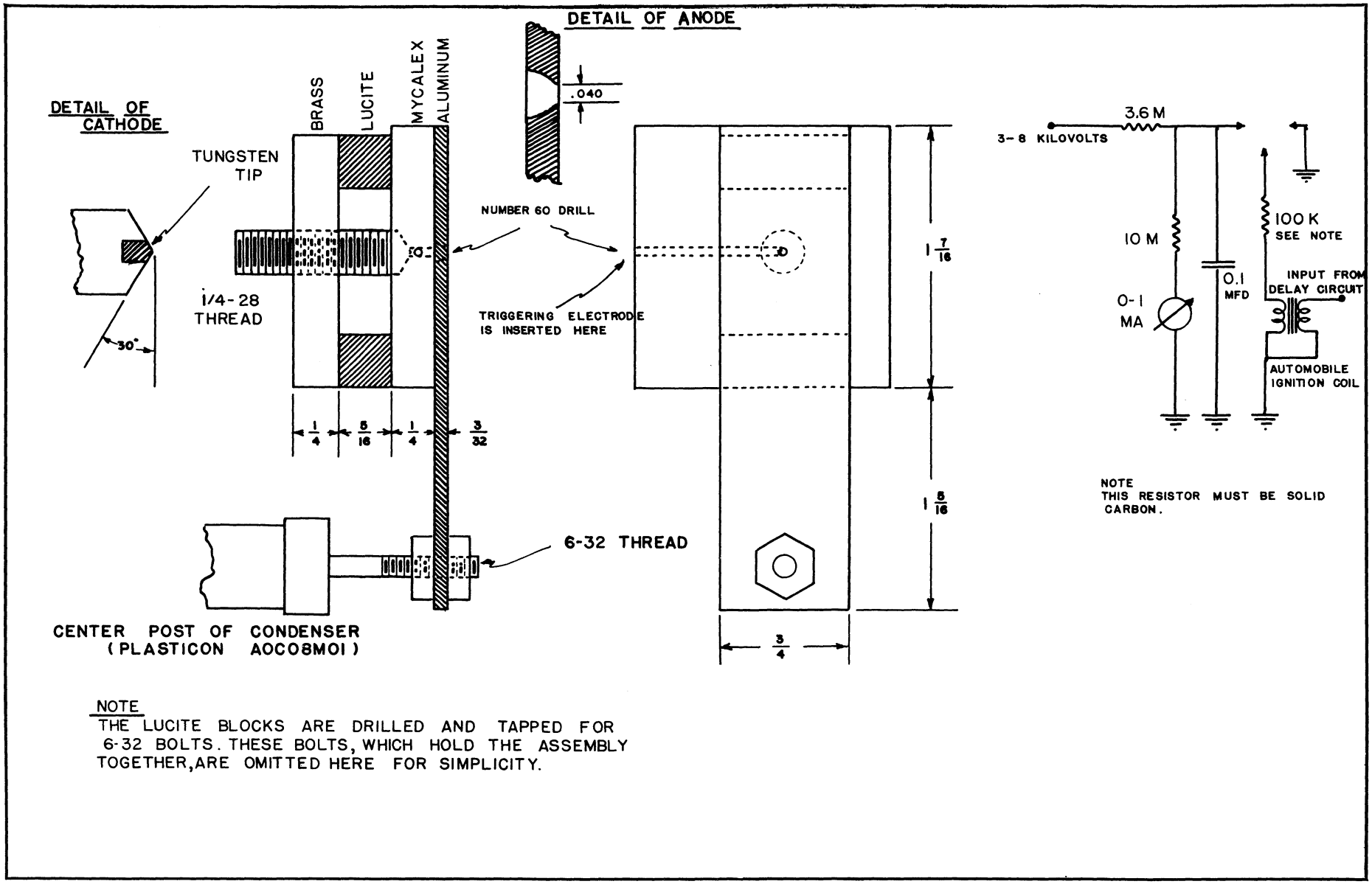

Figure 24

The Spark Gap

ion mobility effects.

The duration and intensity of the spark are determined by the capacitance of the condenser and the voltage to which it is charged. The apparatus described, operating at 4000 volts across an 0.1-microfarad condenser, causes a spark of an effective duration of approximately 0.2 microseconds and sufficient intensity appreciably to darken a 5 x 7 Eastman Process plate when used with an f/2.5 optical system. The duration of the spark was estimated by studying the detail present in photographs of shock waves of known velocities of the order of one millimeter per microsecond.

CHAPTER IV

THE FLOW IN THE SHOCK TUBE

This chapter is concerned with a comparison of the observed flow in the shock tube with that calculated from the theory of the ideal shock tube of Chapter I. Discrepancies between the two are examined with a view to determining the relative importance of effects which cause the tube flow to be non-ideal. The discussion is divided into four parts:

1) The shock strength as calculated from the shock speed is compared with the value as calculated from the initial pressures in the tube.

2) The uniformity (in time) of supersonic flow in air at the test section, both ahead of and behind the contact surface, is investigated. This investigation involves photographing flow patterns produced by a 5-degree wedge and calculating the "apparent flow Mach number" from the angles formed by shock waves attached to the wedge. This Mach number is checked against that calculated from the shock speed. From the results, the time duration of substantially uniform flow is obtained for the air ahead of the contact surface.

3) The time of arrival of the contact surface at the test section is compared with the time at which it would arrive there if the flow

were ideal and with the time the supersonic flow ahead of the contact surface ceases to be uniform. From the latter comparison conclusions are drawn regarding the uniformity of the flow at lower Mach numbers.

4) Finally, shadowgrams taken near the diaphragm show the formation of the primary shock wave and lead to an explanation of some of the results discussed in the previous parts of the chapter.

1. The Initial Pressure Ratio Versus the Pressure Ratio Across the Shock

In using the shock tube, the initial pressures are measured directly, and the pressure ratio across the shock, ξ , is inferred from a measurement of T, the time of transit of the shock between the two light screens:

$$T = \frac{\text{distance between light screens}}{\text{shock speed}} = \frac{405}{a_o\sqrt{\frac{6+\xi}{7\xi}}} = \frac{405}{0.3455}\sqrt{\frac{7\xi}{6+\xi}} \quad (34)$$

for air. This relation is plotted in Figure 25, along with the relation giving the corresponding Mach number. From such a curve the value of T can be determined for any value of ξ , and vice versa.

Equations (20) and (21) give the theoretical relationships between the initial pressure ratio and ξ for air-air and helium-air respectively. For the ranges of ξ for which each has been used, these relationships are plotted in Figures 26 and 27, along with experimentally determined points. There is some scatter in the experimental points, which are somewhat below the theoretical curves. The scatter is partially due to the fact that a_o is dependent on room temperature and on humidity, while

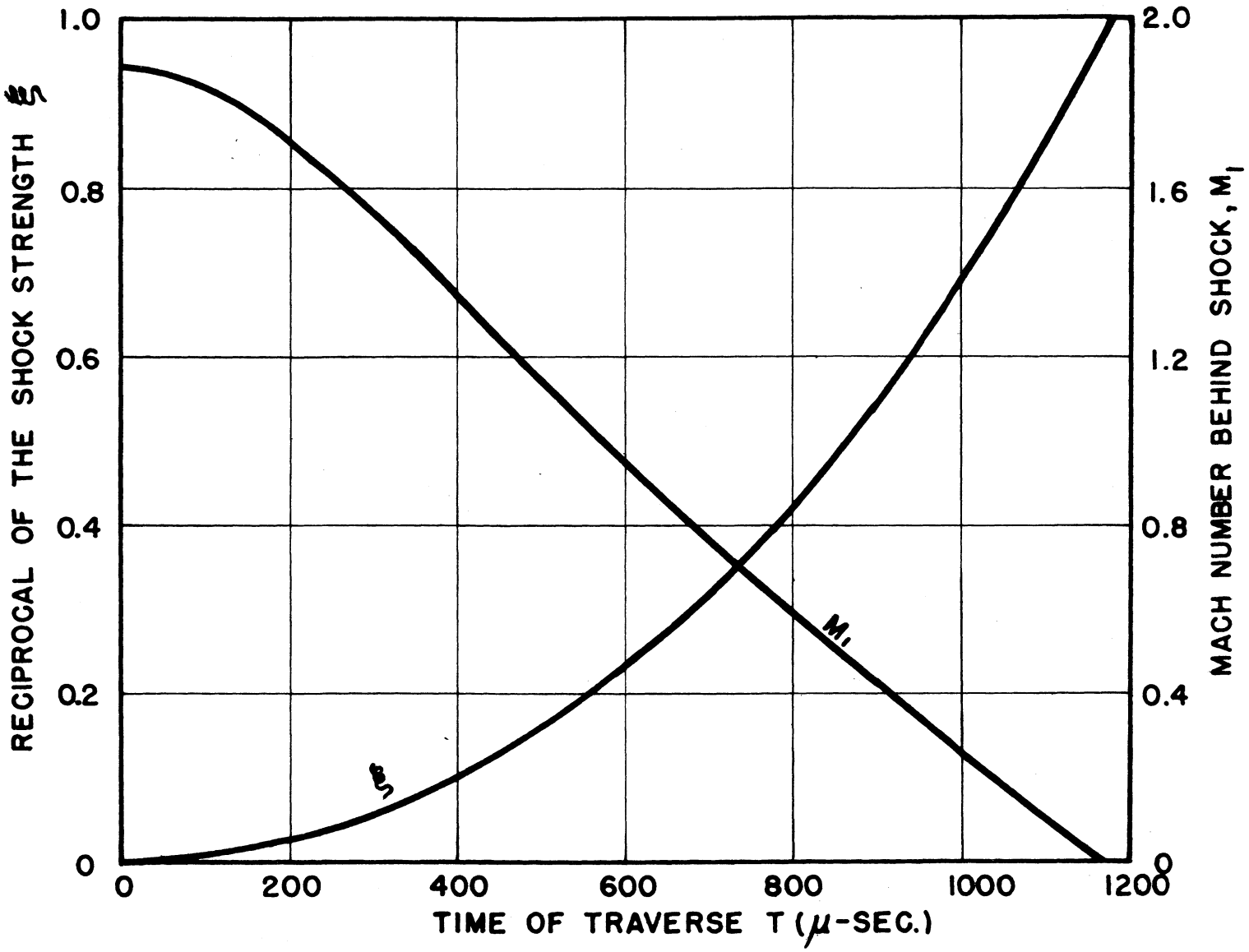

THE RELATIONS BETWEEN M_1, ξ, AND T

Figure 25

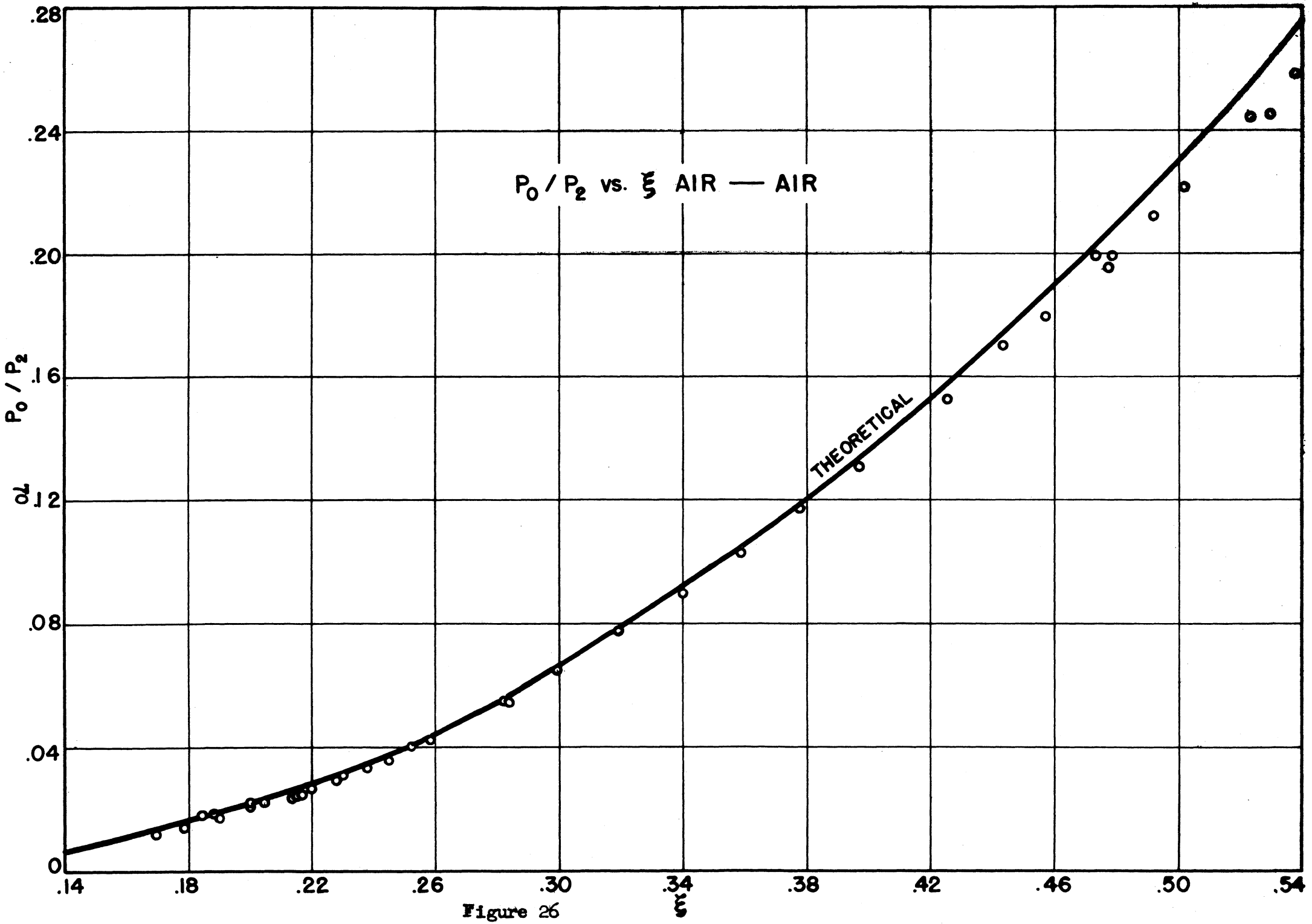
P_0 / P_2 vs. ξ AIR — AIR
THEORETICAL
P_0 / P_2
ξ
.28
.24
.20
.16
.12
.08
.04
0
.14
.18
.22
.26
.30
.34
.38
.42
.46
.50
.54

Figure 26

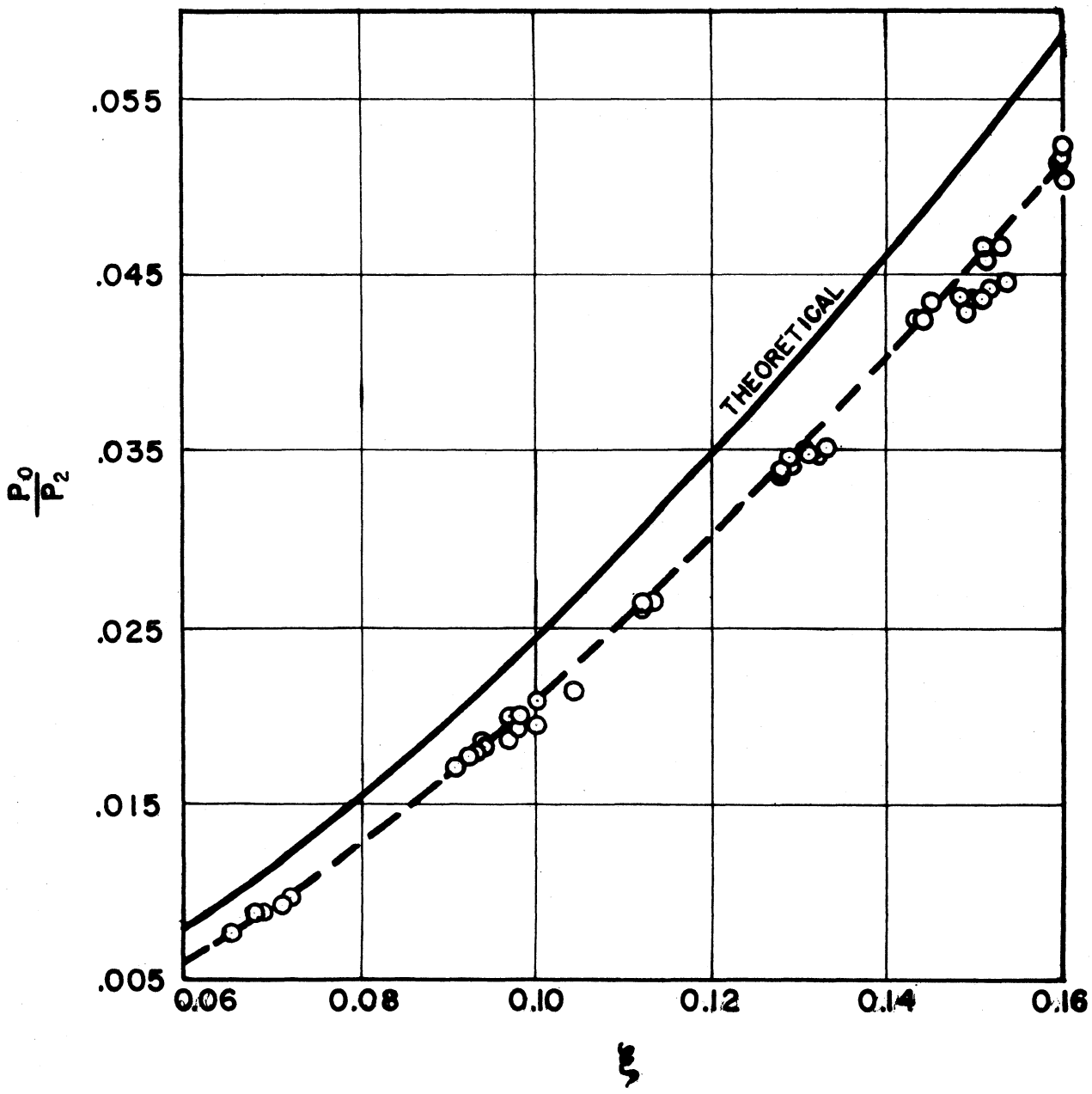

$\frac{P_0}{P_2}$ VS. ξ FOR HELIUM AIR

Figure 27

in the calculations a_o has been treated as a constant. Because the experiments described in this report were carried out during the cool part of the year, when the temperature of the room was thermostatically controlled at very near 68° F., as assumed in the calculations, temperature fluctuations introduced no serious errors.

The magnitude of the error involved is easily computable. It is desired to find the variation of ξ with temperature, θ, at constant shock speed, U. This is found by differentiating Equation (5) of Appendix III, taking into account the temperature dependence of a_o. The result is

$$\left(\frac{\partial \xi}{\partial \theta}\right)_U = \frac{\xi}{\theta} \cdot \frac{6+\xi}{6}$$

According to this equation, a one-percent change in room temperature, 3° C., from that for which the curves were plotted would cause approximately a one-percent change in the value of ξ calculated.

Some of the scatter in the air-air points is undoubtedly caused by a lack of initial temperature equilibrium. After the points had been obtained, a study was made of the temperature distribution in the compression and expansion chambers just before firing. A thermocouple was placed at one point in the expansion chamber (near the far end) and at various points in the compression chamber, and the temperatures were determined using a potentiometer. In the expansion chamber the temperature was substantially room temperature, even during evacuation. On the other hand, when the compression chamber had been brought to atmospheric pressure by admitting air, preparatory to firing, its temperature at all points checked

was higher than room temperature. In fact, in certain places it was as much as 30° C. higher than room temperature. After twenty seconds had elapsed, temperature equilibrium had been established, for practical purposes. A check on the time T, using one value of p_o/p_2, revealed that the difference between firing immediately and waiting twenty seconds could easily amount to four microseconds in that measurement, but that waiting beyond twenty seconds did not further affect the value of T. No such effect was observed when helium was used, so that no waiting period was necessary.

A small source of scatter is due to the error inherent in the timing system. However, a one-microsecond error in T, when converted to an error in ξ , results in an almost undetectable shift of the experimental points.

The helium-air curve will be affected by impurities in the helium used. These may change both the sound velocity and the specific heat ratio. The exact composition of the "helium" used is not known, so that a calculation of the magnitude of this effect cannot be carried out. However, 1/3 mm. (mercury) of air pressure was in the compression chamber when the helium was added. The effect on the curve of this small amount of air was calculated to change the values of p_o/p_2 by at the most 10^{-4} over the range of the curve. This is negligible. Also, the use of slightly incorrect values of the sound velocity and of the specific heat ratio of helium could be expected to have small effects on the curve.

Both the curves and the experimental points would be slightly affected by the use of incorrect values of the sound velocity and specific heat ratio of air.

There is an obvious reason why the experimental points should be below the theoretical curve: The energy required to rip the diaphragm, to tear pieces of it loose, and to accelerate these pieces must come from the flow behind the contact surface. (Pieces of the diaphragm are always found at the far end of the expansion chamber after firing.) Therefore, the compression chamber gas cannot act as a perfect piston, which is believed to be the largest of the factors which contribute to this difference between theory and experiment.

2. The Flow Calibration

If the tube flow is to be used for aerodynamic investigations, it is of prime importance that the Mach number of the flow at the test section be substantially constant for a sufficient length of time. This constancy determines, to a large extent, the usefulness of the flow. It was the fact that the theory of ideal shock tube predicts constant flow both ahead of, and behind, the contact surface which led to the expectation that the shock tube could be used in studying aerodynamic phenomena. The following describes an investigation of the constancy with time of the supersonic flow in the tube.

a. The Method: The only photographic technique which has been employed in experimentation has been the shadowgraph technique. This automatically imposed a restriction on any attempt at flow calibration. Indeed, the only means of determining the Mach number, using this technique, appeared to be through the measurement of the angled formed by the shock waves attached to a wedge in supersonic flow. If interferometry had been available, the examination of the flow uniformity could have been much more accurate and could have been extended to all flow Mach numbers.

The Mach number calculated from the attached shock wave angle will be called the apparent Mach number, M_{ap}, for two reasons. In the first place, non-viscous flow is assumed in the calculation. The existence of a boundary layer on the wedge effectively alters the wedge angle. The amount of such alteration is, in the shock tube, a function of time. Secondly, the relation to be used applies strictly only for steady flow; and the attempt here is to use it in investigating unsteadiness in the flow. In order to observe early the effects of unsteadiness, measurements of the angles were made as close to the leading edge of the wedge as possible.

The value of the Mach number may be deduced from the shock speed also, and this will be referred to as the predicted Mach number, M_p.

If a wedge of half-angle θ is placed in the flow, the apparent Mach number is given, for steady flow, by[1]

$$\frac{1}{M_{ap}^2} = \sin^2\beta - \frac{\gamma+1}{2}\,\frac{\sin\beta\,\sin\theta}{\cos(\beta-\theta)} \qquad (35)$$

where β is the inclination of the bow-wave to the direction of the flow as indicated in Figure 28. The wedge used in the determination of M_{ap} was accurately ground to a total angle of 5 degrees. For this wedge and with the assumption that $\gamma = 1.400$ for air, Equation (35) can be written

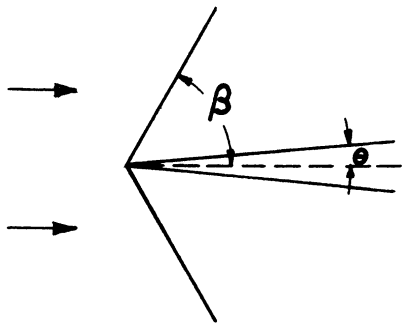

Figure 28
Shock Wave Attached to a Wedge

[1]See, e.g., Liepmann, H. W. and Puckett, A. E., Introduction to Aerodynamics of a Compressible Fluid, Wiley, New York (1947), Article 4.5

$$M_{ap} = \left[\sin^2\beta - 0.05234 \frac{\sin\beta}{\cos(\beta - 2.5°)} \right]^{-\frac{1}{2}} .$$

This equation was plotted and the graph was used in analyzing the data.

In order to obtain the shock wave angle as a function of time, it was necessary to fire the tube repeatedly, endeavoring to make all the shocks in each run of equal strength. The spark delay was varied from shot to shot, the resulting shadowgrams being equivalent to a high-speed motion picture of a single shock wave, with somewhat irruglarly spaced frames.

The experiment served a second purpose. The apparent Mach number was checked against the value of the Mach number, M_p, which would be predicted from the measured value of T. The relation between T and ξ has already been given as Equation (34). That between M_p and ξ , for the flow ahead of the contact surface, is Equation (6)

$$M_p = \frac{5}{\sqrt{T}} \cdot \frac{1-\xi}{\sqrt{1+6\xi}} .$$

This is the second curve plotted in Figure 25. From the curves one can find the value of T corresponding to M_p, or vice versa. On setting p_o to a value such that the measured value of T was that on such a graph corresponding to the desired Mach number, a series of shadowgrams could be made in which only the time delay was varied. For this investigation the value of M_p was varied in steps of 0.05 from 1.15 to 1.50.

Because the relation between T and ξ , (34), is dependent on a_o and therefore on room temperature, the relation between M_p and T is also dependent on room temperature. Again the error involved is not serious for these experiments. Its magnitude is easily computable. It is desired to find $\left(\frac{\partial M_p}{\partial \theta}\right)_U$. Now

$$\left(\frac{\partial M_p}{\partial \theta}\right)_U = \frac{dM_p}{d\xi} \cdot \left(\frac{\partial \xi}{\partial \theta}\right)_U$$

$\frac{dM_p}{d\xi}$ is found by differentiating Equation (6). It is

$$\frac{dM_p}{d\xi} = -\frac{M_p}{1-\xi} \cdot \frac{3\xi+4}{1+6\xi} \tag{36}$$

so that

$$\left(\frac{\partial M_p}{\partial \theta}\right)_U = -\frac{\xi}{1-\xi} \cdot \frac{6+\xi}{1+6\xi} \cdot \frac{3\xi+4}{6} \cdot \frac{M_p}{\theta} \tag{37}$$

The errors in Mach number, computed from (37), for certain values of ξ (or of M_p) corresponding to a temperature error of 10° C. are given below.

Mach Number Error Corresponding to a Temperature Change of 10° C.

ξ	M	$\frac{d \ln M}{d \ln \theta}$	ΔM
0.5	0.47	-1.49	-0.023
0.3	0.79	-0.788	-0.0205
0.2	1.01	-0.54	-0.018
0.1	1.33	-0.304	-0.014
0.05	1.57	-0.169	-0.009

From these it is evident that a temperature error of 2 to 3° C. would be insignificant except at low Mach numbers.

The correction to be applied to the values of T to allow for room temperature variations is as easily computable. One must now find $\frac{\partial T}{\partial \Theta}$ Differentiating Equation (34), taking into account the temperature dependence of a_o, one obtains

$$\left(\frac{\partial T}{\partial \Theta}\right)_{\xi} = -\frac{1}{2} \cdot \frac{T}{\Theta}$$

so that at constant M_p (constant ξ) the changes in T and Θ are related by

$$\frac{dT}{T} = -\frac{d\Theta}{2\Theta}$$

The Mach number may be in error also because of the effects of variation of the humidity on the values of a_o and γ . It was found by calculation that an error in γ of 0.005 would correspond to a maximum Mach number error of 0.009 and that an error in a_o of 0.5 percent would result in Mach number errors less than that. The errors which can be expected to arise from the small variations of the absolute humidity indoors during the winter are well within this limit.

b. Measurement of the Shock Wave Angle: The angle formed by the attached shock wave, 2β , was measured directly from the photographic plates. This measurement was very difficult when the Mach number was low, for then the shocks were very ragged, often curved, and sometimes double. The method

adopted in measuring these was to take the smallest value of 2β for which there was a definite indication. This was done because the non-uniformity in the sharpness of the wedge could cause such an effect and the smaller angle would probably be closer to the correct one. The measurements are given to the nearest half-degree in all cases, but for Mach numbers 1.15 and 1.20 the probable error in the measurement of 2β may not warrant this. For Mach numbers 1.25 and above, the ease in measurement becomes progressively greater.

The error in M_{ap} introduced by an error of one-half degree in the measurement of 2β varies with the Mach number. The magnitudes of the errors, measured from the slope of a graph of M_{ap} vs. β , are:

M_{ap}	1.15	1.20	1.25	1.30	1.35	1.40	1.45	1.50
ΔM_{ap}	0.001	0.002	0.003	0.004	0.005	0.005	0.006	0.007

The theoretical value of the Mach number at which the shock wave just detaches from a 5-degree wedge is 1.143. Since the shape of the wave near the vertex of the wedge is markedly changed when the wave becomes detached, it is not surprising that the wave would respond sharply to small irregularities in both the Mach number of the flow and the sharpness of the wedge at Mach number 1.15.

c. The Wedge: The first 5-degree wedge was made of mild steel, and it was observed that its leading edge deteriorated badly, presumably from the buffeting it received from the cellophane particles, which are driven along the tube at high speed, following the contact surface. Another was made of hardened tool steel, this time with a very fine edge similar to that on a cold chisel; i.e., the wedge angle was greater than

5 degrees for a distance of about 0.005 inch from the edge. This edge held up well.

Both of these wedges were about 1/4 inch thick. When it became desirable to have a 1/8-inch thick wedge with a 5-degree angle, it was made of hardened tool steel, but with the 5-degree angle continued to the edge, as nearly as could be done with standard equipment. In spite of the hardening, this edge became very rough with use. It was then lightly ground to a fine cold-chisel edge on an oilstone, and in this form it was used for the entire set of measurements. The edge had to be reground on two occasions.

d. Determination of Predicted Mach Number: The pressure in the compression chamber was set at atmospheric pressure, and consequently was constant throughout any given run. With the gate circuit set to time the passage of the tube shock past the light screens, the pressure in the expansion chamber was varied until the value of T corresponding to a desired Mach number was obtained repeatedly. The times, T, corresponding to the Mach number used are:

M_p	1.15	1.20	1.25	1.30	1.35	1.40	1.45	1.50
T(μs)	493	467	443	417	393	368	344	319

When the value of p_o had been determined, the gate circuit was switched to measure the spark delay, and a schedule of shots was fired in which p_o was set at the required value, with one shadowgram taken for each shot. At the conclusion of each of several of these runs, a shot was fired with the gate circuit switched back to time the primary shock, as a check on the value of T. In all cases T was found to be within 2 microseconds of the proper value, which corresponds to a maximum Mach number error

of 0.004.

e. Determination of τ: It remains to discuss the method of determining the time, τ, which elapses between the arrival of the shock at the leading edge of the model and the exposure of a given plate. The timer registers a value, say A, which is the time elapsed between the arrival of the shock wave at the second light screen and the exposure of the plate. If a plate could be exposed which would catch the shock just as it reached the leading edge of the model, then the time, say B, which was registered by the timer for this exposure would establish the zero from which all subsequent values of τ would be taken in that run; i.e., τ = A - B. In practice, B was determined from a plate in which the shock wave was visible, but not necessarily touching the edge of the model. The distance, d, between the shock front and the edge of the model was measured (as positive if the wave had passed the edge of the model); and B was determined from d, A(the reading of the timer for this exposure), and from the known speed of the shock wave, U: B = A - d/U.

f. Flow in the Hot Air Ahead of the Contact Surface: For air-air the calibration of the flow ahead of the contact surface was attempted only for M_p = 1.15. At lower Mach numbers the shock wave would have been detached, and the timing system would not operate for appreciably higher Mach numbers. For helium-air, on the other hand, the calibration was attempted in Mach number intervals of 0.05 from 1.15 to 1.50, the last being approximately the highest for which shock waves could be timed for this case. The results are given in Tables I through VIII and are plotted in Figures 29 and 30. Two graphs were plotted in order to minimize overlapping of points from adjacent values of M_p. The question marks in the tables and graphs

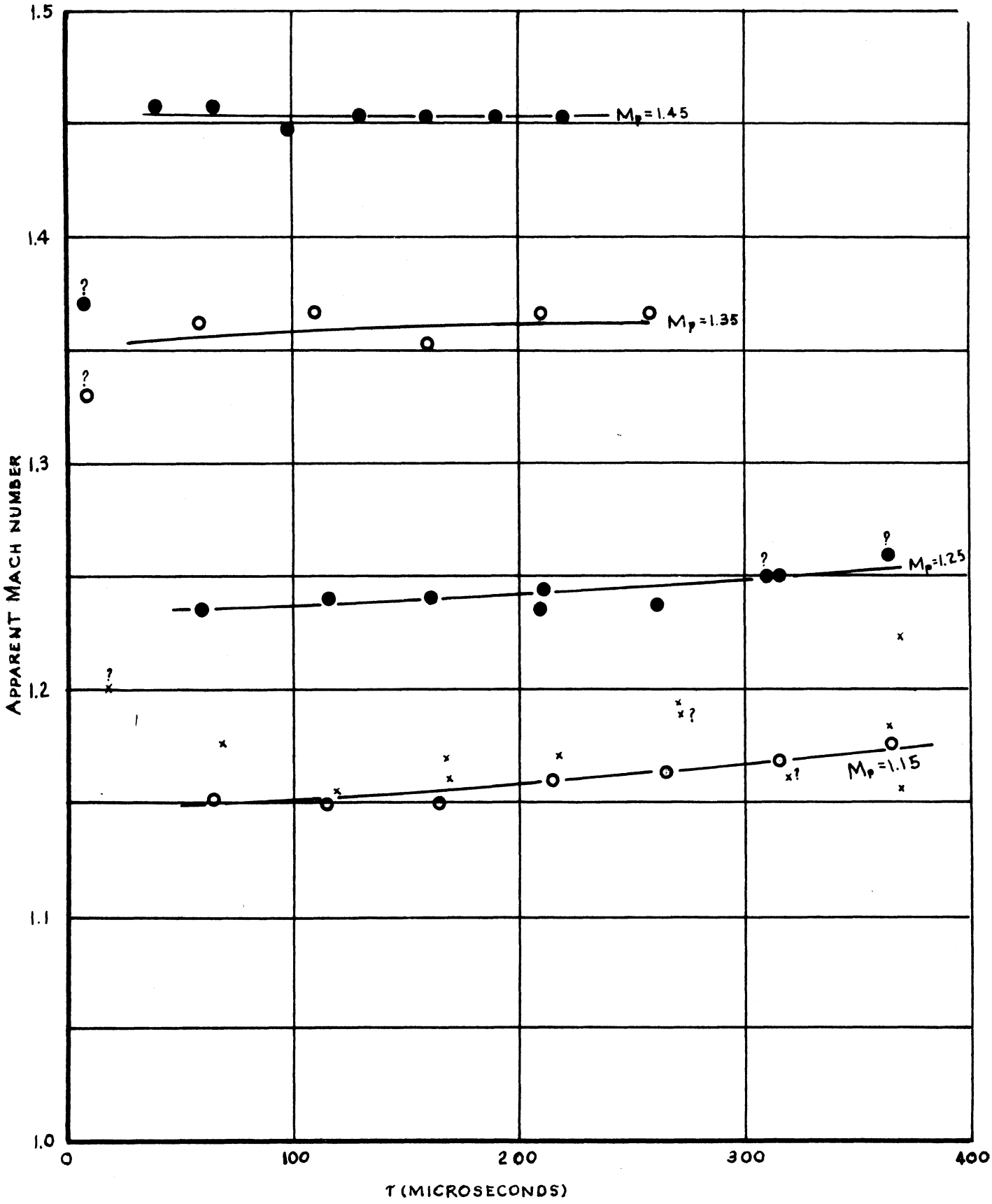

Figure 29

Variation of apparent Mach number with time.

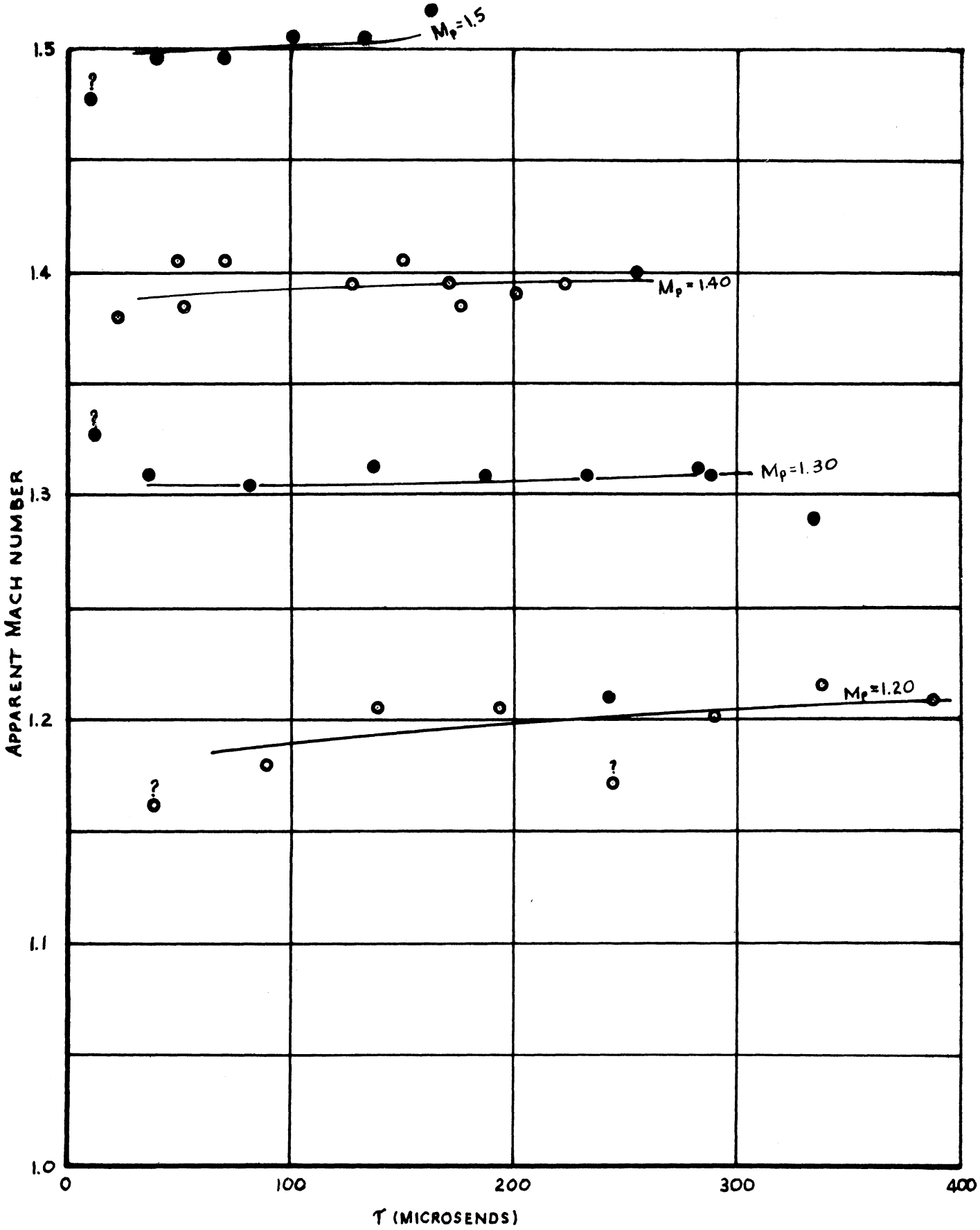

Figure 30

Variation of apparent Mach number with time.

correspond to angles which were difficult to measure.

The points marked with asterisks are those obtained with air in both chambers for $M_p = 1.15$. These data are less reliable than those for helium-air for the reason that the density of the air is lower in the former case, the changes in density produced by the shocks are also lower, and, as a result, less distinct images are produced on the photographic plates.

From the data plotted in the figures one would conclude that for helium-air the flow Mach number is constant to within limits which vary from $\pm$ 0.007 at $M_p = 1.50$ to $\pm$ 0.03 at $M_p = 1.15$, if the earliest datum of each run is ignored, and that the apparent Mach number agrees with M_p to within about the same limits. At the higher Mach number the error would be entirely explained by the accuracy with which the angles were measured. It is not believed, however, that these values of the variations of the apparent Mach number are real, but that they represent upper limits of the variations in the true Mach number.

It can be concluded with some certainty that the flow Mach number is very nearly the desired value and that the results give the time duration of uniform flow.

This duration is plotted from the experimental points in Figure 31. That the points do not lie on a smooth curve is due to the fact that in the measurements the time delays were from 30 to 50 microseconds apart. Because this flow is more uniform than that behind the contact surface, the experiments of the final chapter were performed entirely in this flow.

g. Flow in the Cold Air Behind the Contact Surface: Most of the measurements were made in the hot gas ahead of the contact surface, as just

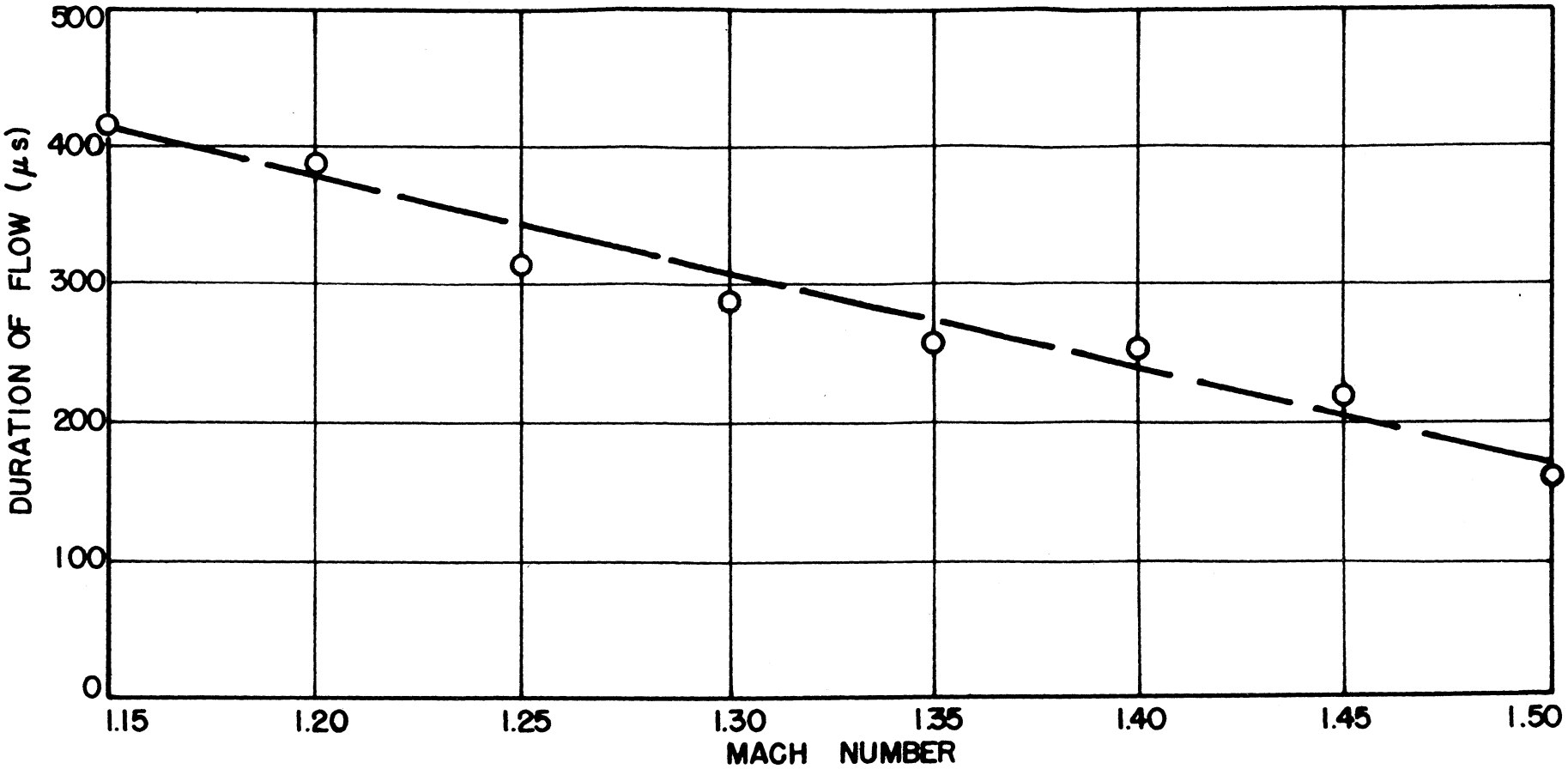

Figure 31

Experimental Duration of Uniform Flow for He-Air.

described. The conjunction with them, one series of measurements was extended into the cold flow behind the contact surface. This was an air-air flow for which the value of T corresponded to a desired Mach number, M_p = 1.15.

The theory of the ideal shock tube predicts uniform flow in the cold air which has issued from the compression chamber, corresponding to the region between points F and C in Figure 6, page 16. According to Figure 9, page 29, at ξ = 0.157, corresponding to M_p = 1.15, the duration of uniform flow between the shock wave and the contact surface should be about 0.91 milliseconds; and the duration of the uniform flow behind that surface should be about 2.04 milliseconds. The theoretical value of the Mach number in the latter flow is M_{1c} = 2.40 as obtained from Equation (V-4) of Appendix V.

A plot of the Mach number vs. time should, then, show a discontinuous rise in the Mach number from zero to 1.15 at τ = 0, then 0.91 milliseconds during which the Mach number remains constant at this value, another discontinuous rise at the end of this time to a Mach number of 2.40, and finally 2.04 milliseconds of constant flow at this Mach number. Beyond this time the Mach number should decrease smoothly as the reflected rarefaction advances into the test section.

The results of the measurements are given in Table I and are plotted in Figure 32, which shows that the results fall far short of the theoretical predictions. The continual decrease in Mach number behind the contact surface could be due to the fact that a finite time is required for the bursting of the diaphragm, with the result that the rarefaction wave extends farther forward into the flow than the theory of the ideal flow predicts.

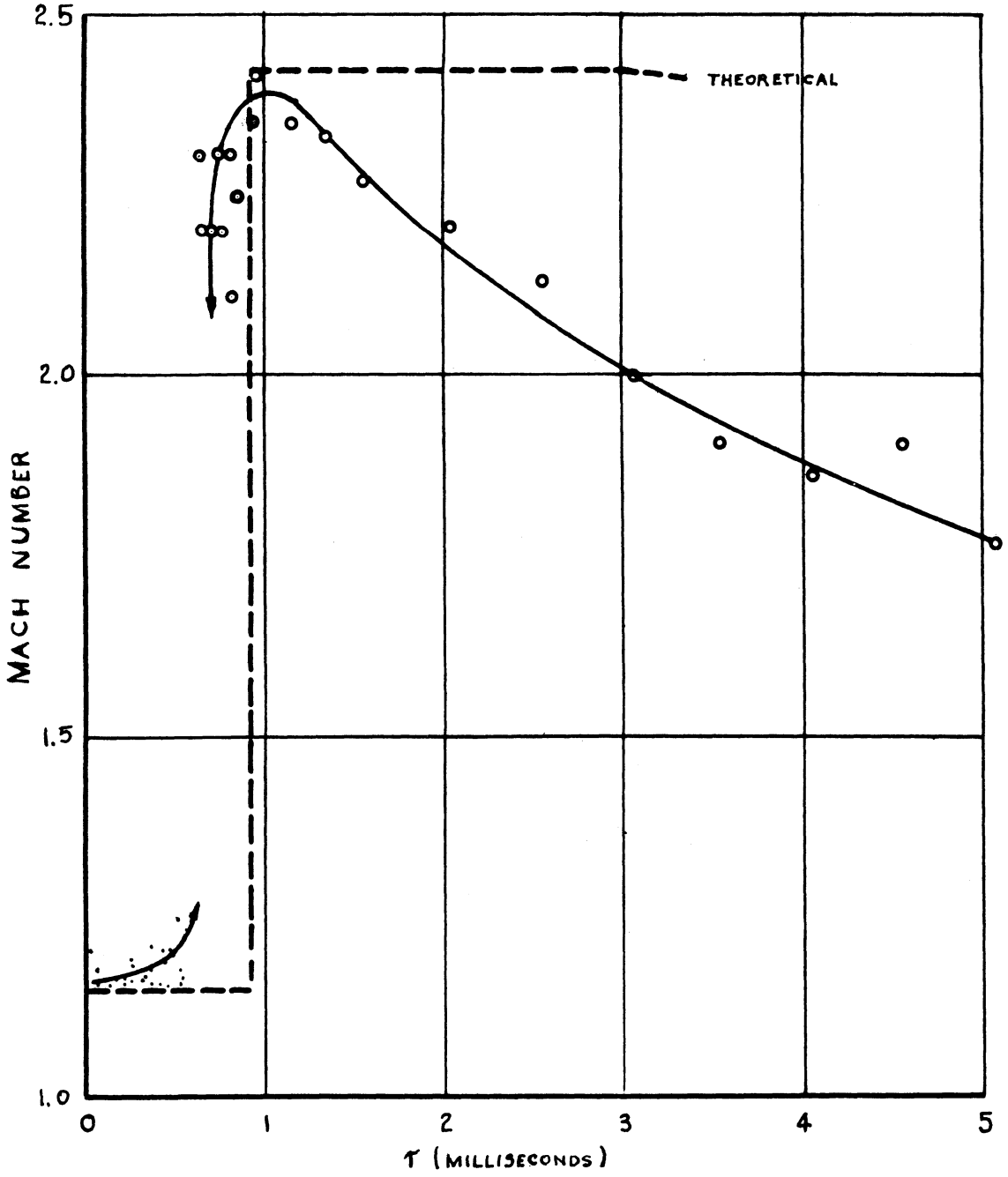

Figure 32

Mach number of the flow in the cold air.

Photographs of the bursting diaphragm, which will be described later, show the formation of a jet of the gas initially in the compression chamber, following the appearance of an opening in the diaphragm, in the initial stages of rupture. This has the effect of producing an extended mixing region instead of a contact surface and of spreading the rarefaction over this region and that following it, which in the idealized theory is one of uniform flow.

If the surmise is correct that this discrepancy is due to the finite time of rupture of the diaphragm, the flow in the cold air might be made to approach uniformity by increasing the length of the shock tube, since the rarefaction becomes less abrupt as it progresses.

Part of the discrepancy is the arrival of the contact surface earlier than predicted. This is certainly connected with the "jet effect" just mentioned, and probably also with the manner in which the shock front is formed.

3. The Relation Between the Uniformity of the Flow and the Contact Surface

According to the theory of the ideal shock tube in Chapter I, for air-air with $\xi \leqq 0.44$ and for helium-air with $\xi \leqq 0.22$ the contact surface arrives at the test section before either of the two reflections from the ends of the tube. These limiting values of ξ are higher than any at which experiments have been performed in the flow for these two cases, so that in the experiments the contact surface should always reach that section first.

The delay times which would place the contact surface at the middle of the window in ideal flow are easily determinable. These are plotted in Figure 33. Also in the figure are two sets of points corresponding to the times at which the contact surface actually arrived at the

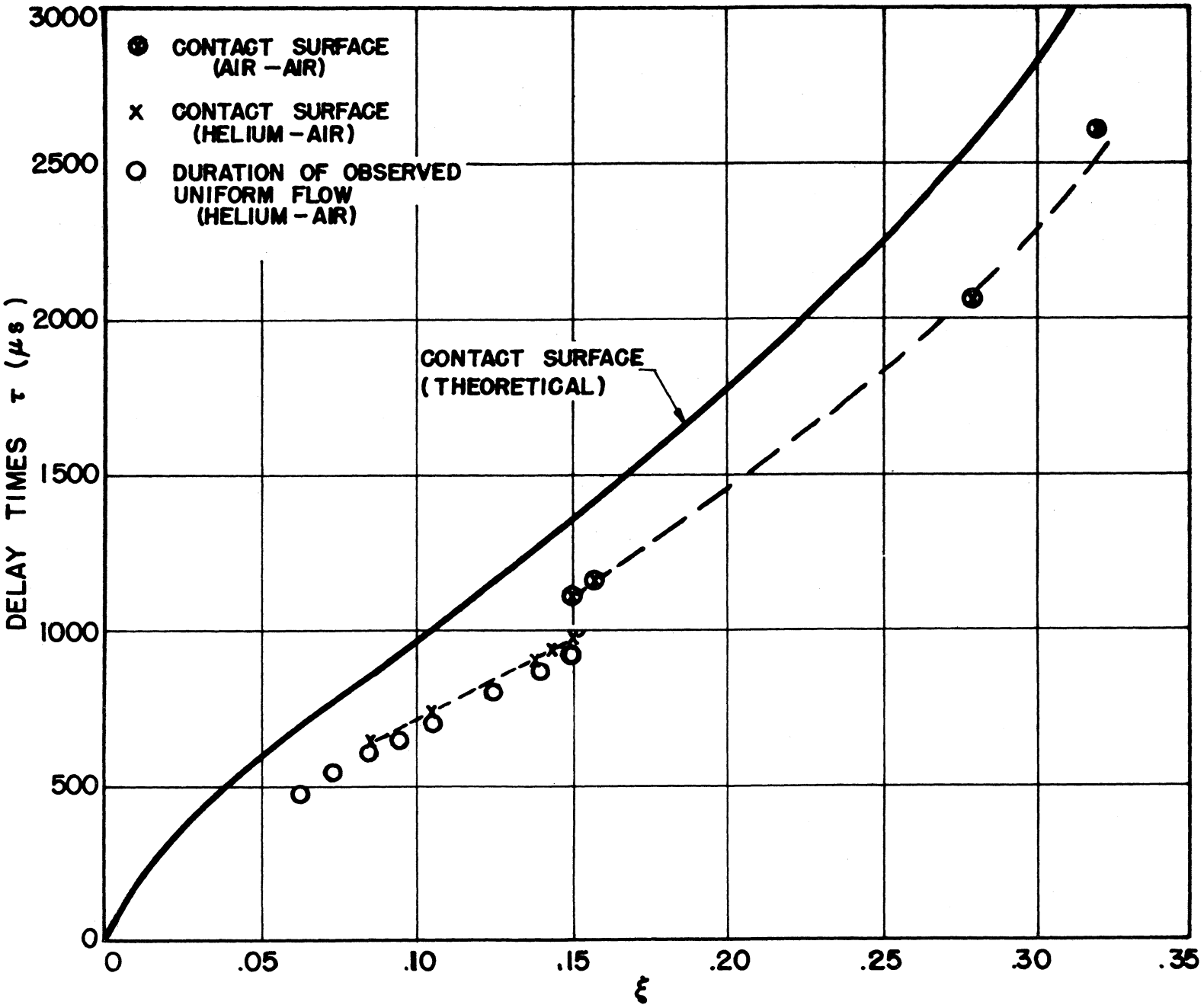

Figure 33

Arrival of Contact Surface.

middle of the test section. One set of points is for helium-air, and the other is for air-air. These points were obtained by varying the delay until the discontinuity was photographed in the window. From the velocity of the discontinuity, calculated from Equation (I-11) of Appendix I, the delays recorded for the photographs were corrected to the time at which the nose of the surface would have been at the center of the window. The third set of points has been taken from the results of the flow calibration. These points represent the latest times at which one can consider the flow to be uniform.

In all pictures the discontinuity is highly curved. The curvature, as will be shown, is largely a result of the way in which the diaphragm breaks. The facts that it is curved and that the plotted times are those of the arrival of the nose in the window mean that an average time of arrival would be later than that plotted. Unfortunately, because the tube is 7 inches high and the windows are but 5 inches in diameter, it was not possible to obtain such an average.

It is not to be expected that obtaining an average time of arrival would result in excellent agreement between theory and experiment. The values of τ for the experiments were obtained by calculation from T. If they had been obtained from p_o/p_2 by calculation, the differences would have been slightly less, although such a step would certainly not be meaningful. It would be advantageous for this comparison to measure times from the instant at which the diaphragm is ruptured.

It is of importance that the flow Mach number becomes variable before the arrival of the contact discontinuity. Nevertheless, according to the helium-air points, practically all of the time between the shock

wave and the contact surface is usable time. The flow may be uniform longer than Figure 33 indicates, because the points taken from the calibration curves are the latest at which the flow was observed to be uniform and the experimental points for the calibration were taken from 30 to 50 microseconds apart. Judging from the figure, one would estimate that somewhat less than the last 10 percent of the time between shock wave and contact surface is unusable. This is the basis on which the extrapolation to air-air and to lower Mach number flows is made. It is simply assumed arbitrarily that this percentage of the flow is not uniform for these Mach numbers as well. In the experiments of the next chapter, the last 10 percent of the flow has been avoided.

This extrapolation may be pessimistic. It is clear from the figure that the contact surface arrives at the test section at closer to the prediced time for air-air than for helium-air; and therefore the flow may be uniform for a greater percentage of the total time for that case.

4. The Bursting Diaphragm and the Formation of the Tube Shock

From photographs taken at the test section it has been observed that the shock wave is very nearly plane, that the flow is not uniform immediately in front of the contact surface, and that this surface is highly and irregularly curved. Studies of the flow in the first 12 inches ahead of the diaphragm yielded information regarding the relations between these observations.

The diaphragm itself has properties which make it admirably suited for its purpose. It withstands at least an atmosphere of pressure differential practically indefinitely without breaking spontaneously and yet is light in weight and tears very easily, once it is pierced. In spite of

these properties, the pictures show that it is relatively far from ideal.

a. Inhomogeneity of the Flow Near the Burst Diaphragm: In order to investigate the manner in which the diaphragm bursts and its effect on the uniformity of the flow, a set of shadowgrams were taken near the diaphragm position during the early stages of the formation of the shock wave. After some preliminary shadowgrams were taken in which the shock wave was unconfined by an expansion chamber, a 12-inch section with 1/2-inch plate glass walls was built and placed in the tube, taking the place of the first section of the expansion chamber. (See Figure 34.)

When the glass section is in use, it is necessary to trigger the delay circuit by means of a signal originating at the time the diaphragm bursts. Such a signal is provided by a beam of light which falls on the diaphragm before the burst and passes on, after reflection from a mirror in the expansion chamber, through a window to one of the 931-A photomultiplier tubes. (It is a convenience that the red cellophane is opaque to the blue and ultraviolet parts of the spectrum, parts to which the phototubes are most sensitive.) A window is placed in the back end of the compression chamber to admit the light beam, which is focused on the region of the diaphragm surrounding the point at which it is punctured by the plunger. The focusing is necessary to reduce fogging of the plates by the beam, not to provide high intensity in the beam. This method of starting the delay circuit was good enough to allow definite time delays to be assigned to the photographs, although these delays should not be taken as the times starting from the instant the diaphragm was pierced.

In the first series of experiments the compression chamber, which already contained air at atmospheric pressure, was filled, using helium, to

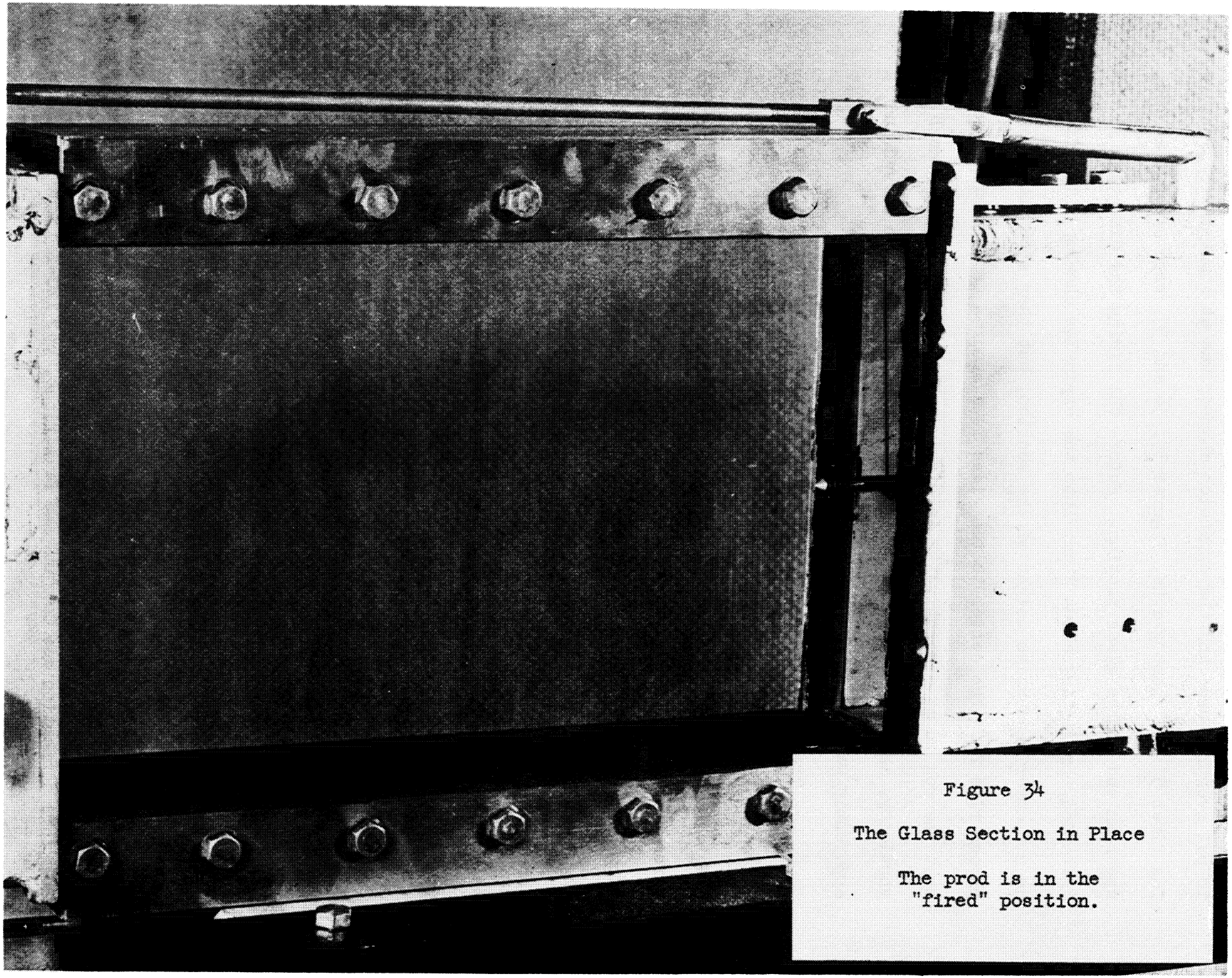

Figure 34

The Glass Section in Place

The prod is in the "fired" position.

10 psi overpressure; and the expansion chamber was at atmospheric pressure. The first 5" x 7" photographs, Figures 35, 36 and 37, were exposed at the upstream end of the glass section. Before the firing the diaphragm is distended, projecting about 2 cm. into the expansion chamber. The figures do not cover the entire height of the section, but they show that the diaphragm rips from the center to the sides in a hundred or so microseconds, that the region of discontinuity is highly turbulent and contains much vorticity, and that the shock wave (barely visible in 36) is curved and is apparently weak.

The weak appearance of the shock is only partially due to its curvature. One would expect that, for the same velocity of the forward position of the contact discontinuity, in three-dimensional flow the shock strength would be less than in one-dimensional flow. In one-dimensional flow this would be, in a sense, equivalent to a piston problem in which the piston, rather than moving initially with a constant velocity, initially has velocity zero and then accelerates. In this case the shock wave would be formed from the steepening of compression waves, and, once formed, it would increase in strength and velocity.[1]

Figures 38 and 39 show the shock farther along the tube. The plates covered the far end of the glass section. In 38 there appear to be two shock waves, and Figure 39 shows that Mach reflection has occurred at the walls and that the "heads" of the Mach shocks are very nearly normal to the walls.

The situation is ther illuminated by Figures 40 and 41, which were taken on 8" x 10" cut film. Here the film covers the entire height of

---

[1]In this connection see Courant and Friedrichs, pp. 110-115 and 171-172.

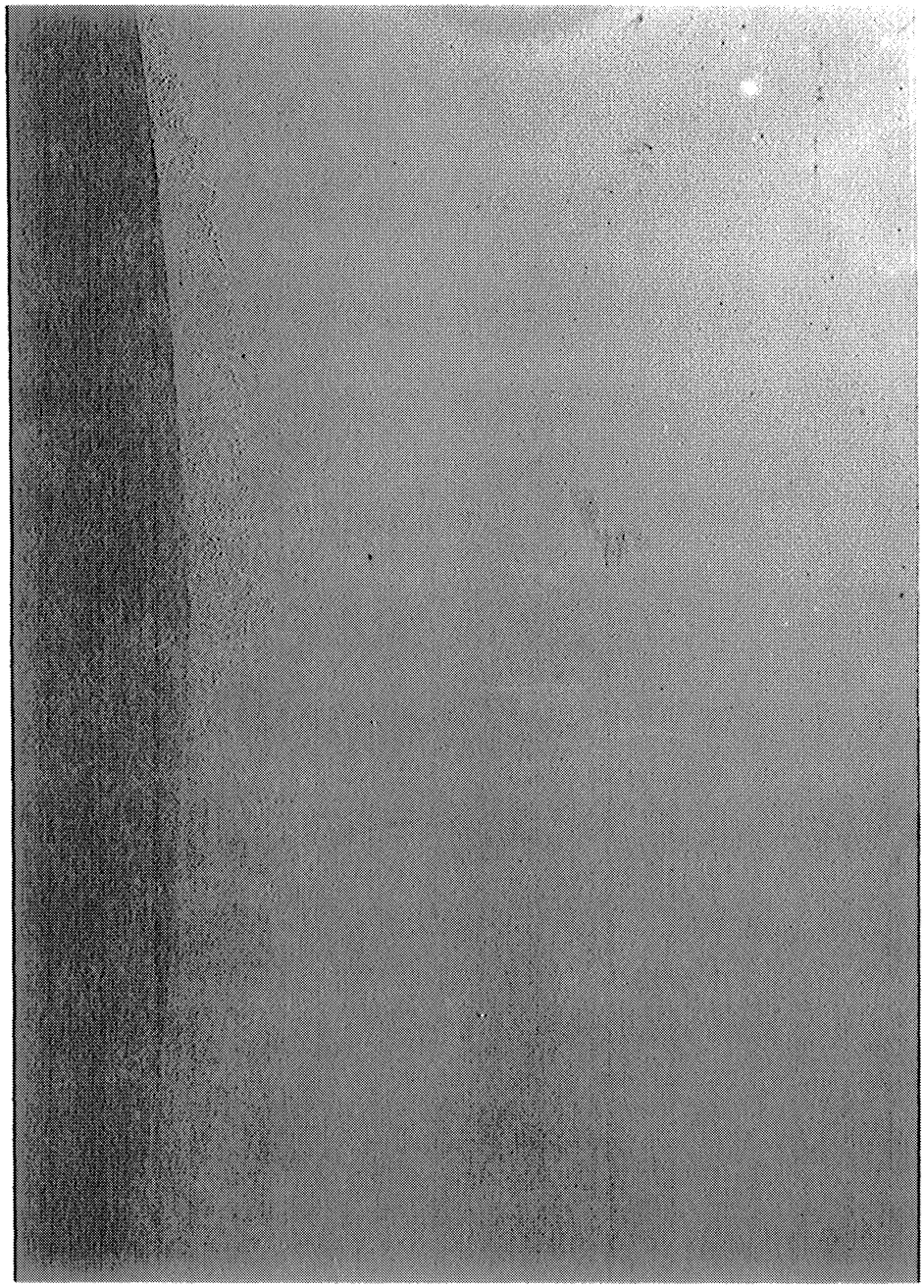

Figure 35

The Bursting Diaphragm

T = 99

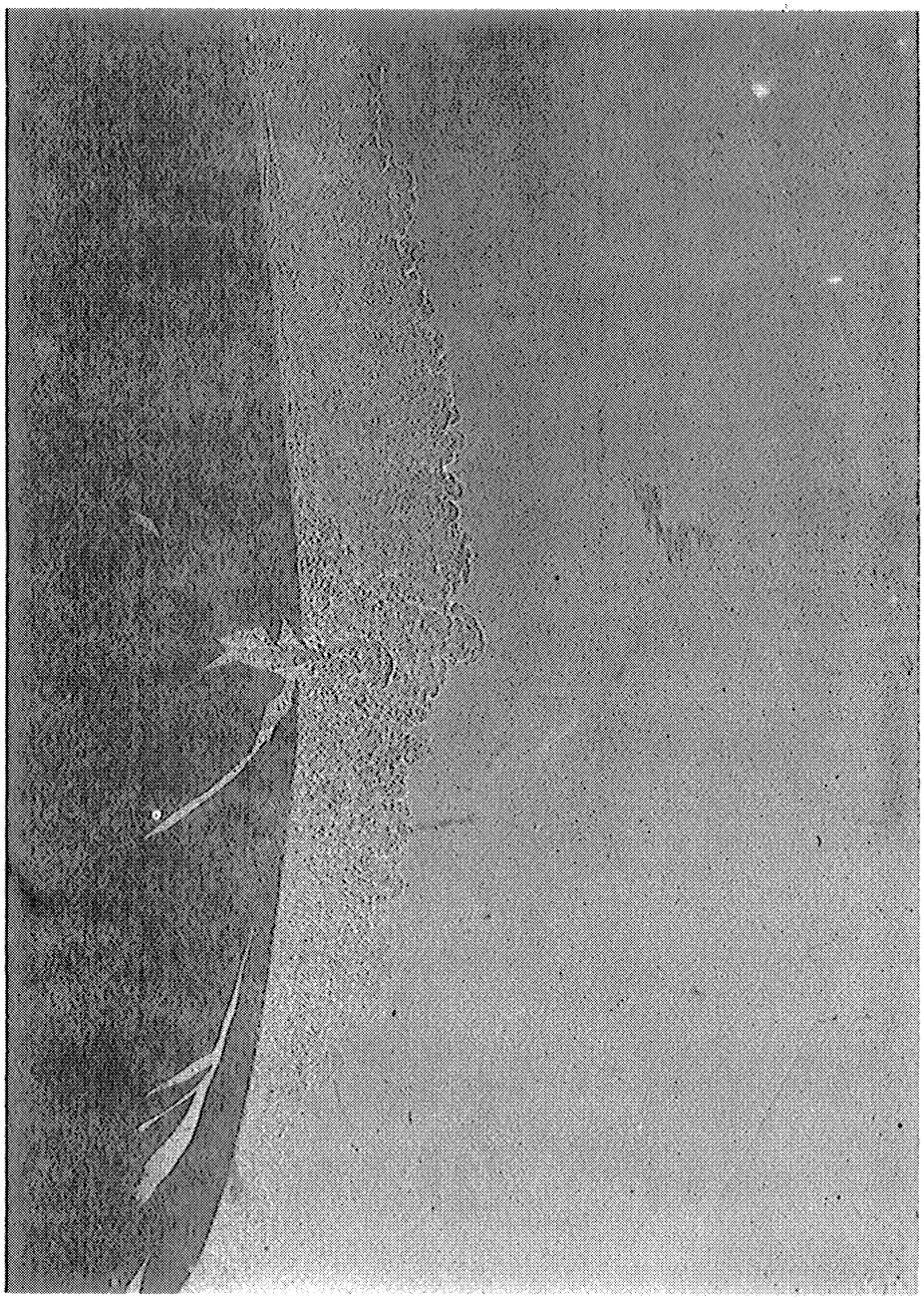

Figure 36

The Bursting Diaphragm

T = 196

Figure 37

The Bursting Diaphragm

T = 403

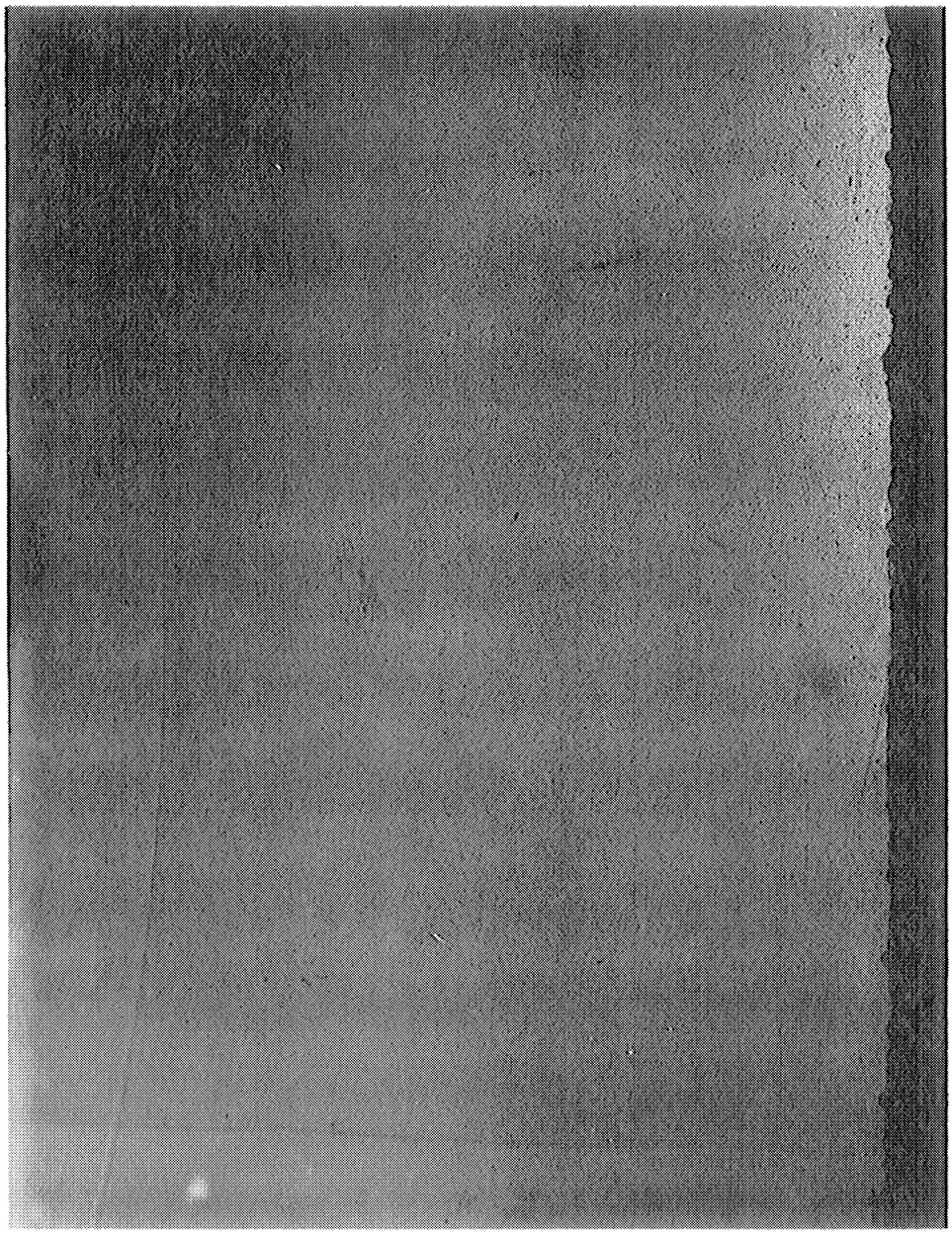

Figure 38

The Formation of the Primary Shock Wave

T = 637

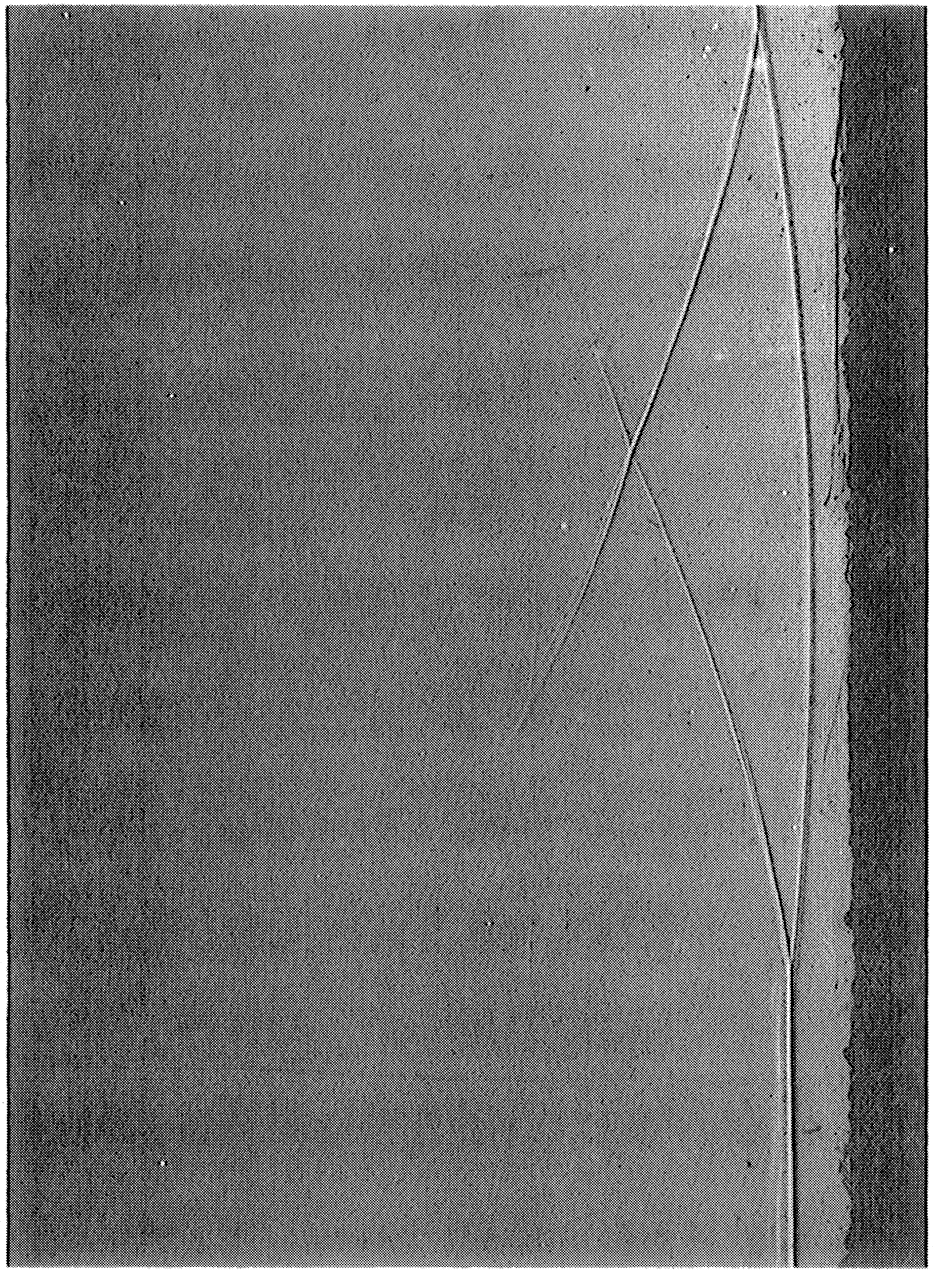

Figure 39

The Formation of the Primary Shock Wave

T = 844

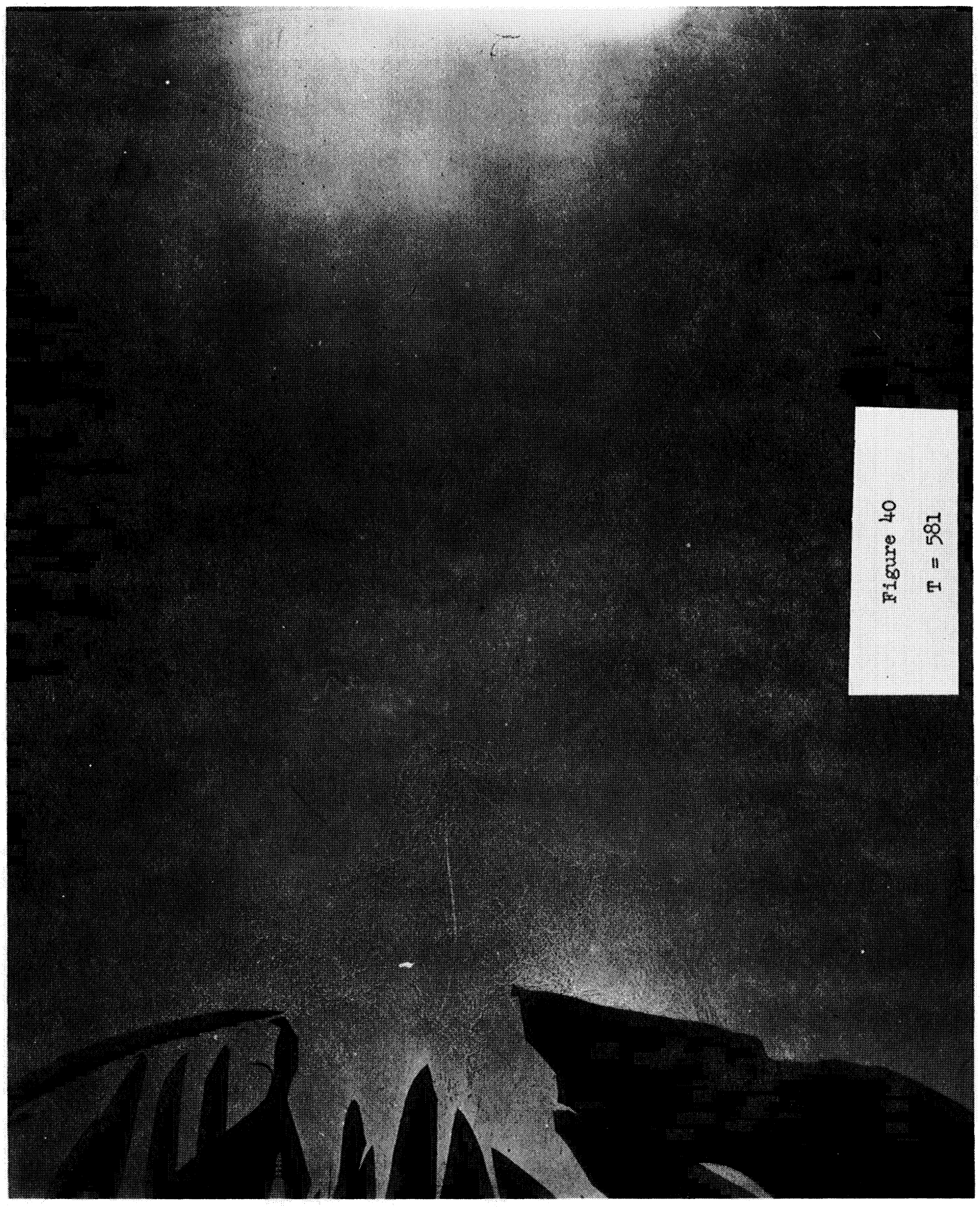
Figure 40
T = 581

Figure 41
T = 796

the tube.

In connection with Mach reflection, Smith[1] observed that, in the case in which the shock to be reflected is plane and of constant strength, the Mach intersection follows a straight line through the point of its first occurrence. Since these shocks are slowly losing their curvature and are presumably strengthening as they proceed, one would not expect his result to apply to the present case. However, his observations give a qualitative indication as to the path of the Mach intersection points.

From the above photographs one can draw certain conclusions regarding the formation of the shock wave and the nature of the flow. Very early in the flow there are probably three-dimensional compression waves which steepen to form shock fronts as in the case of the simple compression wave in one-dimensional flow. These shock fronts are further strengthened by compression waves overtaking them from the rear. If there exist several such fronts, following one another, the most forward one is eventually overtaken by the rest, and a single shock wave results. The most forward shock, which at first undergoes "regular" reflection from the walls, gradually loses its curvature as it progresses. It reaches the stage beyond which regular reflection is impossible[2], and Mach reflection occurs. The heads of the Mach shocks grow until one nearly plane wave crosses the tube. This wave may later be modified slightly, but is substantially the tube shock as observed at the test section.

Up to the time at which the tube shock is plane there are discontinuities in entropy, density, and velocity and gradients of pressure, density,

---

[1]loc. cit. ante, p. 39.

[2]See, e.g., von Neumann, loc. cit. ante, p. 18.

entropy, and velocity in the flow between the shock and the contact discontinuity. There is also vorticity in this flow, and of course none of this flow is one-dimensional. The lack of one-dimensionality is particularly marked just ahead of the contact surface and, indeed, in the "surface" itself. Here, because of the vorticity, there is mixing of the gas initially in the compression chamber with that initially in the expansion chamber. This may partially account for the fact that the contact surface arrives at the test section too early.

b. Discussion of the Possible Failure of the Timing System Because of Incompletely Formed Shock Waves: The above experiments revealed the way in which the shock wave is formed and other phenomena which occur in the tube. The examination of two cases of practical importance yielded information pertinent to the operation of the tube. These were helium-air at $\xi = 0.2$ (Figures 42 and 43) and at $\xi = 0.1$, where the shocks do not show up well enough for reproduction in this report. For these experiments the compression chamber was at atmospheric pressure, and the expansion chamber pressures were simply taken from the previously determined experimental values corresponding to the stated values of ξ. Examination of the plates revealed that in the latter case ($\xi = 0.1$), if one assumes that Smith's result applies, there is question as to whether the shock would be completely formed by the time at which it passed the first light screen. The screens were designed assuming the shock to be plane. They involve, effectively, a very narrow vertical beam of light which passes through the tube in the plane of the assumed wave half-way up the side of the tube. If the shock were not plane, the electronic system might fail to function because insufficient light was deflected into the first phototube. The fact that in normal operation the shock waves were timed at

Figure 42

T = 303

= 0.2

Helium-air

Figure 43

T = 433

= 0.2

Helium-air

values of ξ down to 0.060, using helium-air, indicates either that the shock was properly formed at these values of ξ or that the process of formation was very close to completion.

It is noteworthy, in this connection, that the light screens used by Smith were redesigned and improved on two occasions, but that for air-air, the only case for which there is a cross-check between the three arrangements, the cutoff values of ξ were apparently unaffected by the improvements. The indications are, then, that the cutoff values of ξ in this tube are associated with the formation of the shock wave rather than with the lack of a sufficient difference in the density across it and that, in order to obtain lower usable values of ξ or higher usable Mach numbers, one should lengthen the section of the tube between the diaphragm and the first light screen.

CHAPTER V

AERODYNAMIC TESTS IN THE SHOCK TUBE

1. Introduction

For the purpose of investigating types of experiments which can be performed in the tube flow, two-dimensional models have been mounted between the windows; and supersonic, transonic, and subsonic flows past these models have been photographed, varying the time delay. Although conclusions other than those concerned with the formation of steady-flow configurations are drawn, no attempt to analyze the processes of formation in detail has been made. There are a relatively large number of partially understood phenomena involved, and the study of any one of these could well be made the subject of several investigations. As a matter of fact, a detailed investigation of most flow patterns should probably not be attempted using shadow photography alone. The present investigation, in which shadow photography has been utilized exclusively, should be regarded as exploratory for these reasons.

Before discussing the experiments, it is well to consider the effects of models on the flow. Flow disturbances are produced at any point

on the model as soon as the principal or tube shock passes that point. These disturbances travel with the local sound speed and are responsible for the formation of shock waves and other phenomena. Because of the finite velocity of propagation of the disturbances, the time required for the formation of a steady-flow field should, strictly speaking, be infinite. However, in the vicinity of the model the flow will attain a stationary condition after a very short length of time, while nevertheless at greater distances nonstationary conditions may and do persist longer. This has been implicitly assumed in the flow calibration, in which angles formed by the attached shock waves were measured as close to the nose of the wedge as possible.

Experiments on the detached shock wave, which are to be presented, clearly demonstrate that the forward part of that wave, which is close to the model causing it, in certain cases reaches an equilibrium position within the time available in the tube. However, far from the models, the position and shape of the shock waves involved were changing long after the flows near the leading edges of the models had apparently become fixed.

The experiments referred to above were performed at initially supersonic flow speeds at which, if one neglects effects due to the finite cross section of the tube, pressure disturbances can be transmitted only finite distances forward from a model. At subsonic flow speeds, on the other hand, although they are propagated throughout the entire fluid, their intensity diminishes as they travel; and the flow infinitely far from the model is not affected (in a perfect fluid, at least). There is reason to believe that also in initially subsonic flow substantially steady flows will be formed near models in very short lengths of time. As will be

shown, this proves to be the case.

There is a difficulty involved if the flow speeds are subsonic but very close to the sound speed. Then pressure disturbances are propagated forward very slowly, and the lengths of time required to reach approximately steady flow can be expected to be relatively large.

In one respect this may be an advantage rather than a disadvantage. The confining effect of the walls of a wind tunnel on the flow in it are known to be most serious at free stream Mach numbers near unity. It is here that the phenomenon called choking becomes of importance. Because of this there is, for a given model and tunnel, a free stream Mach number range, which includes unity, in which experimentation is impossible. The advantage of the shock tube lies in the fact that one can carry out certain experiments in the Mach number range in which the wind tunnel would be choked. The initial flow Mach number, at least, can be placed anywhere in this range.

The remainder of this chapter is concerned with experiments in that part of the tube flow between the primary shock and the contact surface. There are two reasons for the choice of this particular flow. In the first place, the flow calibration has shown that this flow is more uniform than that behind the contact surface. Secondly, since there is no flow ahead of the shock wave, boundary layers, in particular, are nonexistent ahead of that wave.

The phenomena photographed include starting vortices and a shock wave-boundary layer interaction in supersonic flow, the detached shock wave, shock wave-boundary layer interactions at transonic speeds, the choking of a duct at initially supersonic speed, and certain high Mach number

flows in gases other than air.

It should be realized that comments in the chapter on whether approximately steady flows have been formed apply only to the particular models tested. The employment of shorter models would also shorten the time required for that formation. One would expect to be able to express the formation in terms of a similarity rule or of similarity rules; however, the particular forms which these rules would take are not obvious.

2. The Detached Shock Wave

The study of the detached shock wave can fortunately be placed on a quantitative basis. For Mach numbers greater than unity for which detached shock waves will occur in steady flow, the detached wave in the tube originates at the time when the primary shock reaches the nose of the model and proceeds upstream from the model, approaching a stationary or limiting position, provided that the tube does not become choked. The distance from the most forward part of the wave (nearest the model) can be measured from photographic plates; and that distance can be plotted as a function of time, as is done here.

Such a wave also occurs in the shock tube when the oncoming flow is subsonic. Then it moves upstream, becoming weaker as it moves. In this case, of course, no equilibrium position is reached. The experiments of this section deal with the supersonic case.

Before the experiments are discussed, it should be noted that it is easily possible for the detached wave to reach its equilibrium position ahead of the model before any semblance of stationary flow has been reached in the neighborhood of the trailing edge or at some distance from the model. An example of the first possibility for the case of the attached shock wave

is shown in Figure 103, Page 157. In this case the flow near the nose is substantially steady although the tube shock has not reached the trailing edge of the model. That the second is true was shown by the fact that at some distance from the models used in these experiments the positions and shapes of the detached waves were changing long after the measured distance had apparently become fixed.

The models used for the experiments were in the form of wedges, and the parameters which were varied were wedge thickness, wedge angle, and the Mach number of the oncoming flow.

Three models of the shape indicated in Figure 44 were constructed, with the dimension "d" equal to 1/16 inch, 1/8 inch and 1/4 inch, making an effective total of six models to be studied.

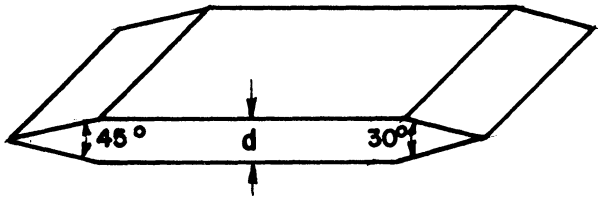

Figure 44
Models Used in
Detached Bow Wave Study

The detached waves from the edges of these models were photographed, and their distances from the leading edges of the models were measured directly from the plates and plotted as functions of time, with the Mach number of the oncoming flow set at values from 1.1 to 1.5 in steps of 0.1.

At each value of the Mach number, a series of shots was run in which each wedge was used twice, once with the 45-degree edge and once with the 30-degree edge forward. However, when a preliminary shot showed that the "detachment" (distance from the wave to the leading edge of the model) would be too small to measure, the series was abandoned. This

occurred with the combinations of wedge thickness, wedge angle, and Mach number which are represented by the blacked-in areas of Figure 45.

A typical photograph from which the data were taken is shown in Figure 46. The plates were triply exposed, with the downstream half of the test section masked off; then the plate was turned so that three more exposures could be made. There were thus six data available from each plate.

The data are given in Tables IX to XIV, those taken with the 45-degree wedge angle forward are plotted in Figure 47 and those with the 30-degree wedge angle forward in Figure 48. The combinations of Mach number, wedge angle and wedge thickness with which a stationary state is observed, i.e., with which the curve of x vs. t reached a horizontal asymptote, are summarized in Figure 45.

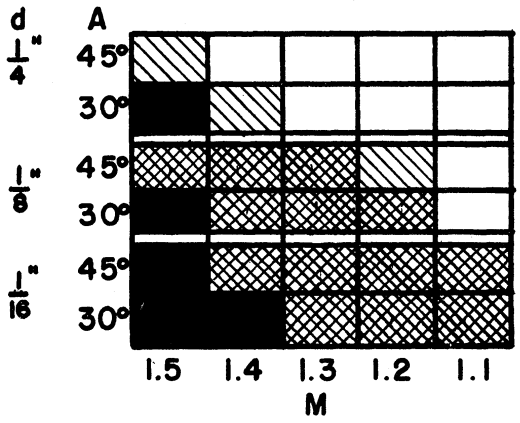

Figure 45
Combinations of Mach Number, M, Wedge Thickness, d, and Wedge Angle, A, with which Stationary Detached Waves Were Observed (Cross-hatched) Doubtful cases are singly cross-hatched, and combinations which were not employed are blacked-in.

In forming conclusions from these results, it is unsafe to extrapolate to blunter objects, such as plates which are square in front (180-degree wedge angle) or plates which are rounded, taking the form of the conventional subsonic airfoil, for example. However, it is probably safe to extrapolate the curves to arrive at results which could be expected to

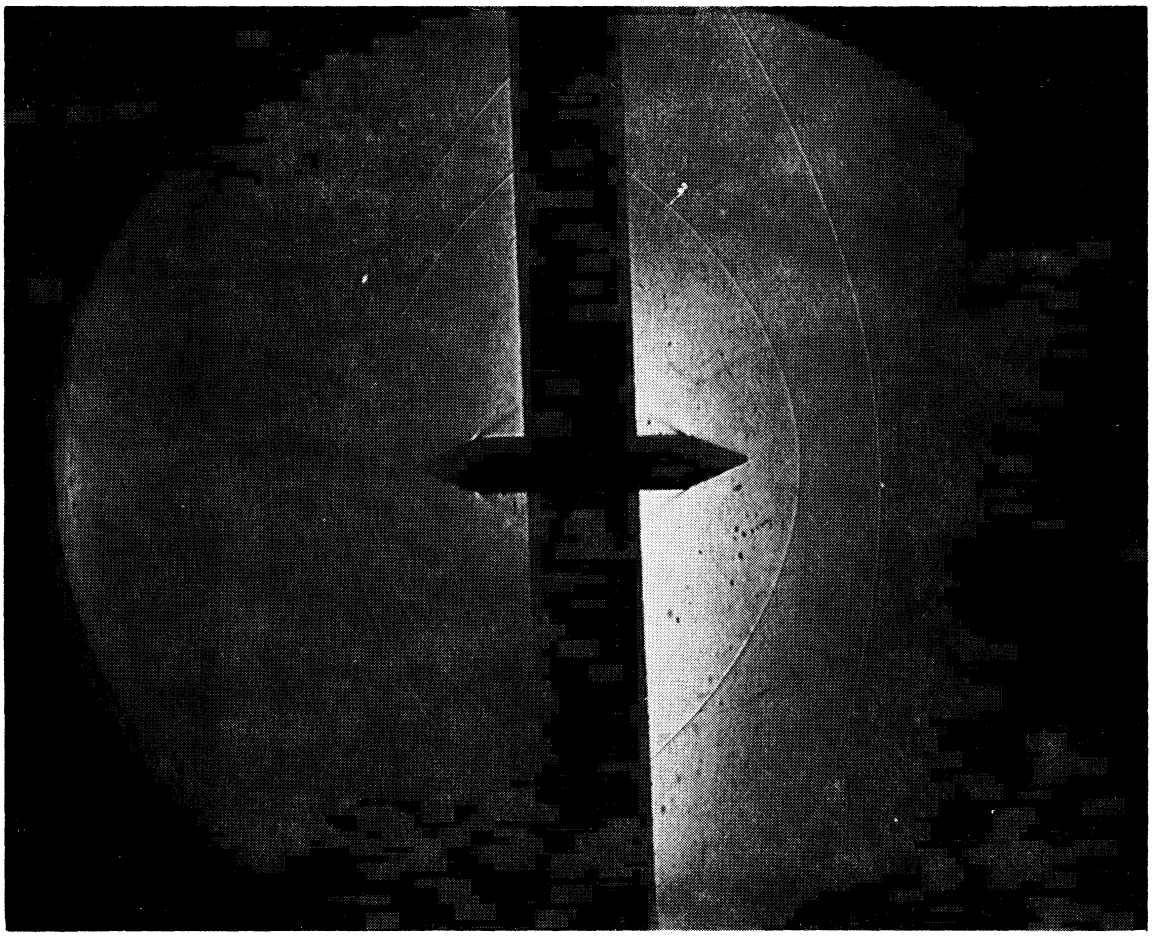

Figure 46

Typical Plate of Detached Bow Wave

M = 1.1, 1/4-inch, 45-degree wedge

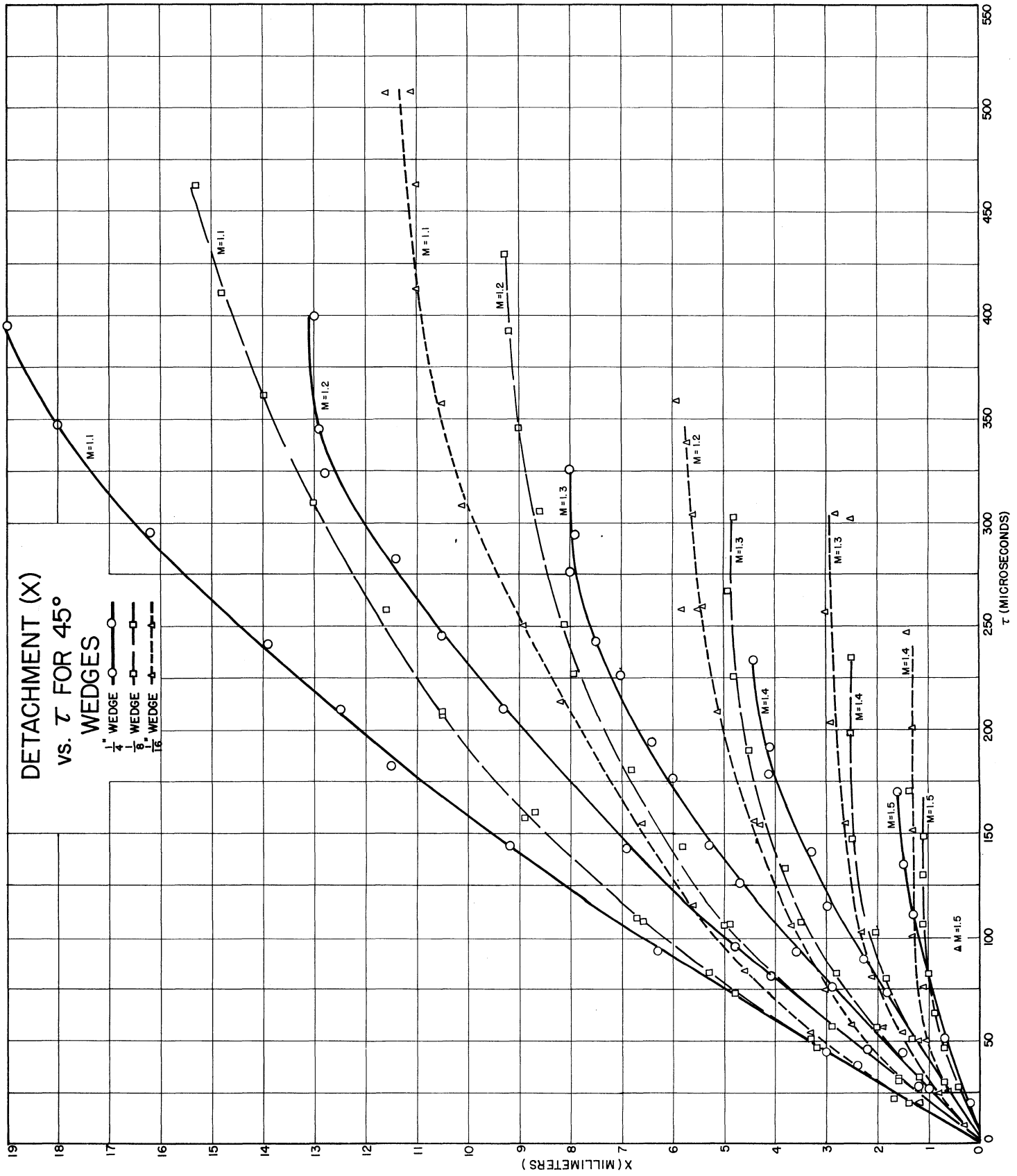

Figure 47

Detachment Versus Time, 45-Degree Wedge

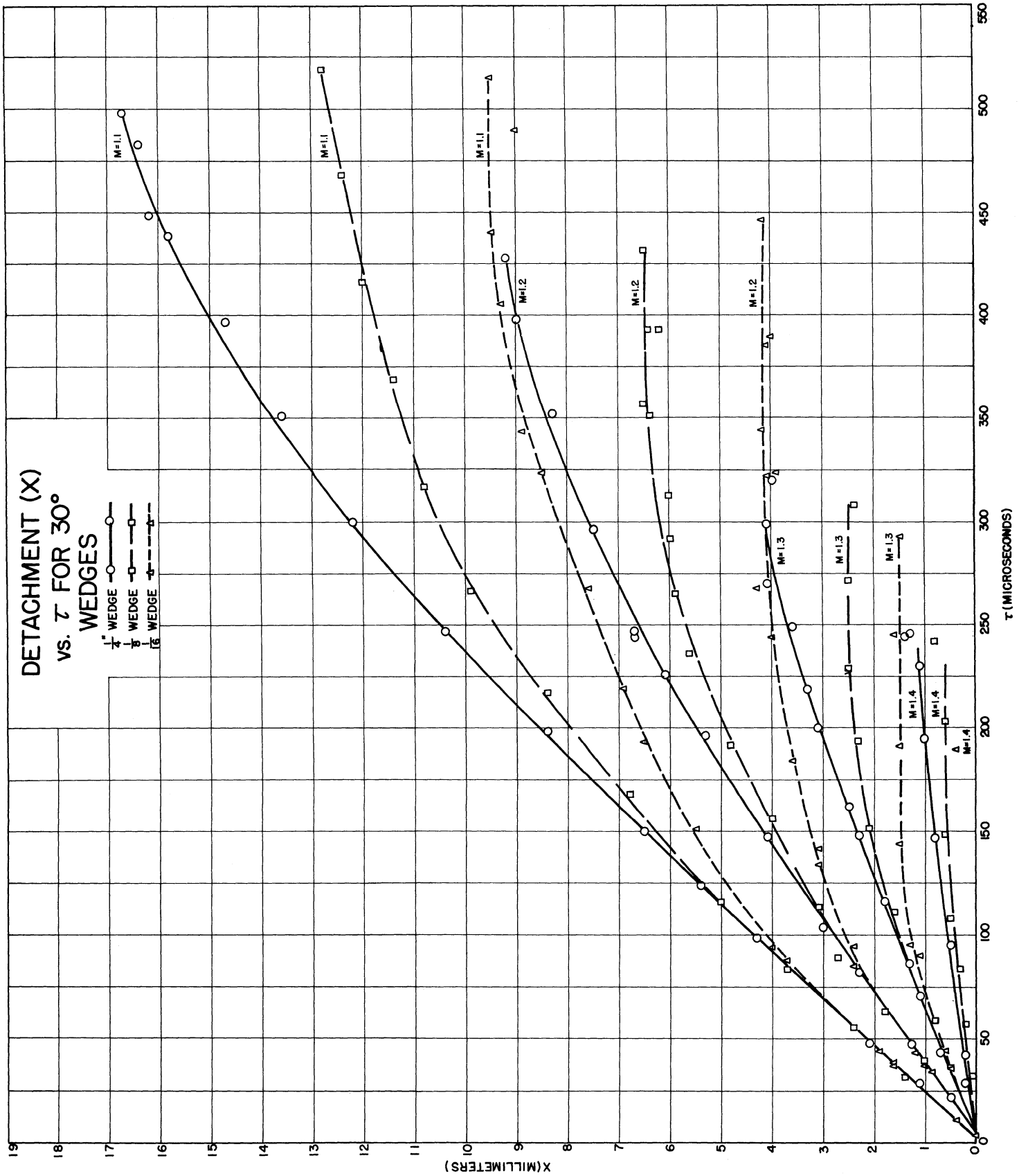

Figure 48

Detachment Versus Time, 30-Degree Wedge

apply when longer periods of time are available, i.e., when a longer shock tube is used.

There are three characteristics of the curves worthy of note. The first is related to the behavior of the curves near the origin. Observe that for the same wedge angle and Mach number the curves for the various thicknesses coincide there. This is to be expected because the detached waves are at first unaware of the presence of the corners of the wedges. In other words, these portions of the curves would be the same if the wedge and tube were infinite in extent.

The second refers to the steady state configurations. The effect of doubling the thickness at constant wedge angle and Mach number is, according to the curves, to less than double the stationary displacement distance. This is certainly unexpected. In making the measurements, it was observed that the line representing the detached shock was broad at first, and the distance was measured from the downstream edge at all times. The breadth of the line (0.5 mm. at most) was never great enough to account for the lack of proportionality between model thickness and displacement distance. Moreover, the consistancy of the data at the origin indicates that the measurements were properly made. This matter should perhaps be investigated further in wind tunnel tests in which larger models (in larger tunnels than the shock tube) are used.

The third point is that there appear to be straight steady portions of most of the curves and the origin. These are unexplained.

3. Starting Vortices and a Shock Wave-Boundary Layer Interaction in Supersonic Flow

Starting vortices were first photographed in water, an almost incompressible fluid, by Prandtl[1] in 1923. For incompressible flow it follows from the theorems of Thompson and Stokes that the sum of the strengths of the vortices produced is equal to the circulation produced about the body responsible for the vortices. The fact that circulation is generated is explained on the basis of viscosity.

Viscosity is also necessary to explain the origin of circulation in subsonic flow, but not in supersonic flow; i.e., in supersonic flow it can exist in a fluid assumed to have zero viscosity. Thompson's theorem is valid for compressible non-viscous flows if the gradients of temperature and of entropy are parallel or if either gradient is zero[2]. The subsonic or supersonic (not transonic) flow over a model behind the tube shock is approximately isentropic if the model is thin and at a low angle of attack. However, there is question as to whether the path of integration involved in Thompson's theorem can cross the tube shock, which can be considered either as a discontinuity or as a continuous flow involving viscosity. For these reasons one can expect to observe starting vortices in the tube flow although there is serious question as to whether the sum of the strengths of these vortices is equal, even approximately, to the circulation produced about the model. That starting vortices have not been previously observed in compressible flow (either subsonic or supersonic) is due to the earlier experimental difficulty involved in suddenly producing a finite flow Mach number.

---

[1]See in this connection Prandtl and Tietjens, pp. 216-221.

[2]The proof of this statement is given by Courant and Friedrichs, pp. 19-20.

The model for the experiments was a 5-degree wedge on the forward end and a 35-degree wedge on the other. It had a 1/4-inch maximum thickness and a chord (length) of 3.2 inches. The tube was operated at a Mach number of 1.15.

In Figures 49-52 the model is at an angle of attack of 2-1/2 degrees. From 49 it is evident that the part of the tube shock on the upper surface arrived at the trailing edge ahead of that on the lower surface and therefore turned the corner around that edge before the other part arrived there. It was also of different strength from that on the lower surface. The resulting flow was not symmetrical, and a vortex was formed. This particular vortex, then, is produced in a very special way; and one cannot expect it to be the only one formed.

As the remaining photographs show, this vortex moves downstream, and the region of the flow affected by it increases. (The forward boundaries of that region, to which one can refer as the "tails" of the principal shock, would move upstream against subsonic flow. The tails of the principal shock arise when the flow which is deflected around the corners by the expansions there reaches the trailing edge of the model. The tails are shocks which return the flow to a direction parallel to the axis of the wedge.) As the flow over the airfoil gradually is adjusted towards a steady state configuration, smaller secondary vortices appear. In the first of these, at least, the direction of rotation is the same as that in the original vortex. This undoubtedly means that the circulation about the model is increasing.

In 49 there is a small shock between the position of maximum thickness (the corner) and the trailing edge. It apparently originates at the corner. As time passes it is swept downstream, and it finally

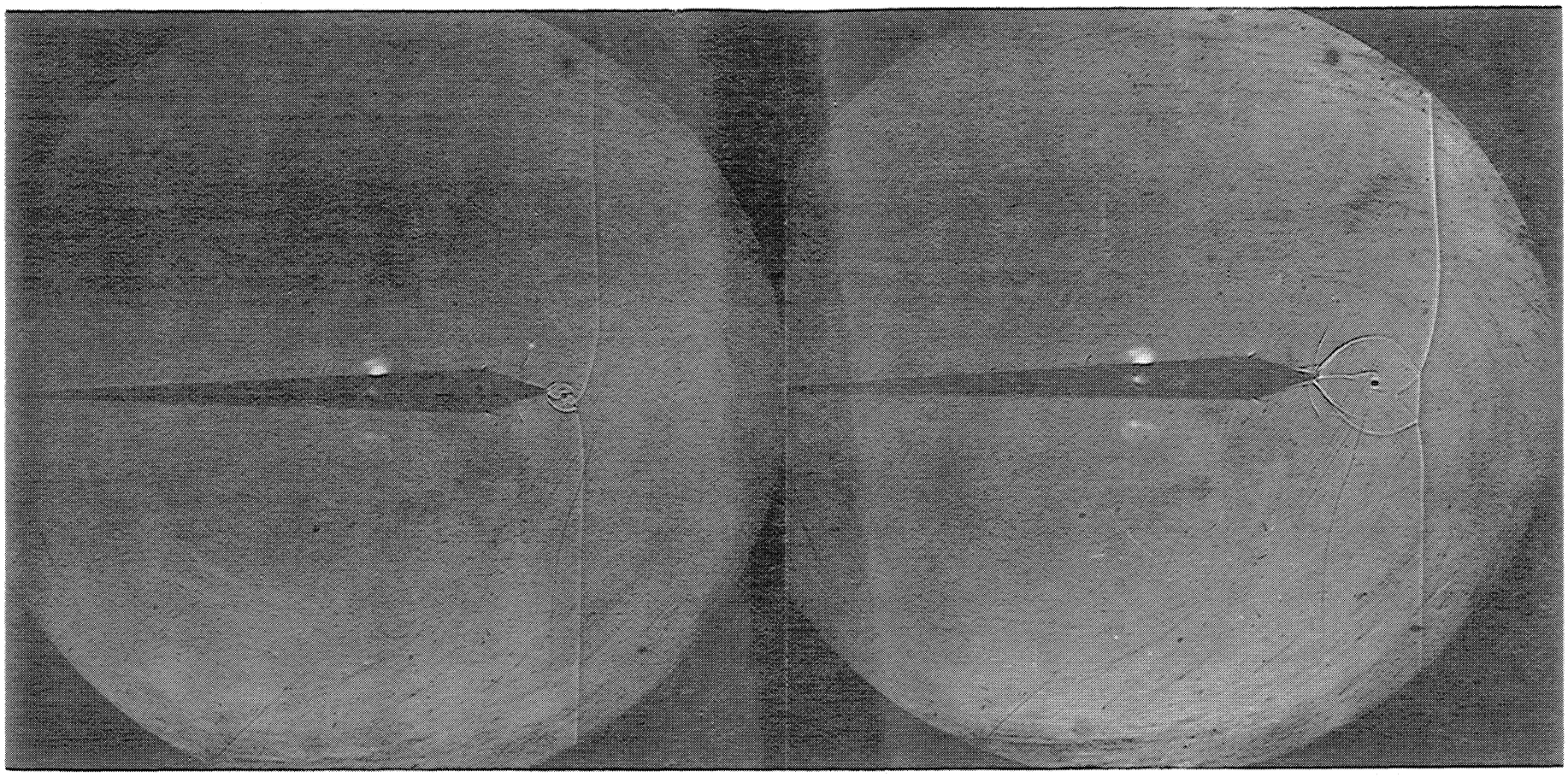

Figure 49

τ = 102
M = 1.15
Angle of Attack = 2.5°

Figure 50

τ = 111
M = 1.15
Angle of Attack = 2.5°

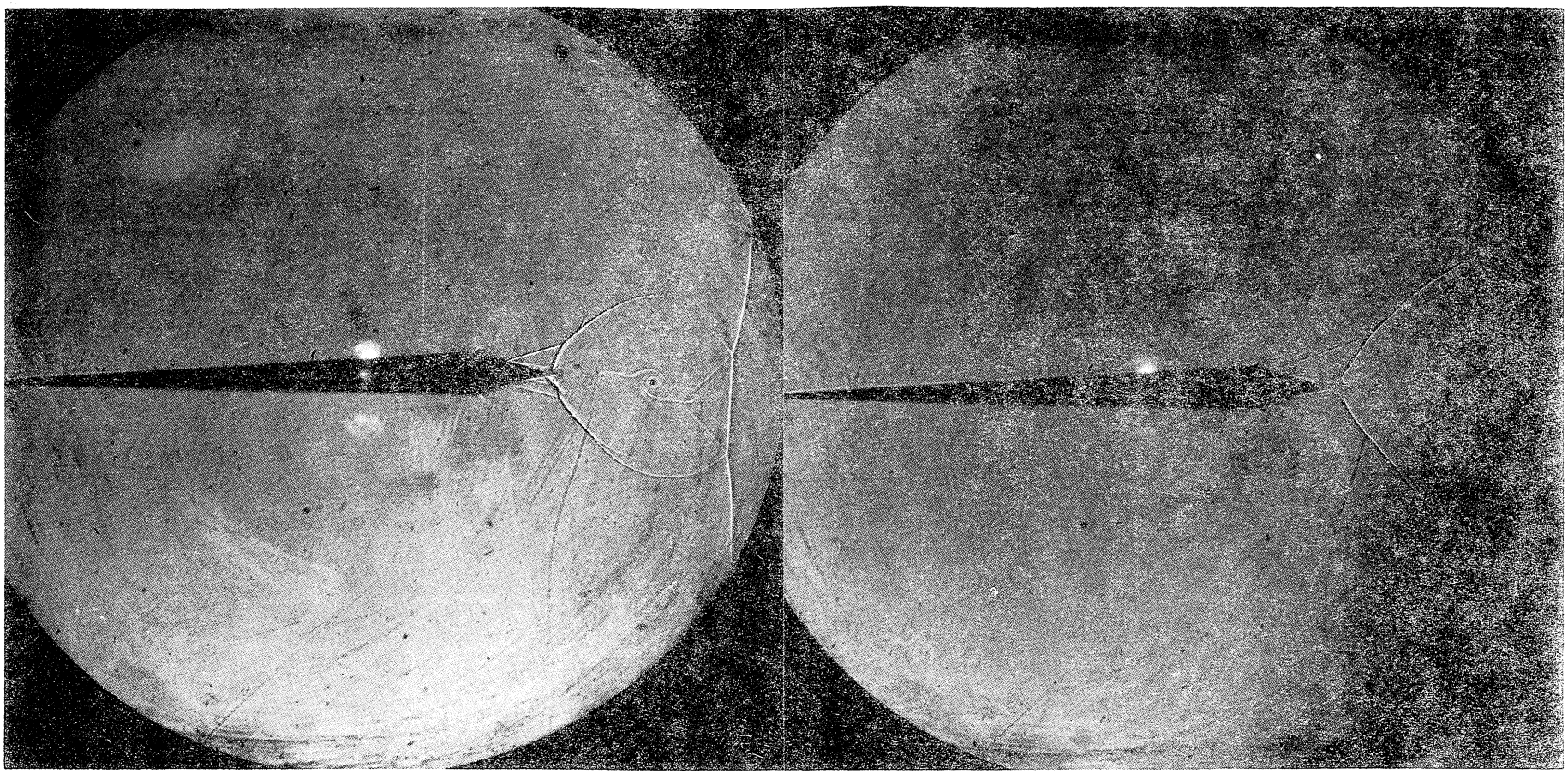

Figure 51

γ = 129
M = 1.15
Angle of Attack = 2.5°

Figure 52

γ = 150
M = 1.15
Angle of Attack = 2.5°

interacts with the shock at the trailing edge. Similar waves are always observed behind such a corner (in the shock tube) in supersonic flow, so that the phenomenon is not to be associated with this particular model.

During this time the boundary layer, which at first was nonexistent, has been building up. It finally forms a noticeable wake and causes the oblique shock observed for the first time in Figure 50. The point of thickening of the boundary layer moves forward with this wave.

In photographs of wind tunnel flow it is not unusual to observe a shock wave directly behind the expansion region (not visible in these shadowgrams) at a sharp corner. Because this wave is not a necessary part of the theory of the flow past a wedge which includes shock waves but omits viscous effects, once sometimes says that this wave is associated with "overexpansion" at the corner. The preceding experiment indicates that this shock could be attributable directly to viscous effects. In order to investigate this a second set of photographs, Figures 53-56, was taken with the model at about zero angle of attack and using considerably longer time delays. The plates show that the wave formed does indeed move to the corner along with the apparent point of thickening of the boundary layer and therefore that this wave, in steady flow, is attributable to the boundary layer.

4. Transonic Flow About a Symmetrical Double Wedge Airfoil

The primary concern of this section is with that part of the transonic range in which the oncoming flow is subsonic. Series of photographs are discussed for one angle of attack with different Mach numbers. For purposes of comparison, photographs in which the entire flow is subsonic are included. A brief investigation is made in the Mach number range in

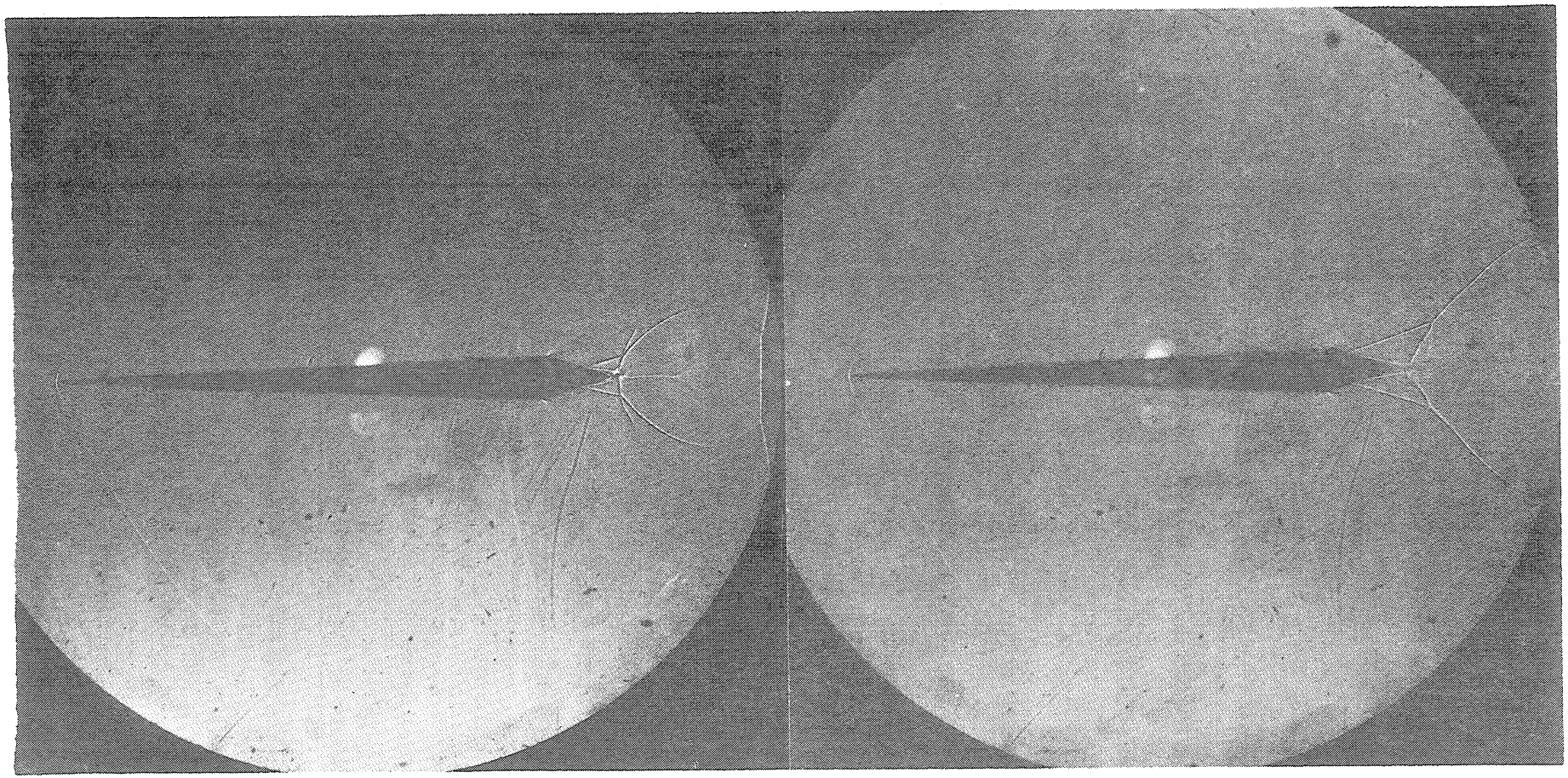

Figure 53

γ = 145
M = 1.15
Angle of Attack = 0°

Figure 54

γ = 181
M = 1.15
Angle of Attack = 0°

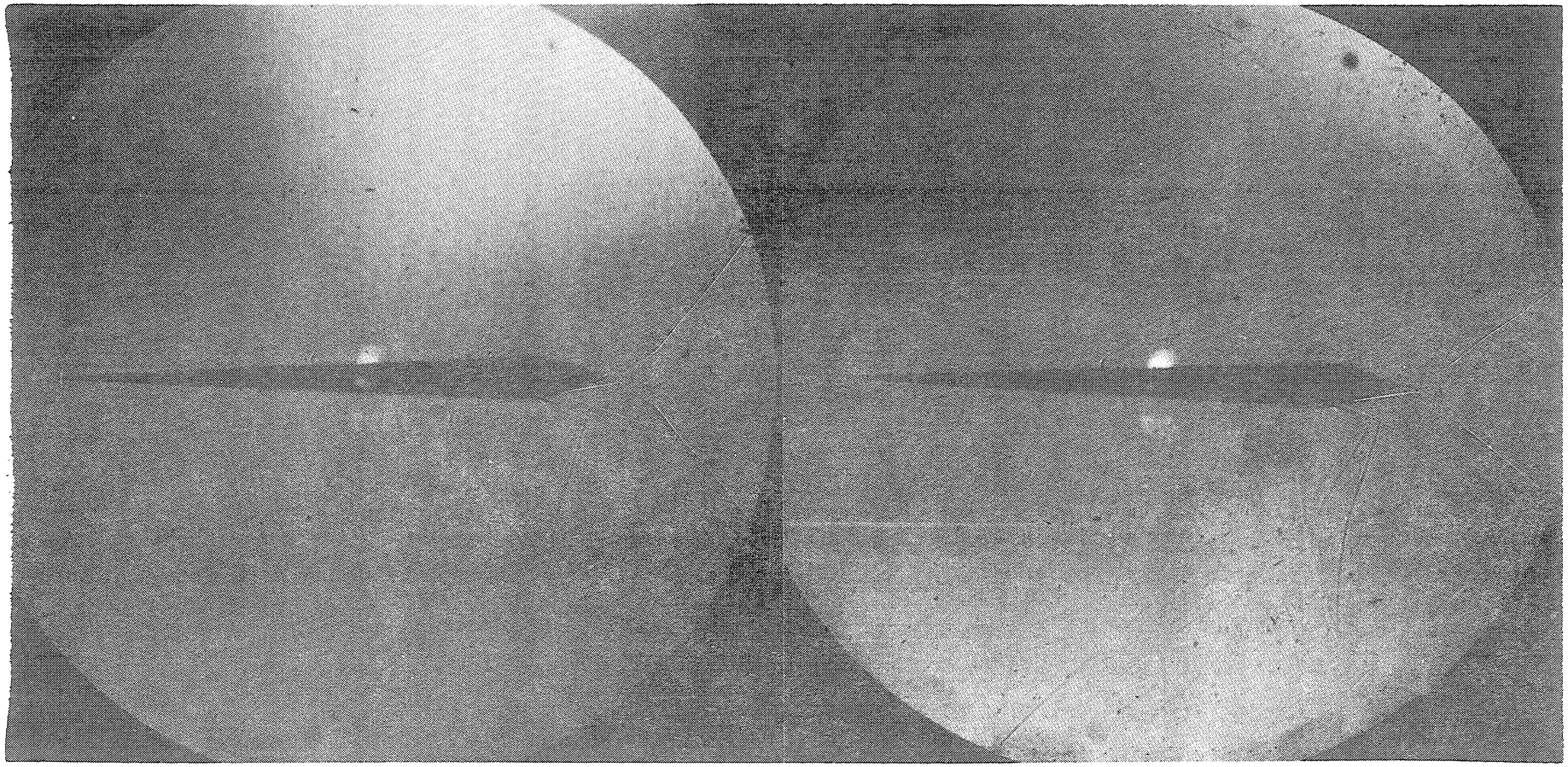

Figure 55

τ = 229
M = 1.15
Angle of Attack = 0°

Figure 56

τ = 507
M = 1.15
Angle of Attack = 0°

which the wind tunnel would be choked.

A double wedge of length 2.6 inches and with a 10-percent thickness ratio served as the model. The reason for choosing this particular supersonic airfoil is that Bartlett and Peterson[1] employed it in subsonic and transonic wind tunnel investigations, so that many of the steady state configurations are available.

a. Zero Angle of Attack: Figure 57, a late photograph taken at M = 0.70, is an example of the boundary layer and wake in steady subsonic flow[2]. The boundary layer has thickened suddenly behind the maximum thickness position and probably becomes turbulent there.

In Figures 58-61, photographed at M = 0.79, the flow is transonic. In 58, the primary shock has already passed; and the tail of that shock, previously referred to in Section 2, has moved upstream to a point on the model about half-way between its trailing edge and the position of maximum thickness. Lambda shocks occur just behind the corners, and these are followed by approximately normal shocks. In 59, the boundary layer has become thick, if not separated, behind the corner; and the tail of the tube shock is interacting with the lambda shocks. In 60, the boundary layer is definitely separated; the tail of the tube shock, far from the model is apparently too weak to be observed; and the size of the lambda shocks has increased. In 61, they have tipped forward, and they project farther towards

---

[1]Bartlett, G. E. and Peterson, J., "Wind Tunnel Investigations of a Double Wedge Airfoil at Subsonic Speeds," Cornell Aeronautical Laboratory Report No. AF-360-A-6 (1946).

[2]The black line which appears to the left of the model is a plumb line which may be used to determine the angle of attack of the model. The line parallel to the airfoil is due to improper line-up of the optical system with respect to the model. It results from the reflection of light from the spark off the model.

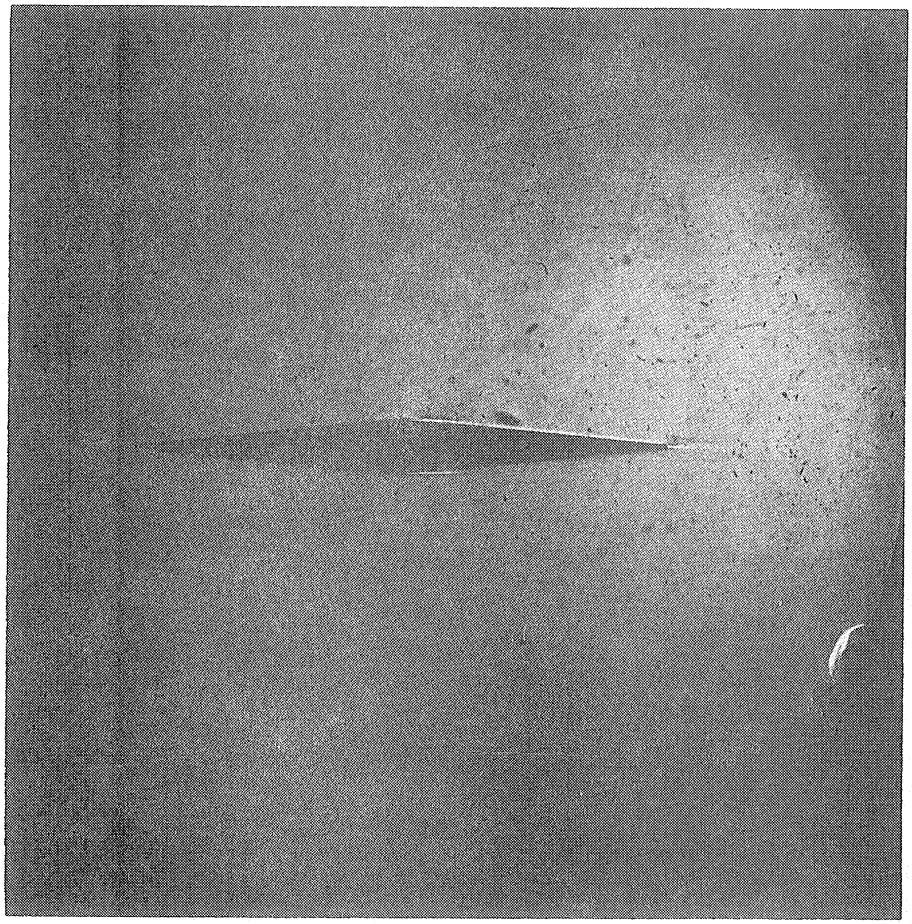

Figure 57

γ = 658
M = 0.70
Angle of Attack = 0°

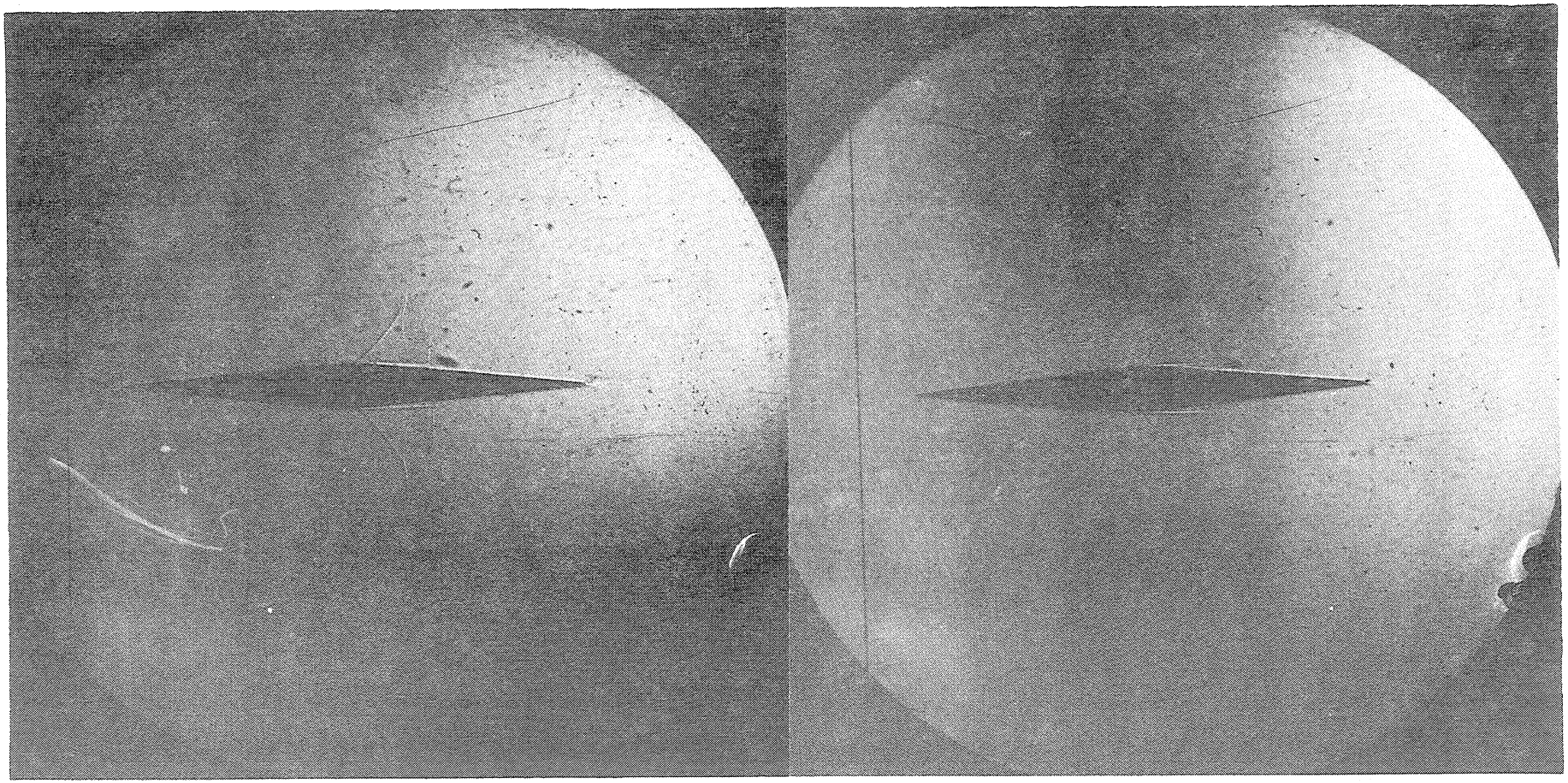

Figure 58

τ = 373
M = 0.79
Angle of Attack = 0°

Figure 59

τ = 745
M = 0.79
Angle of Attack = 0°

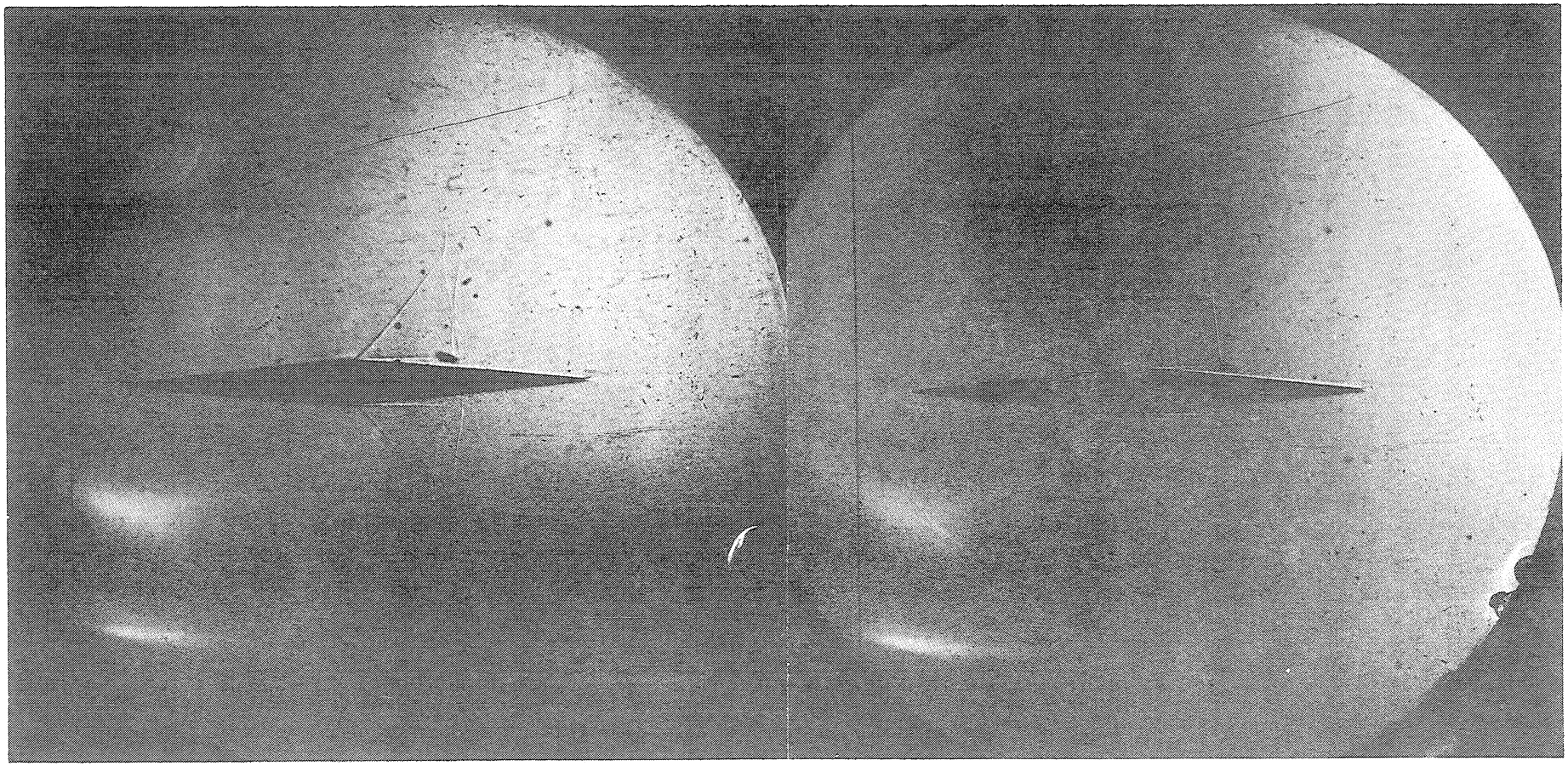

Figure 60

= 1090
M = 0.79
Angle of Attack = 0°

Figure 61

= 1478
M = 0.79
Angle of Attack = 0°

the walls (top and bottom) of the tube. This may be indicative of wall interference but is more probably an interaction of the tail of the primary shock with the Mach configuration. A regular reflection of the rear foot of the lambda shock seems to occur on one surface of the airfoil. Such reflections have been observed in wind tunnel tests by Ackeret, Feldman, and Rott[1]. A steady flow has not been obtained in this case, although the steady state is known to contain these lambda shocks.

Three photographs, Figures 62-64, have been taken at an initial Mach number of 0.90. (The limiting Mach number for choking is computed to be approximately 0.82). Early in the process, as the photographs show, the flow is similar to that at M = 0.79, with the exceptions that the second shock does not appear here and that the lambda shocks in this case are much larger than in the preceding one. Note the reflection from the model, a head wave which in this (subsonic) case moves forward without limit. At the time of the final photograph, if the curvature and apparent strength of the heads of the lambda shocks are used as an indication, the effect of choking has become pronounced. These waves probably extend to the top and bottom of the tube, although the limited diameters of the windows do not allow one to determine this. If one were to investigate the choking phenomenon in detail, one would surely require windows which not only extend from top to bottom of the tube but also cover an appreciable length of the tube.

b. 6-Degree Angle of Attack: At subsonic speeds the steady flow at a 6-degree angle of attack is characterized by the separation of the boundary layer on the upper surface at or very near to the leading edge

---

[1]Ackeret, J., Feldman, and Rott, "Untersuchungen an Verdictungsstossen und Grenzschichten in Schnell Bewegten Gasen," Mitteilungen aus dem Institut für Aerodynamik, No. 10 (1946).

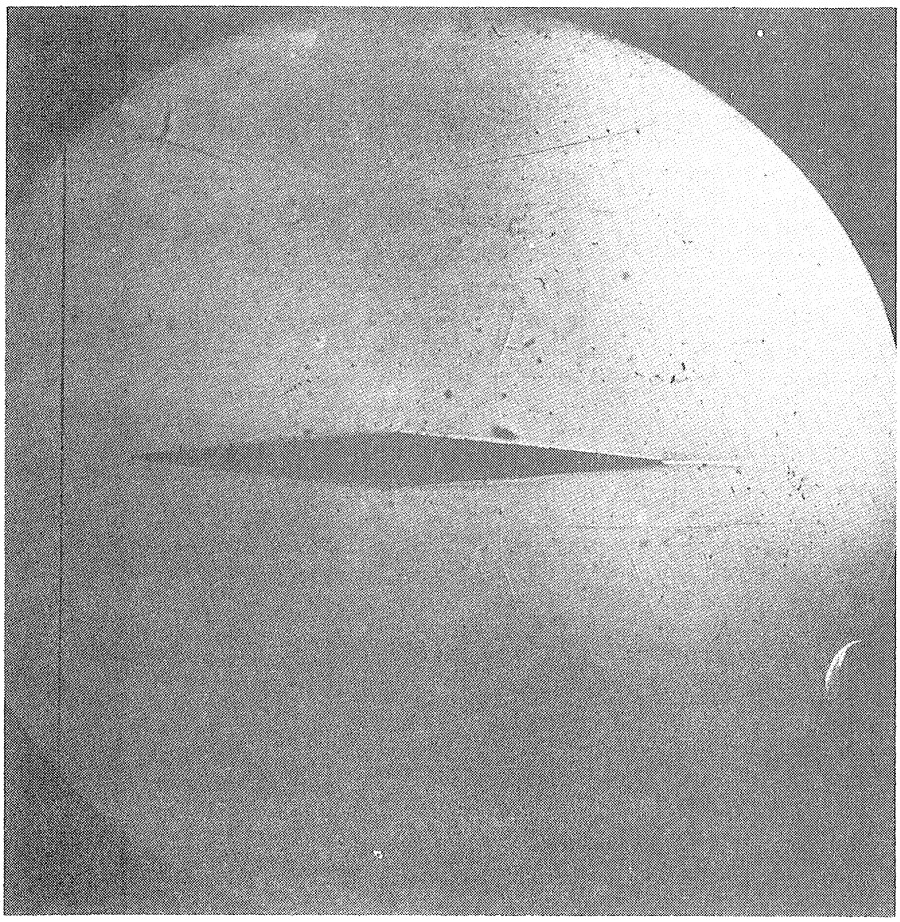

Figure 62

γ = 253
M = 0.90
Angle of Attack = 0°

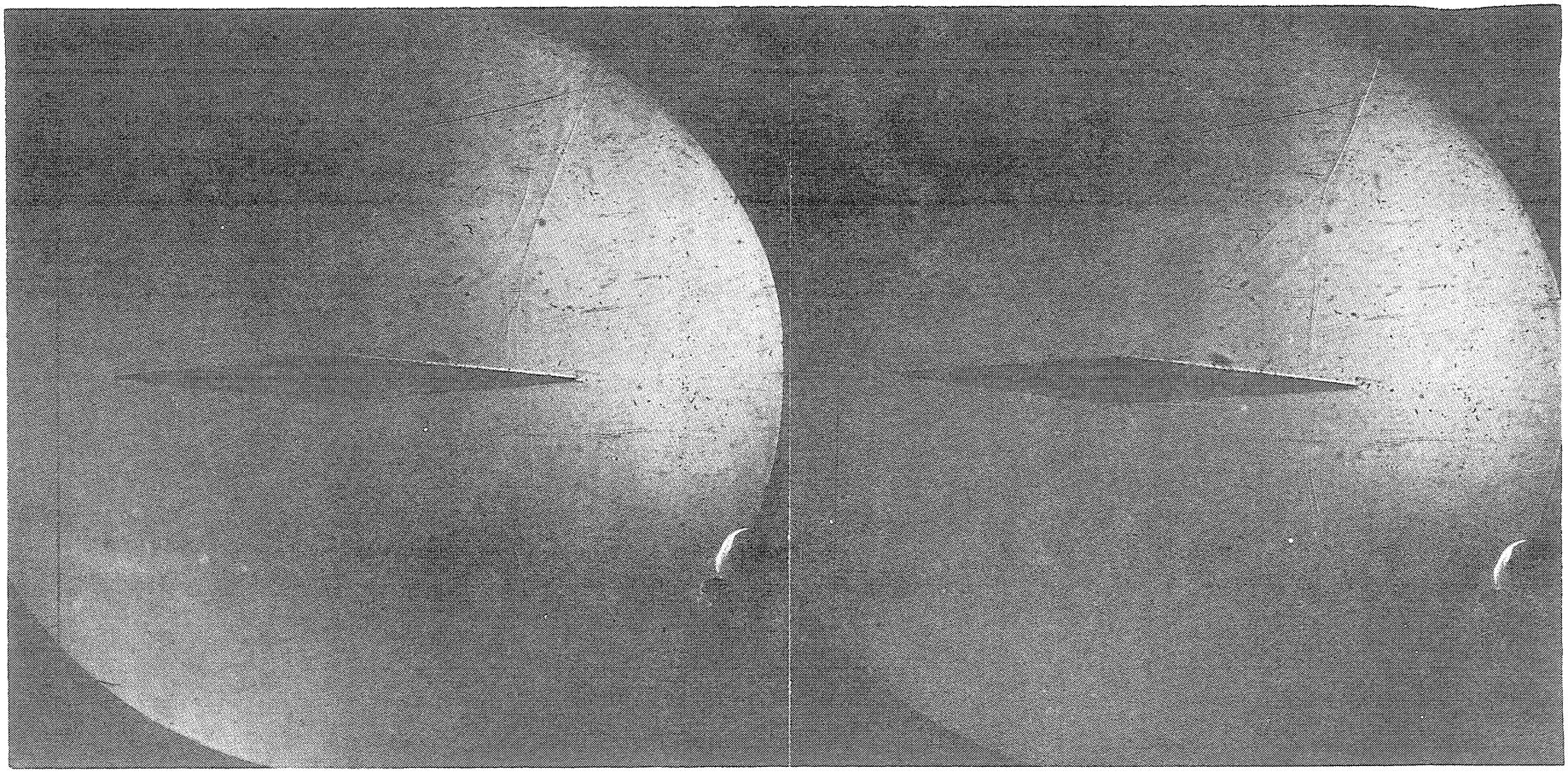

Figure 63

γ = 427
M = 0.90
Angle of Attack = 0°

Figure 64

γ = 751
M = 0.90
Angle of Attack = 0°

of the airfoil. Figure 65 is an example of this at M = 0.60. (M = 0.70 is transonic at this angle of attack.) Comparison of the plate with a series of shock tube photographs (not shown) indicates that the flow represented is substantially a steady state. Opposite the position of maximum thickness the separated layer is almost as thick as the model. The "bubble" which appears at the leading edge of the model in this plate and in the rest of the plates of this section is also observed in wind tunnel photographs and is most probably a result of the high velocity and density gradients which exist in the neighborhood of that edge[1].

The development of approximately steady flow at M = 0.79 is shown in Figures 66-71. At first the flow is very similar to that at zero angle of attack, in that lambda configurations occur behind the corners. Some separation of the flow occurs as at M = 0.60, although the thickness of the separated layer is much less here. The shock on the lower surface almost disappears when the tail of the tube shock passes, but it is reformed. On the upper surface the tail reinforces the lambda shock, and the latter increases in size. A small shock appears on the thin region of separated flow in 68; and this grows, eventually turning into a third lambda configuration. Figure 71 is very similar to the corresponding wind tunnel photograph.

Two photographs, Figures 72 and 73, were taken with the initial Mach number unity. In the early stages the flow appears to be very similar to that at M = 0.79 with the exception that the lambda shocks are very much larger at the higher Mach number. It is recalled that the same conclusion was drawn in comparing photographs at M = 0.90 and M = 0.79 at zero angle

---

[1]Behind the leading edge is a piece of cellophane which lodged there during a previous firing of the tube and which had not been removed.

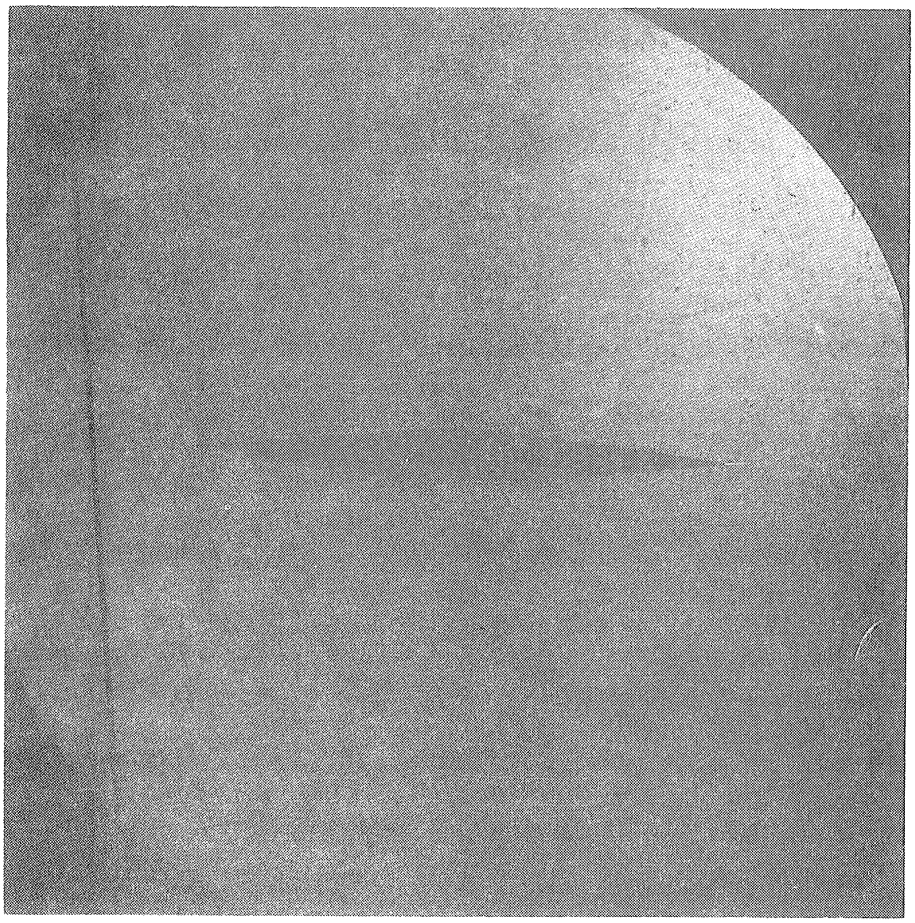

Figure 65

γ = 1084
M = 0.90
Angle of Attack = 6°

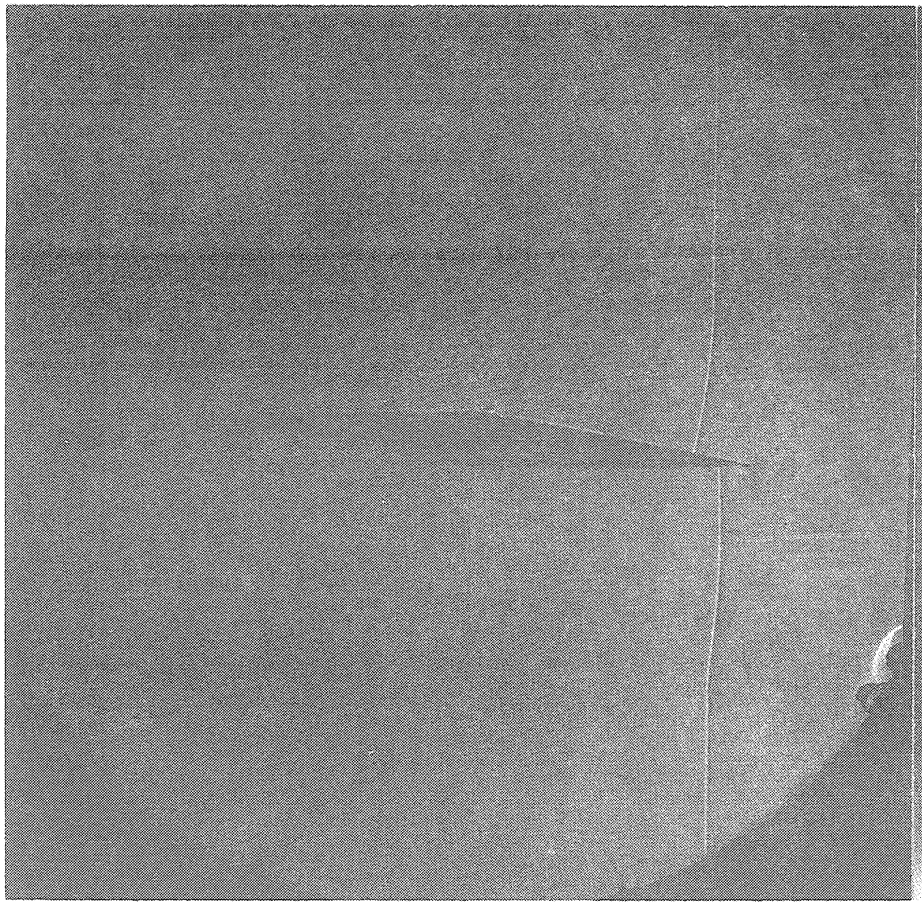

Figure 66

τ = 104
M = 0.79
Angle of Attack = 6°

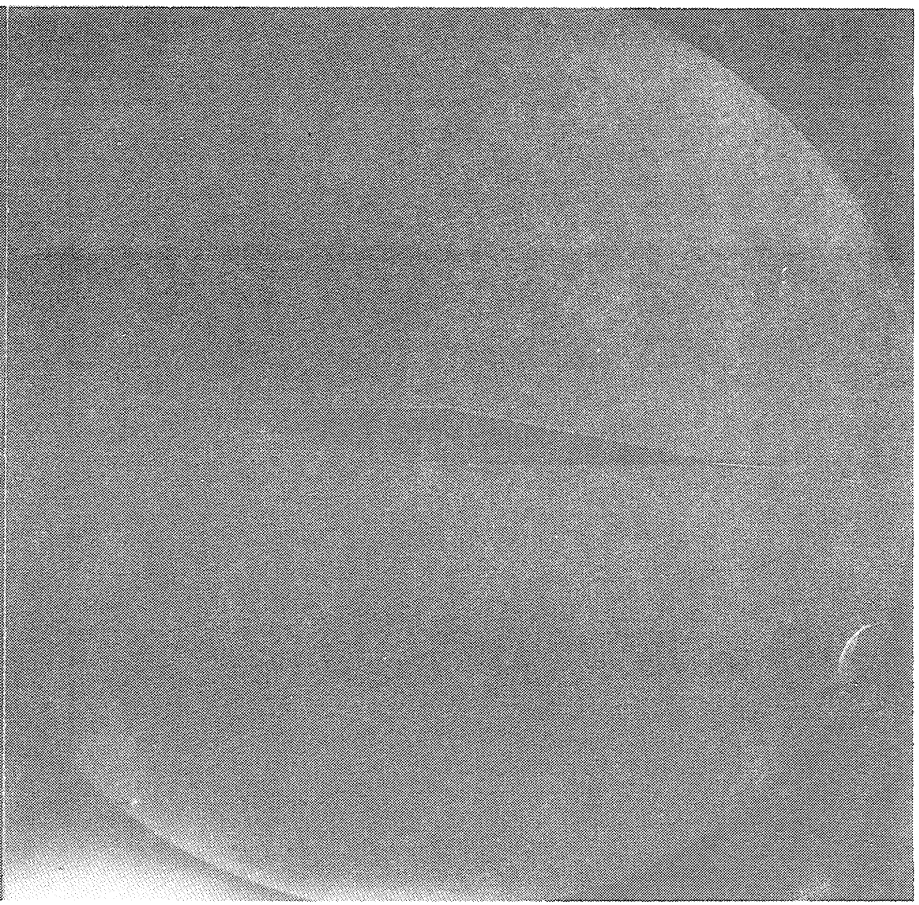

Figure 67

τ = 257
M = 0.79
Angle of Attack = 6°

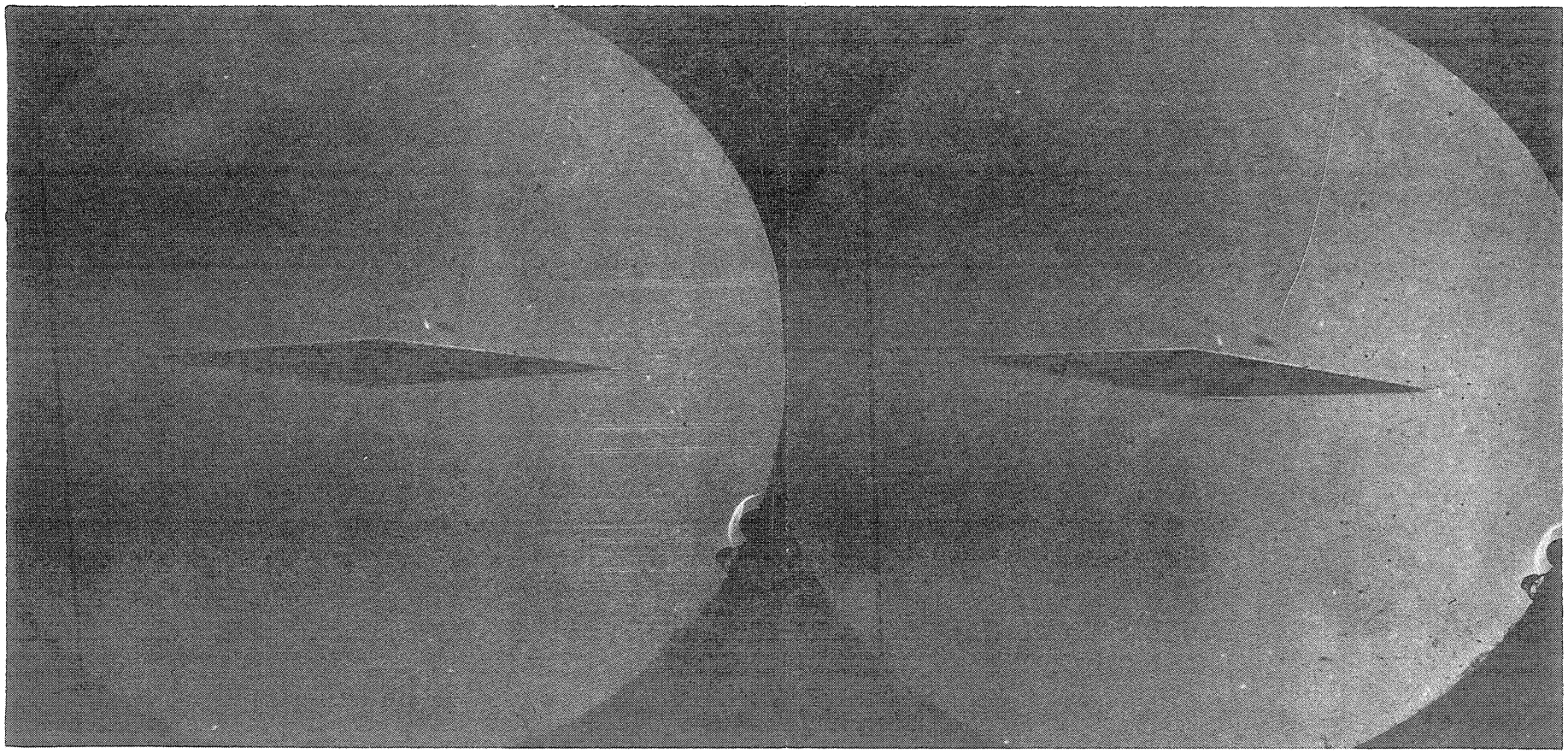

Figure 68

τ = 358
M = 0.79
Angle of Attack = 6°

Figure 69

τ = 761
M = 0.79
Angle of Attack = 6°

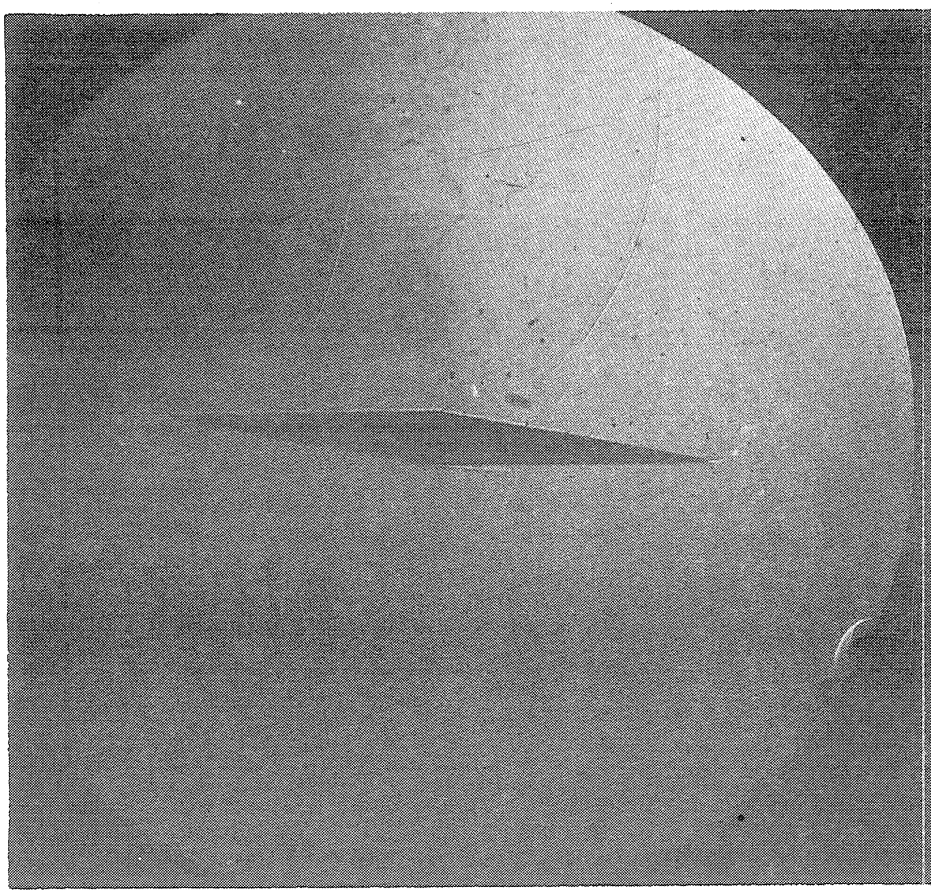

Figure 70

τ = 1257
M = 0.79
Angle of Attack = 6°

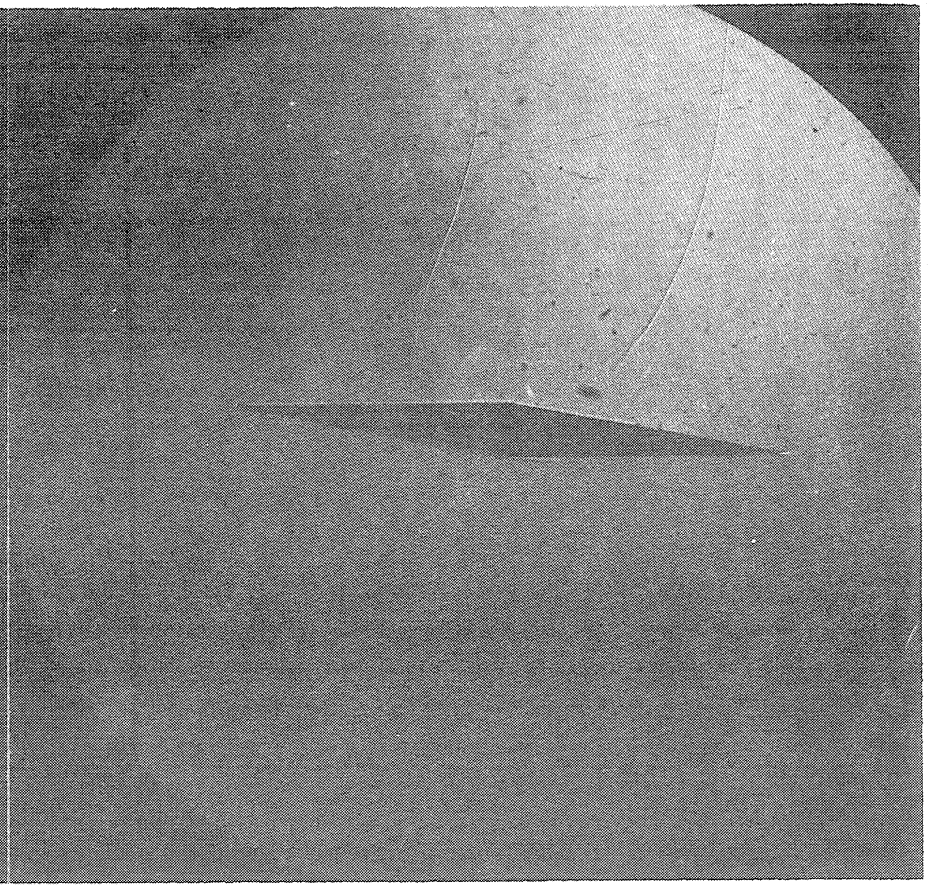

Figure 71

τ = 1454
M = 0.79
Angle of Attack = 6°

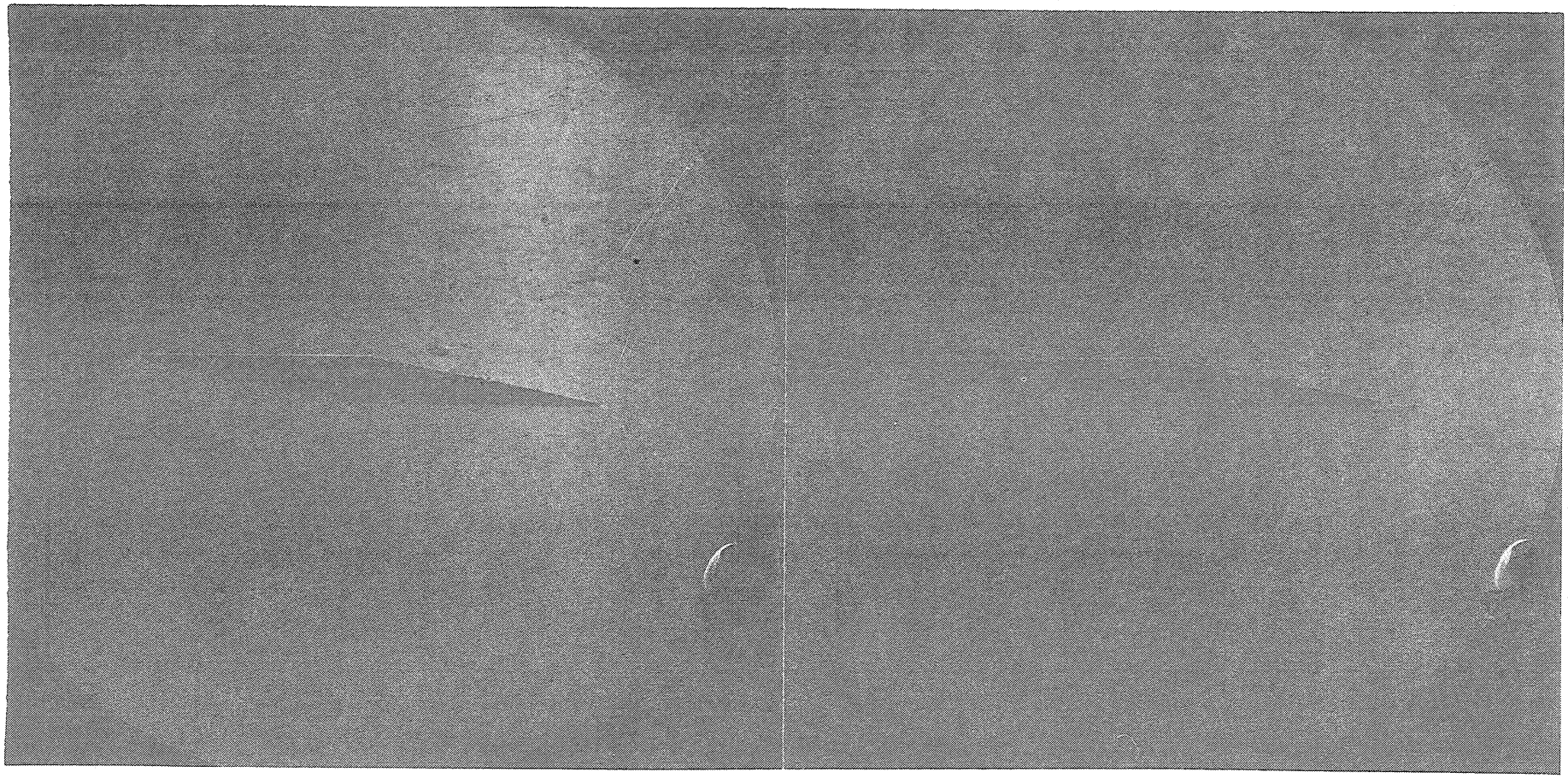

Figure 72

τ = 379
M = 1.00
Angle of Attack = 6°

Figure 73

τ = 783
M = 1.00
Angle of Attack = 6°

of attack. Because of the limited diameters of the windows and because of the fact that the shadowgraph method has been used here, it is difficult to draw any conclusions from the photographs regarding the choking phenomenon. Figures 74 and 75 show an early and a late stage of the development of the flow with M = 1.30. Near the leading edge is a detached shock wave; and on the upper surface, attached to the leading edge, is an oblique shock which is apparently part of a lambda shock.

c. 8-Degree Angle of Attack: A series of pictures, Figures 76-79, illustrates the buildup of the detached or separated layer in subsonic flow (M = 0.60). Opposite the position of maximum thickness, the width of the layer increases to approximately that of the airfoil. The phenomenon which occurs behind the trailing edge in 76 requires some explanation. After the starting vortex is formed, a vortex sheet extends from the trailing edge of the airfoil to that vortex. This sheet becomes unstable and develops into a turbulent wake. The nature of the instability may be similar, at least qualitatively, to that in transition from laminar to turbulent flow on a surface.

At high angles of attack the shock waves which occur on this airfoil markedly decrease the thickness of the separated layer. For example, at M = 0.70, shown in Figures 80-84, the final thickness of that layer is considerably less than at M = 0.60. (Note the well-formed starting vortex and the tail of the principal shock in Figure 80). There is some room for question as to whether the forward foot of the lambda shock formed at this Mach number would move to the nose of the airfoil if more time were available.

The last set of pictures, Figures 85-90, indicates that this might happen. Further, in 85 there appears to be a whole set of shocks on the

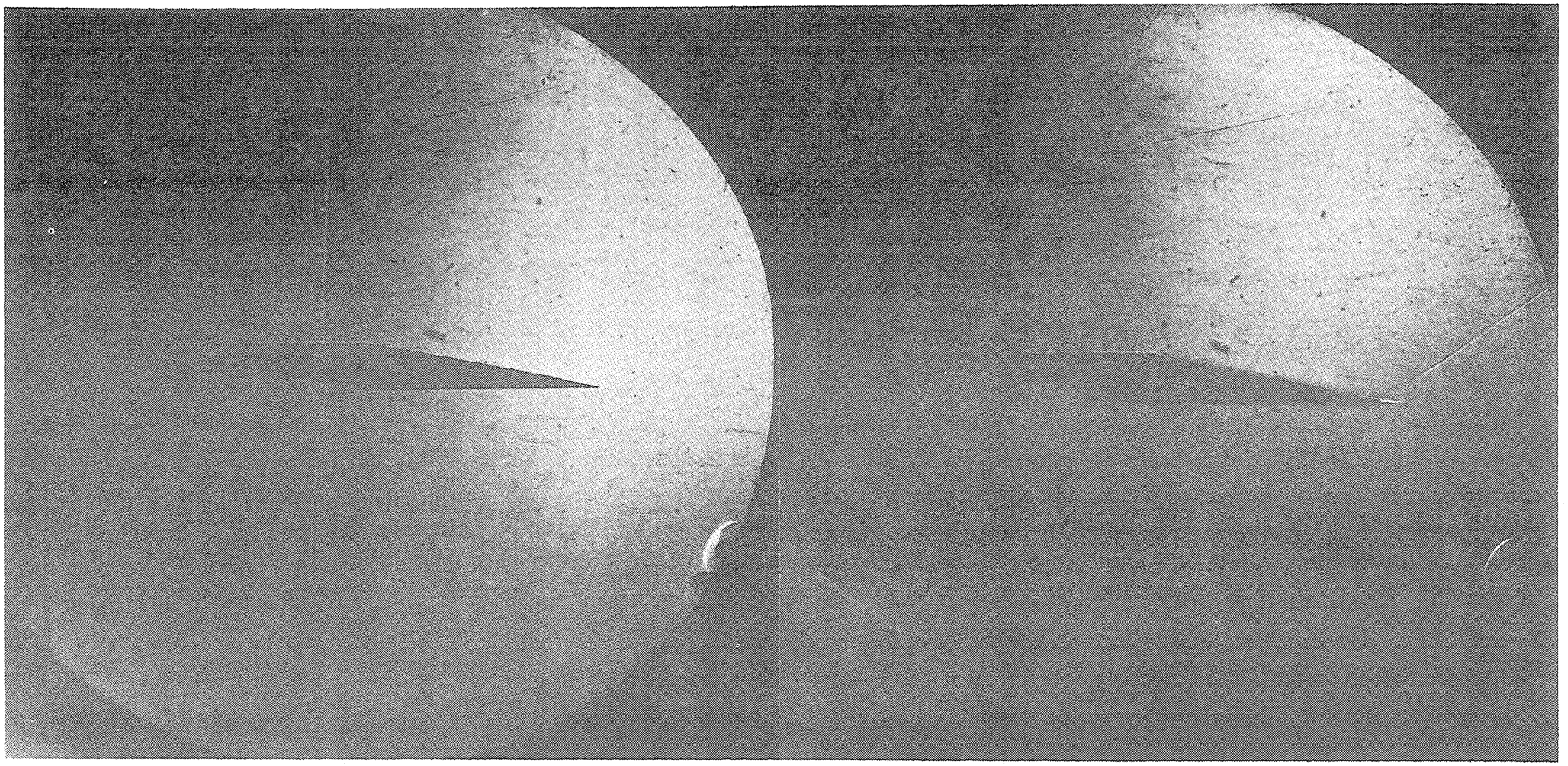

Figure 74

γ = 27
M = 1.30
Angle of Attack = 6°

Figure 75

γ = 315
M = 1.30
Angle of Attack = 6°

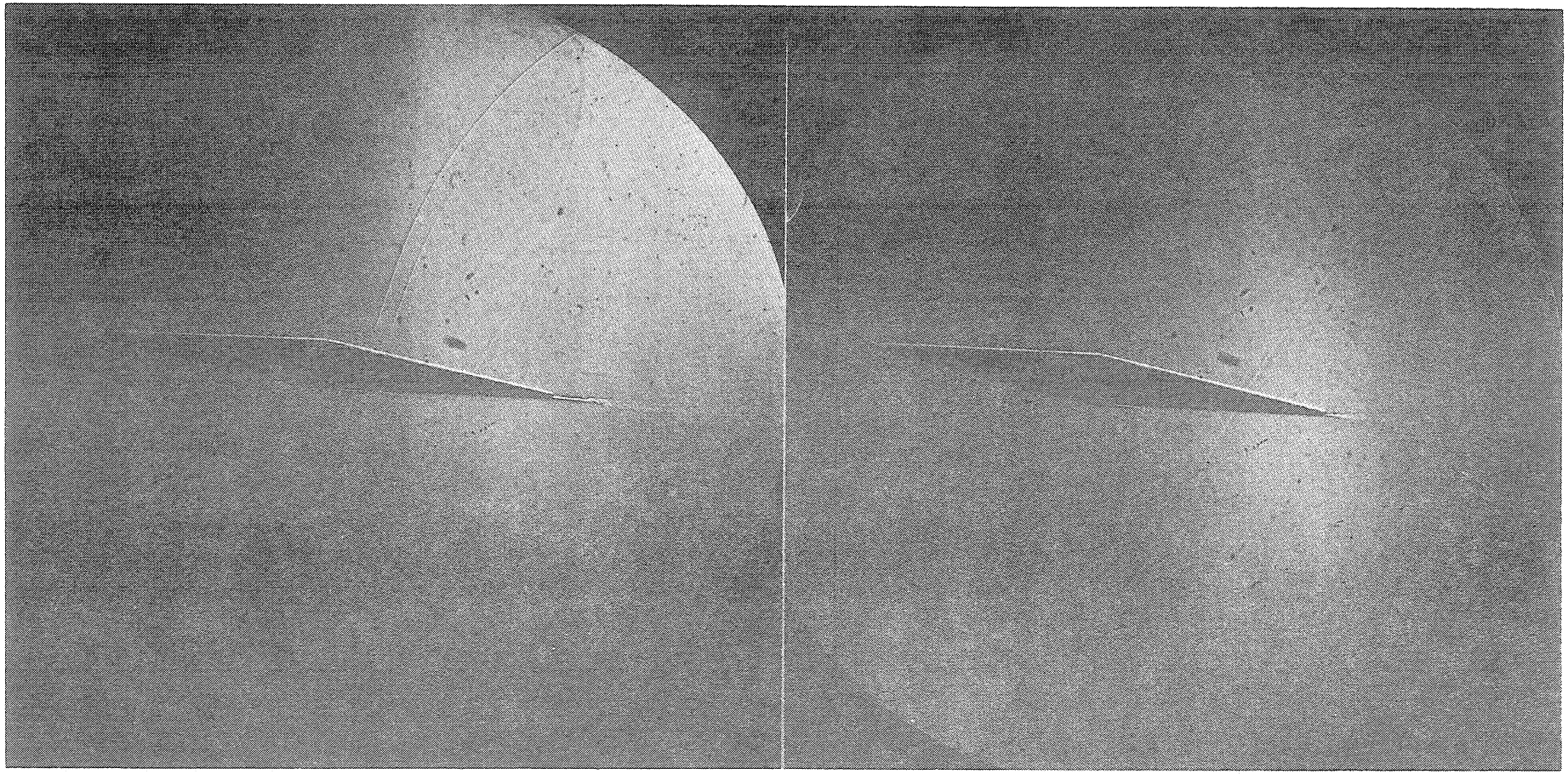

Figure 76

τ = 307
M = 0.60
Angle of Attack = 8°

Figure 77

τ = 605
M = 0.60
Angle of Attack = 8°

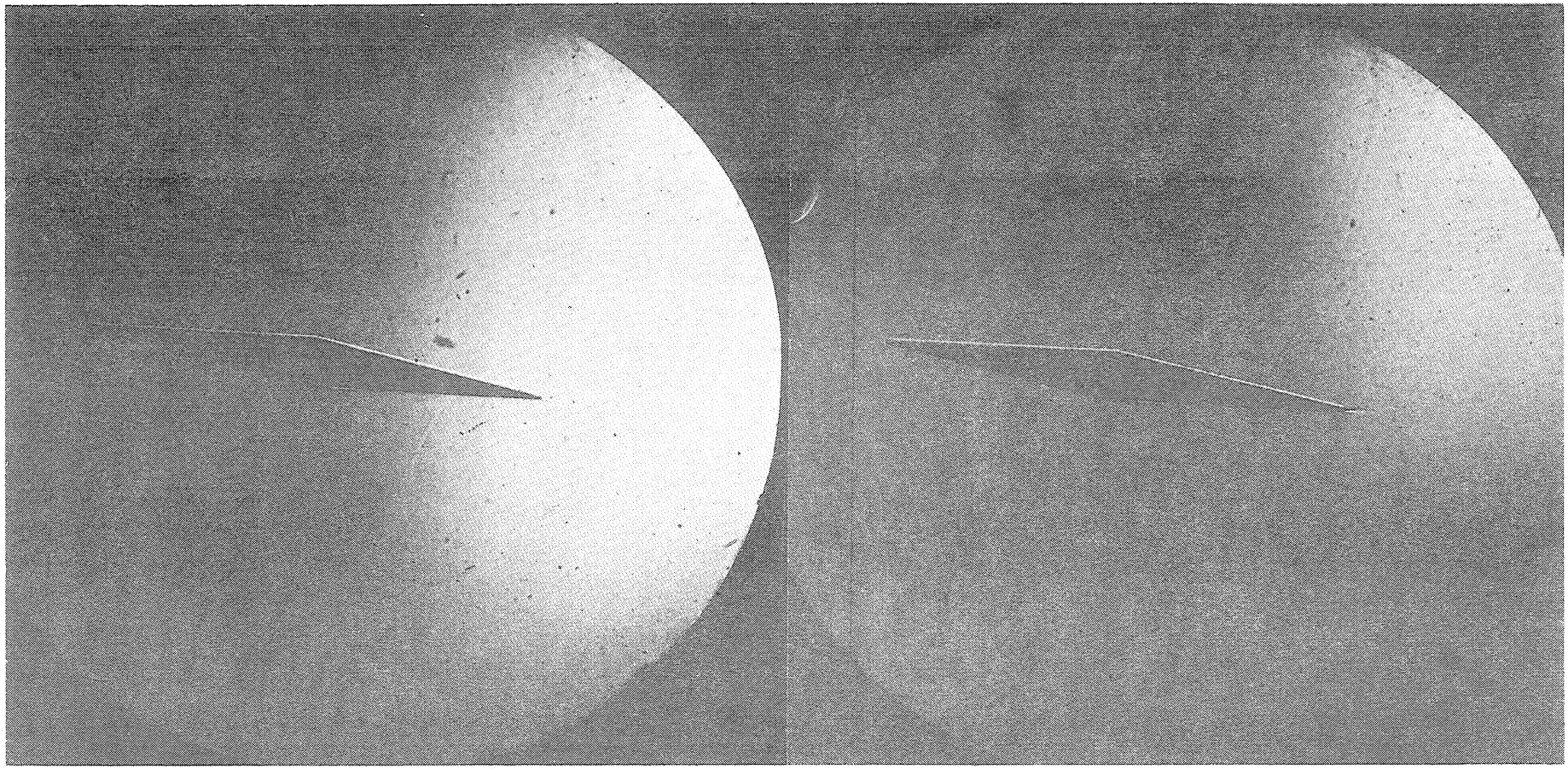

Figure 78

γ = 1005
M = 0.60
Angle of Attack = 8°

Figure 79

γ = 1805
M = 0.60
Angle of Attack = 8°

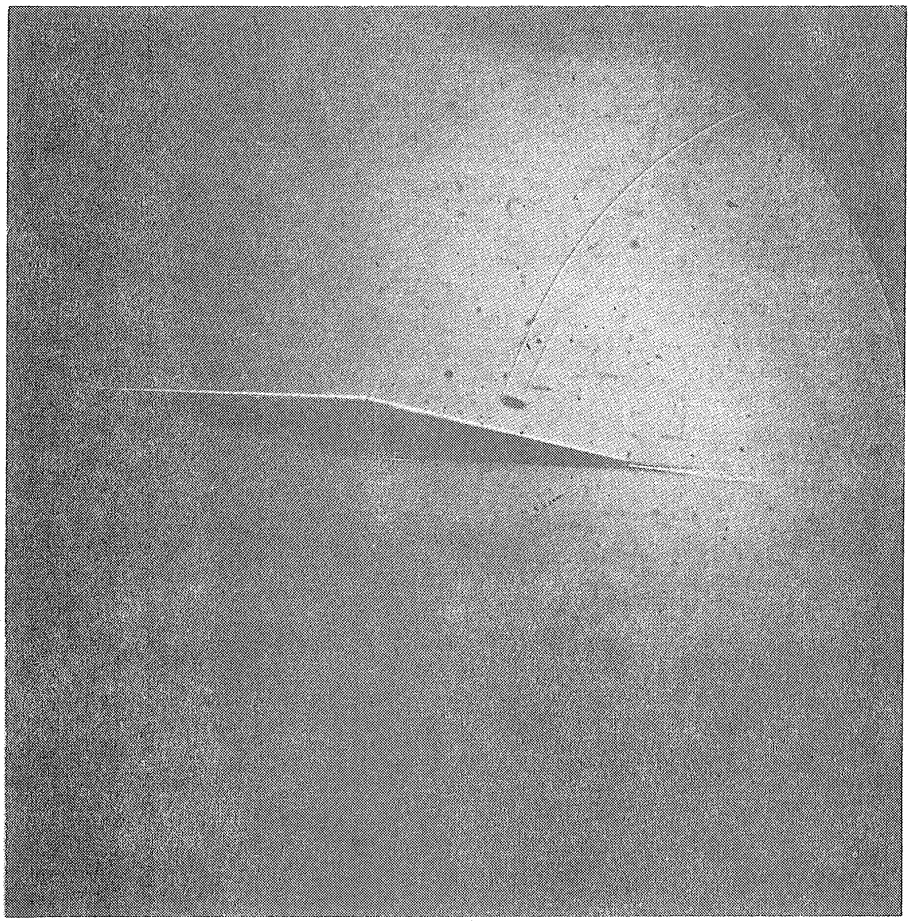

Figure 80

γ = 254
M = 0.70
Angle of Attack = 8°

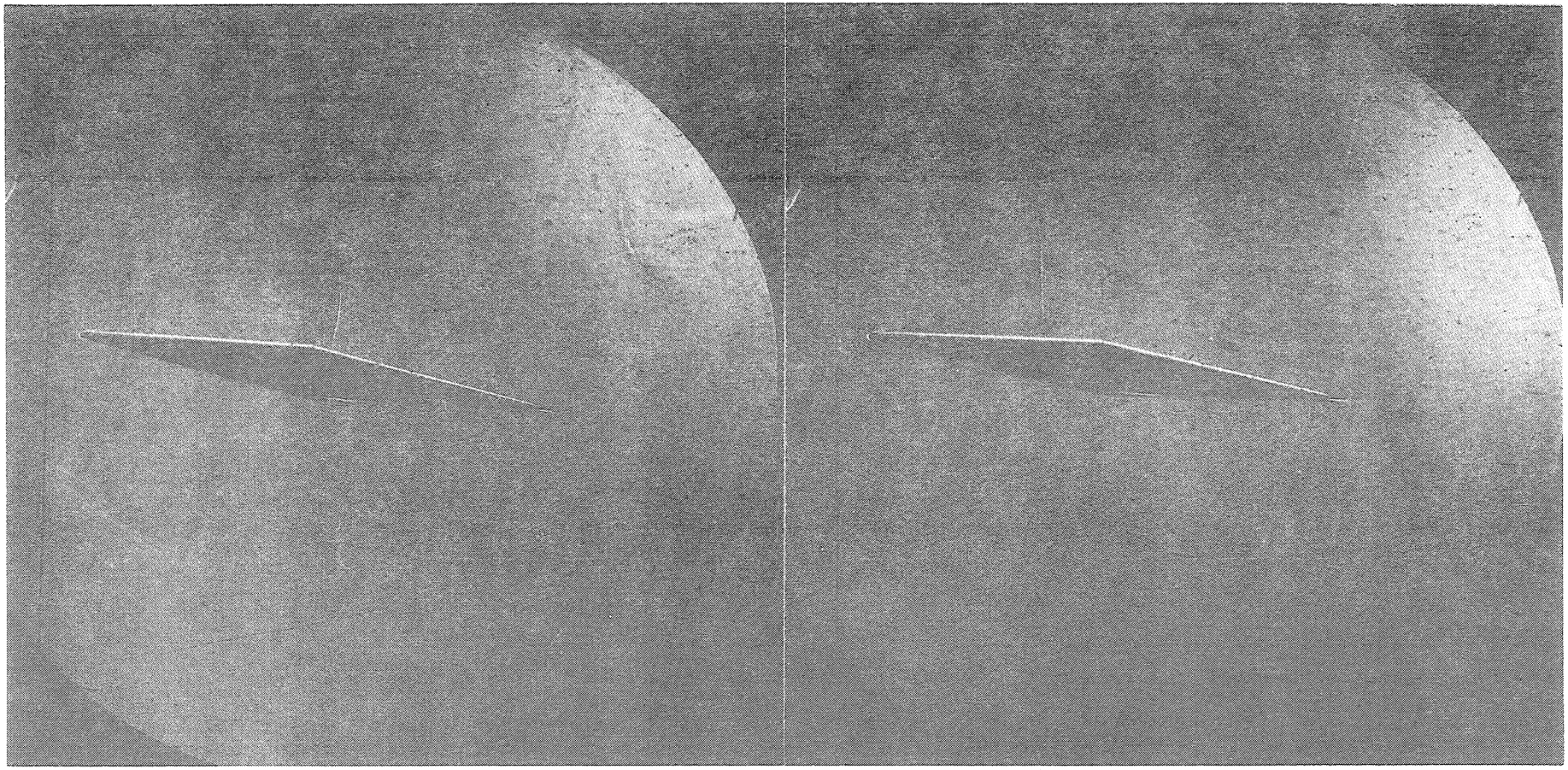

Figure 81

γ = 55½
M = 0.70
Angle of Attack = 8°

Figure 82

γ = 85½
M = 0.70
Angle of Attack = 8°

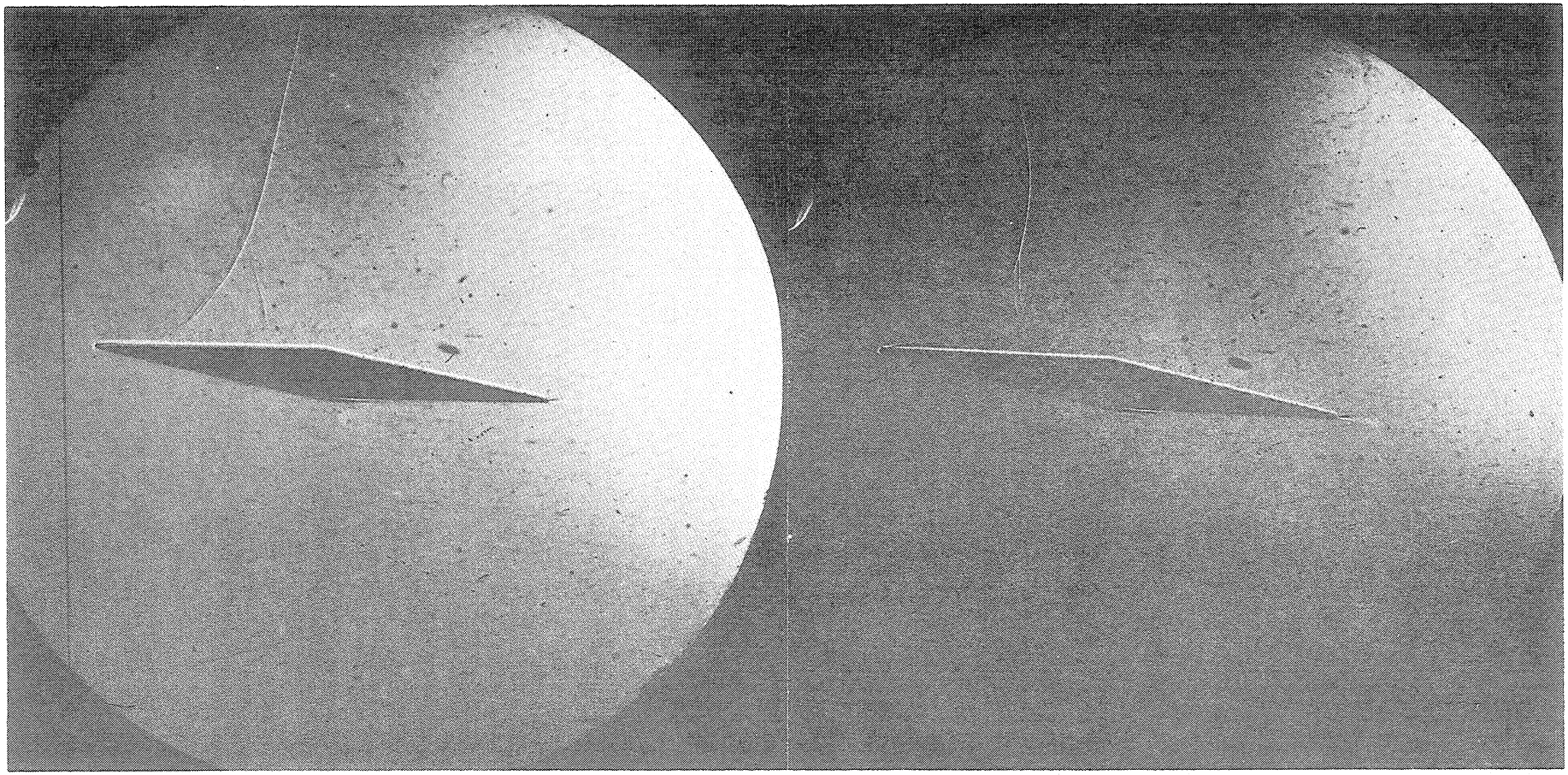

Figure 83

τ = 1259
M = 0.70
Angle of Attack = 8°

Figure 84

τ = 1649
M = 0.70
Angle of Attack = 8°

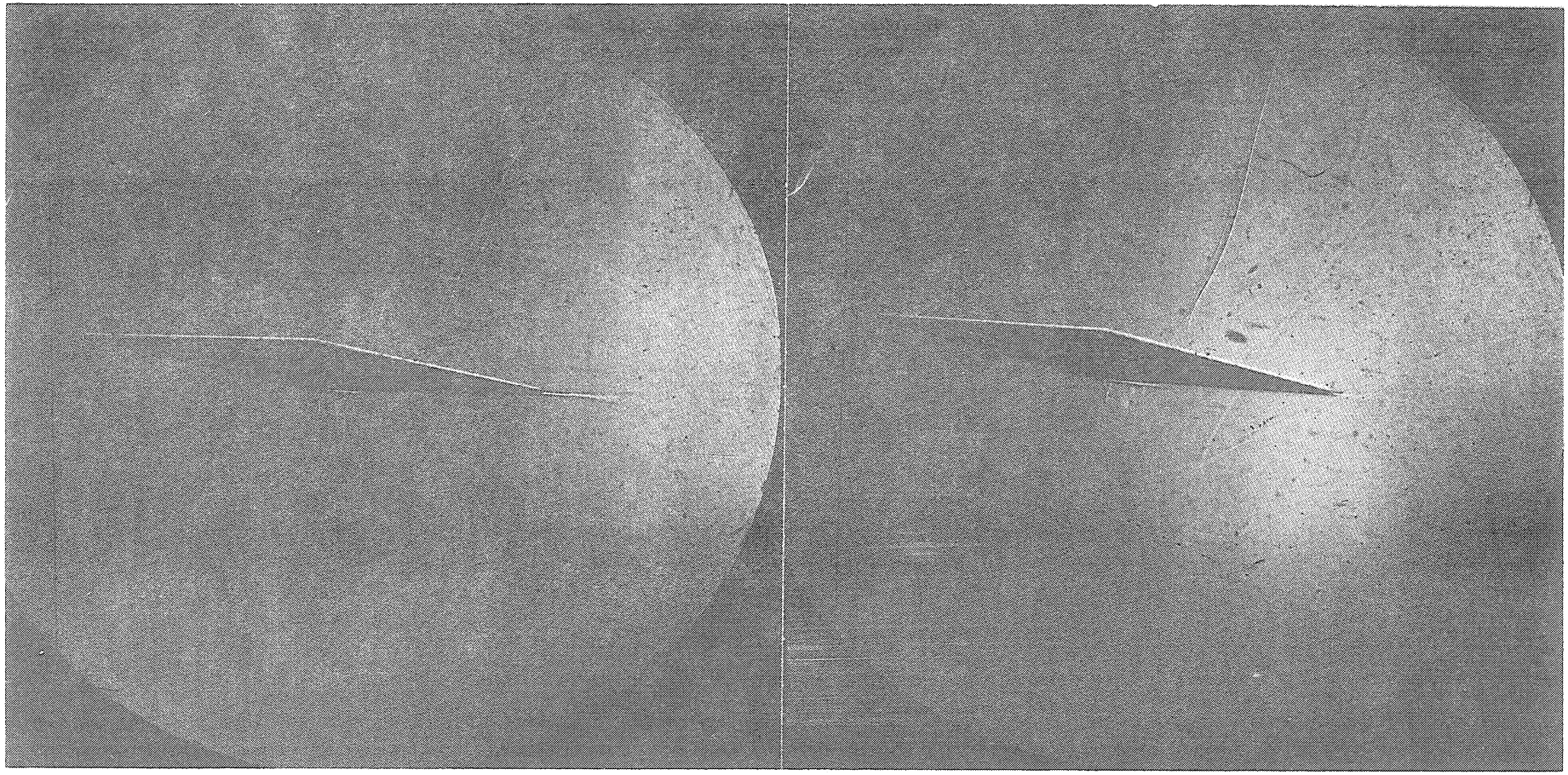

Figure 85

τ = 295
M = 0.79
Angle of Attack = 8°

Figure 86

τ = 497
M = 0.79
Angle of Attack = 8°

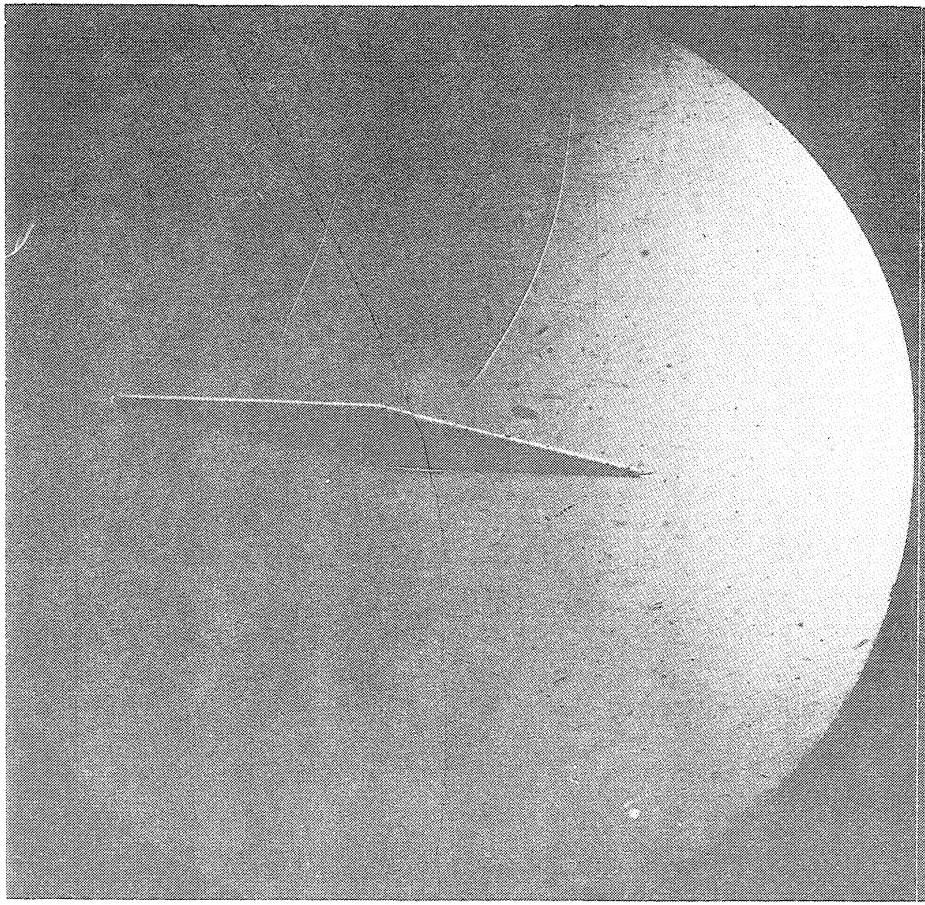

Figure 87

γ = 1015
M = 0.79
Angle of Attack = 8°

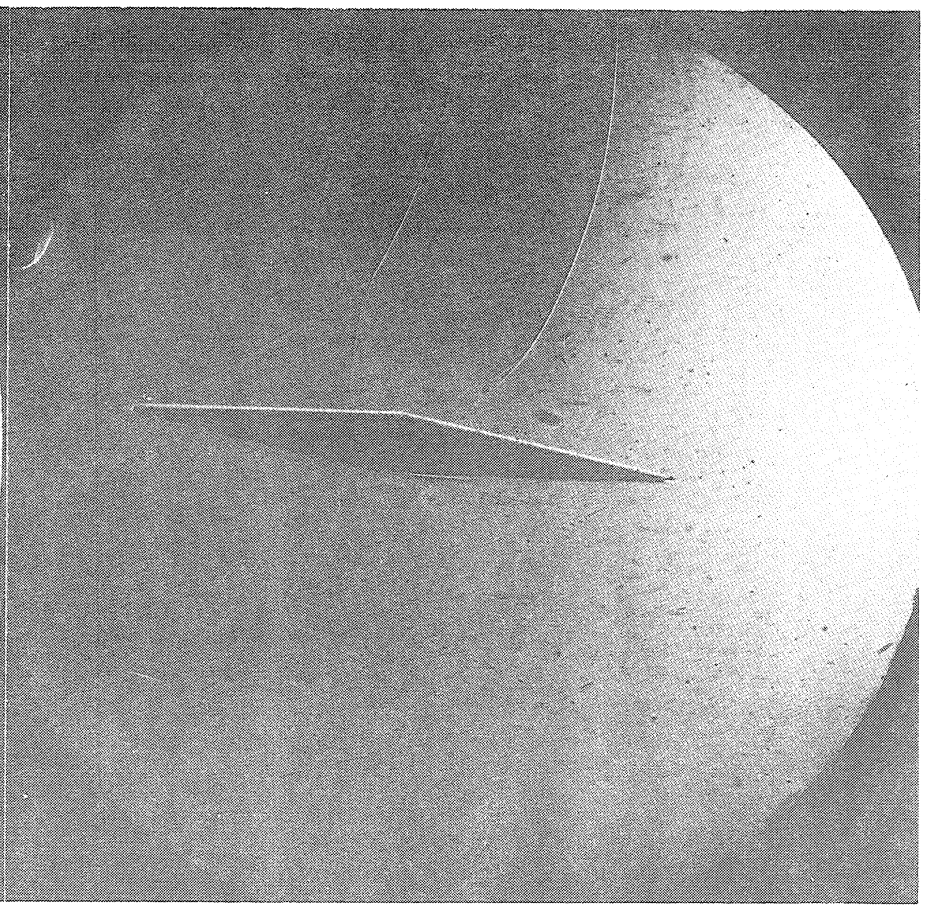

Figure 88

γ = 1195
M = 0.79
Angle of Attack = 8°

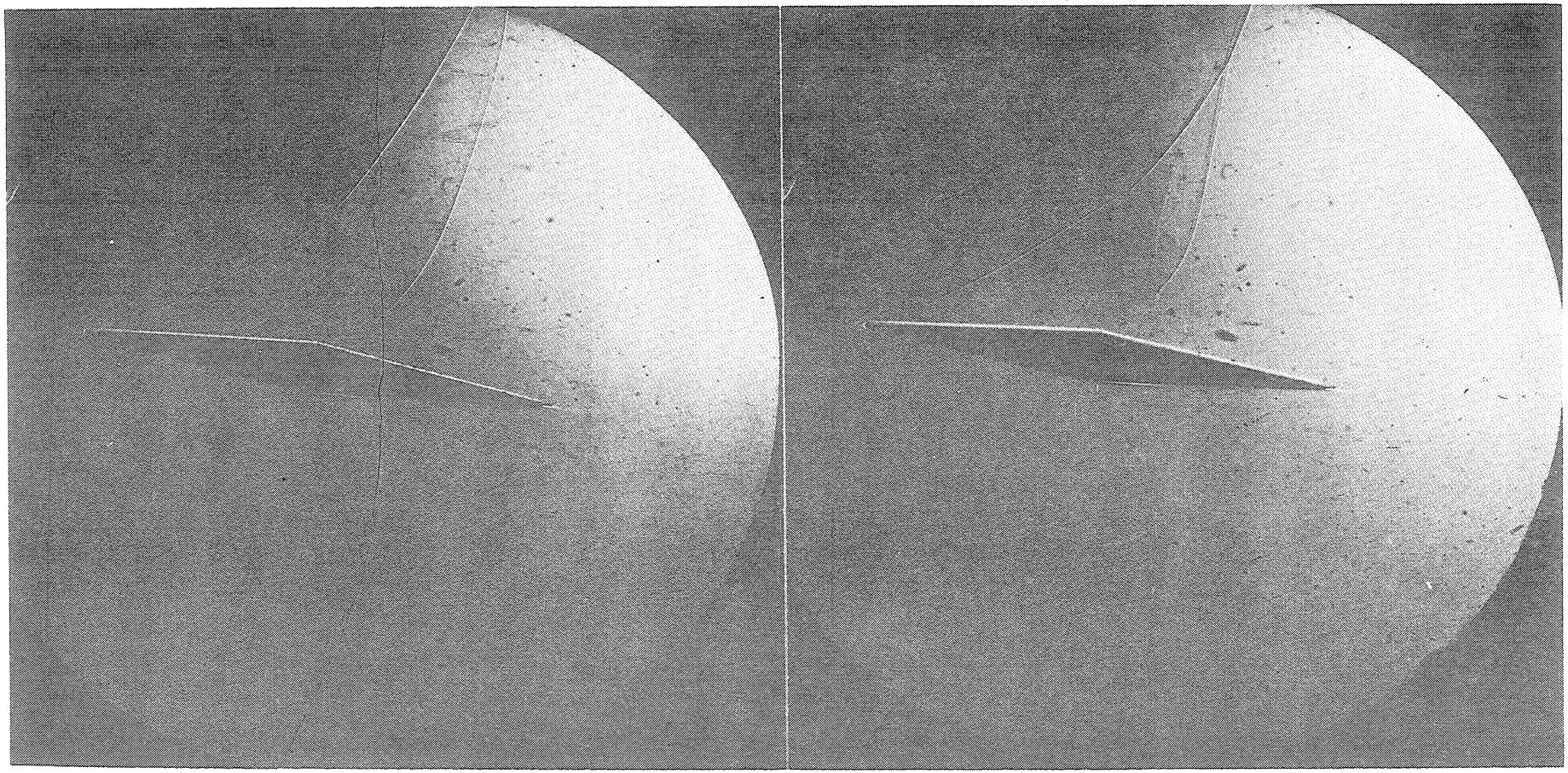

Figure 89

γ = 1397
M = 0.79
Angle of Attack = 8°

Figure 90

γ = 1495
M = 0.79
Angle of Attack = 8°

lower surface. The first of these, at least, is a lambda shock. Such configurations have also been observed by Ackeret, Feldman , and Rott[1] in wind tunnel tests in connection with a laminar boundary layer ahead of the first shock. They are made possible by the acceleration of the flow in the neighborhood of the corner. After passing through the first shock, the flow is again accelerated to supersonic speed, and another shock is possible. It appears that this can occur only for slightly supersonic speeds.

When the tail of the tube shock passes, these shocks disappear, but later at least the first of them reappears. The latest photograph of the set is probably indicative of a choked condition. The strong lambda shock formed would probably extend to the walls of the tube.

5. The Choking of a Duct in Initially Supersonic Flow

Because the flow in the shock tube is established suddenly, the phenomenon of the choking of a ducted body in the shock tube takes place in a manner different from that observed in the wind tunnel.

In order to photograph this process, a model consisting of two 5-degree wedges placed side by side at approximately zero angle of attack was mounted in the tube (see Figures 91-99). The distance from the most forward part of the duct to its minimum section was approximately one inch. The leading edges of the wedges were 3/4 inch apart. This was found (by trial and error) to be approximately the maximum distance which would allow the choking process to occur in the time available at the Mach number of the test, 1.16.

In 91 the tube shock has just passed the upper airfoil. The intersection between the two bow waves is apparently regular; and one of these

---

[1] loc. cit. ante, p. 128

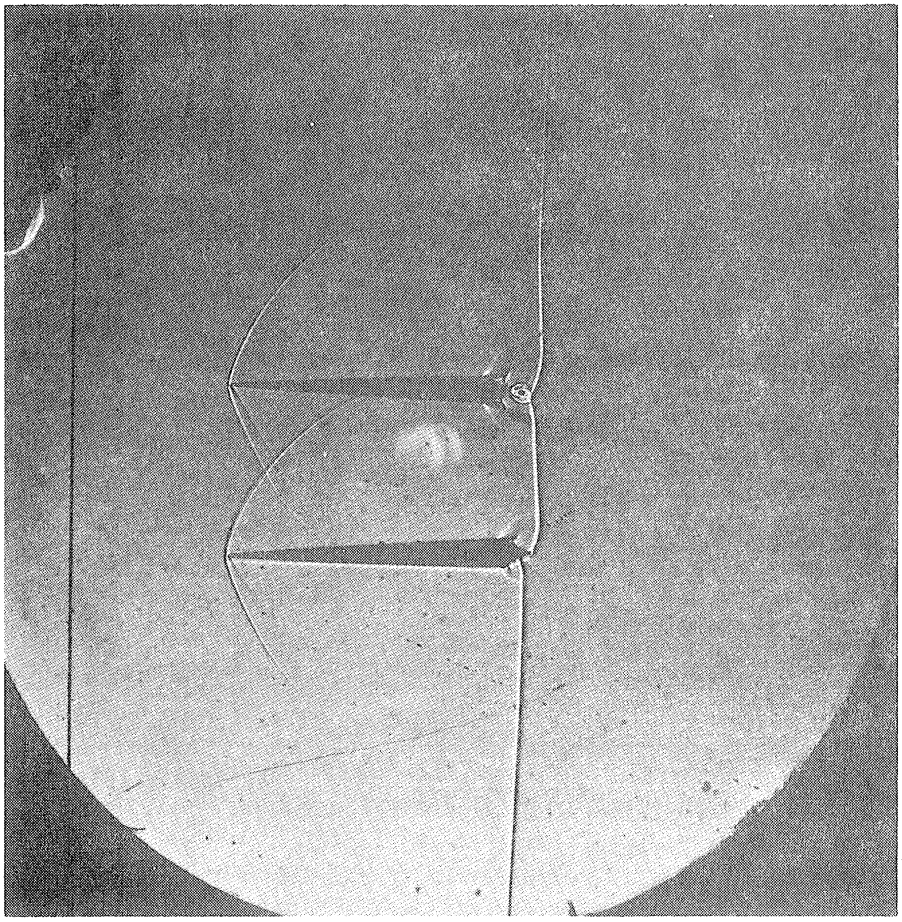

Figure 91

τ = 45

M = 1.16

Figure 92

γ = 75
M = 1.16

Figure 93

γ = 75
M = 1.16

Figure 94
τ = 111
M = 1.16

Figure 95
τ = 146
M = 1.16

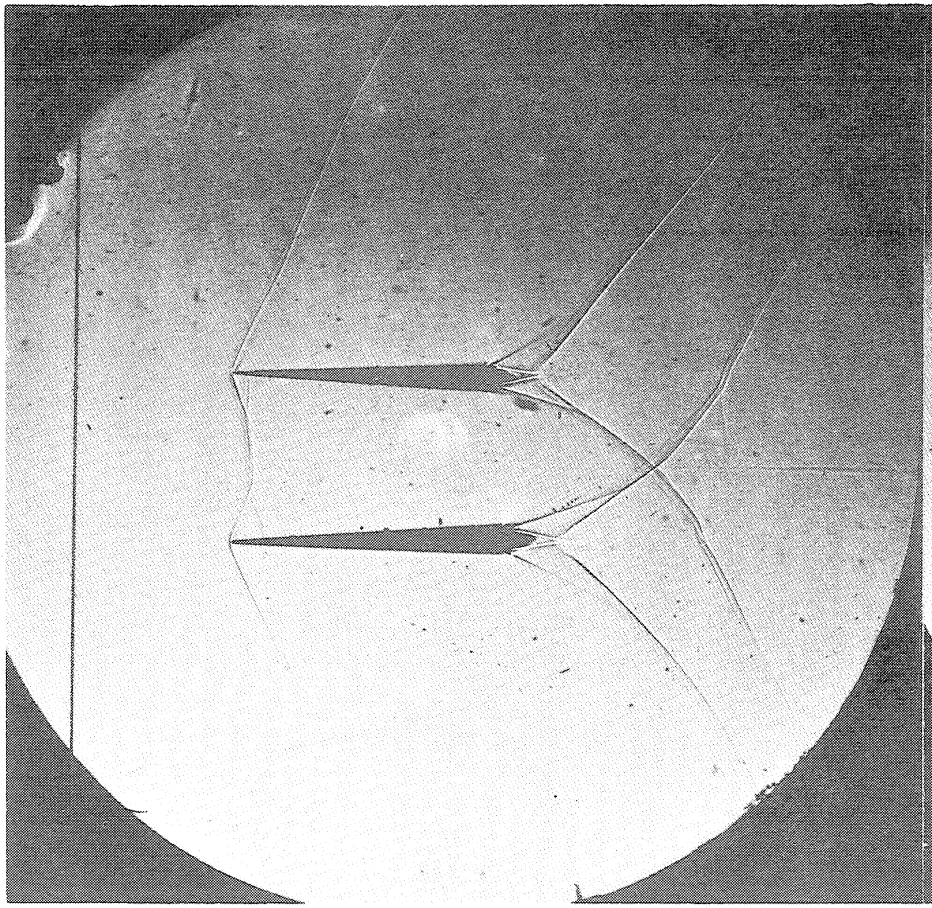

Figure 96

τ = 195
M = 1.16

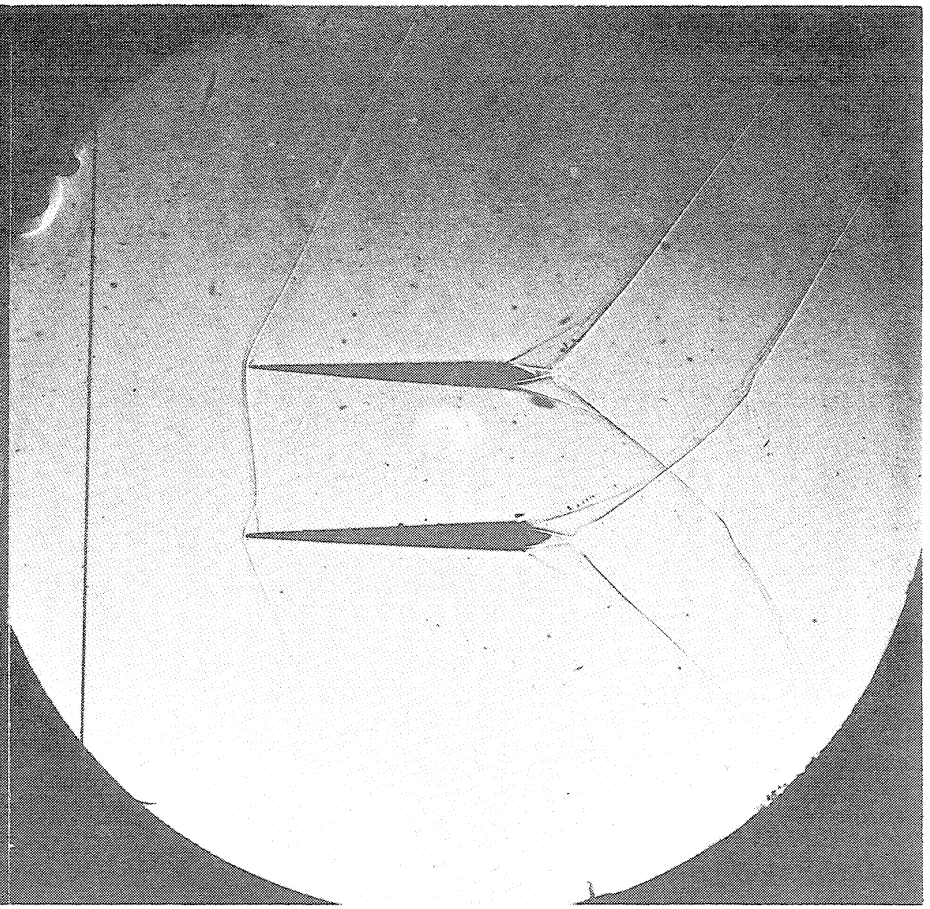

Figure 97

τ = 244
M = 1.16

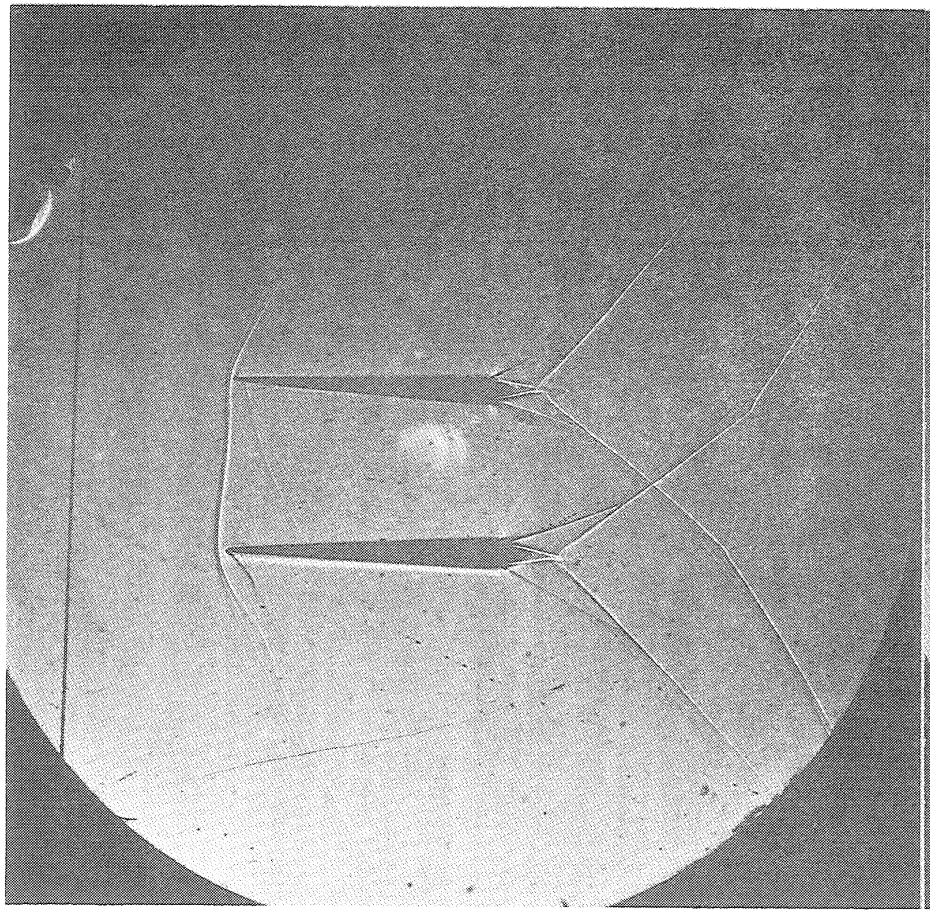

Figure 98

τ = 296
M = 1.16

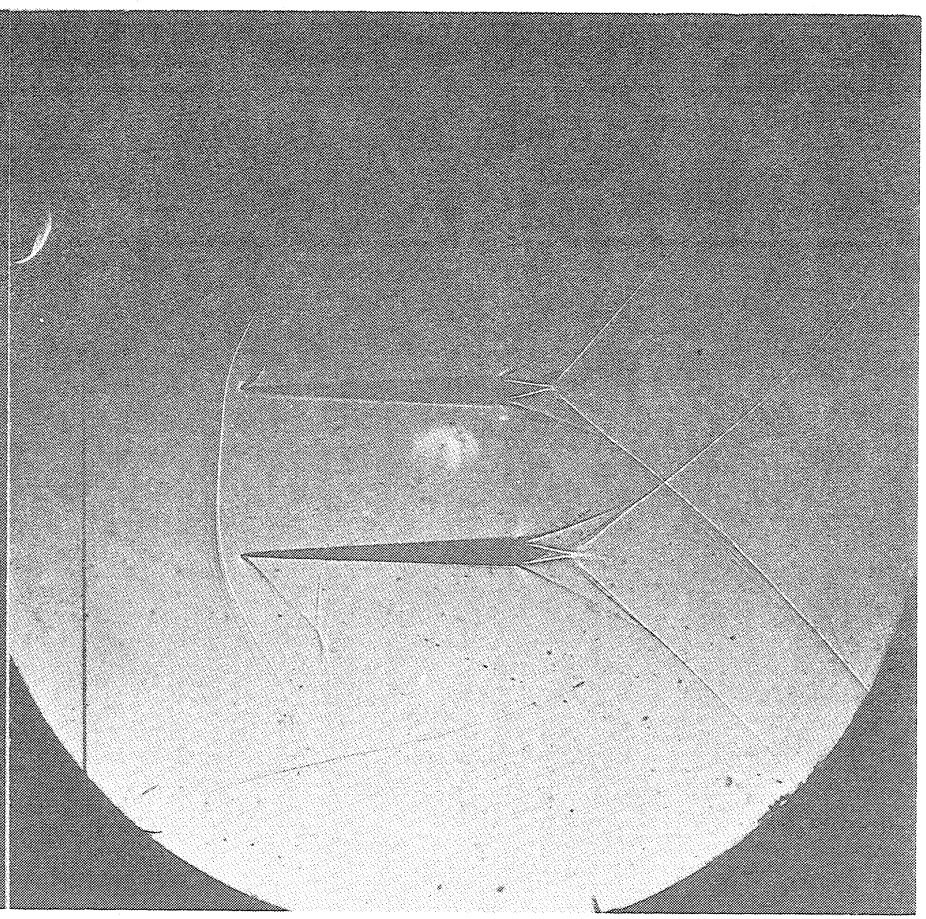

Figure 99

τ = 407
M = 1.16

waves is reflected from the model opposite that at which it originated.

Figures 92 and 93 are duplicates in terms of time delay[1]. They are remarkably similar: the positions, magnitudes, and directions of rotation of the numerous trailing vortices appear to be identical, and the tube shocks, which travel at approximately one millimeter per microsecond, occupy on each plate nearly the same position. This seems to indicate that the vortices appear in an ordered rather than in a random fashion.

In the remainder of the development, the distances between the primary Mach intersections increases, leaving behind an increasing area of subsonic flow, until finally these intersections reach the two airfoils, and a detached shock wave is formed. During this time the reflections which have occurred move forward, eventually overtaking and strengthening the main wave.

In wider ducts, in which choking would still occur at the same Mach number, the time available in the flow is too short to allow observation of the phenomenon. Photographs taken with the wedges at over three times the separation which they have here indicate that the choking process had started as in the above photographs but that no steady state, choked or not, had been reached in the available time. For such investigations, one would very definitely require a longer duration of constant flow.

There are two other points worthy of mention. The first is that in Figures 92 and 93 there are oblique shocks associated with the point of separation or of sudden thickening of the boundary layer behind the minimum

---

[1]After 92 had been developed, the small piece of cellophane caught between the model and the window near the nose of the upper airfoil was detected. It caused the small detached shock wave visible in the photograph. This piece was removed and a second photograph, 93 was taken with the same time delay. The upper airfoil has slipped slightly in the second photograph.

section, and that they move to positions just behind the expansion regions at the corners, where they remain. This is the second observation of these waves. The first was in Section 3. Their cause is the same here as in the previous experiments.

The second point is that if these experiments had been performed in a supersonic wind tunnel of the size of the tube, undoubtedly the tunnel itself would have been choked. The relatively thick boundary layers which occur in wind tunnels interact with the shock waves formed and are generally considered to be partially responsible for choking. These experiments indicate that either the boundary layer in the tube is very thin (which is certainly to be expected since it has been in existence for such a short time) or that there has not been sufficient time for choking of the tube to develop, or both. In any case, it seems established that the shock tube has considerable potentialities in the low supersonic range.

6. Higher Mach Number Flow in Gases Other than Air

A few exploratory photographs have been taken using carbon tetrachloride vapor and freon-12 in the expansion chamber. These gases were chosen because they exhibit unusually low values of sound speed, and hence can be expected to give correspondingly high Mach numbers, other things being equal. Their behavior can be expected to depart from that of an ideal gas, and consequently the formulae which have been developed in Chapter I may not be applicable. It is a happy accident that the index of refraction is high in both gases, with the result that the shadowgrams show high contrast.

In one experiment, it was desired merely to exhibit a very high value of the Mach number. For this purpose, carbon tetrachloride vapor

was used in the expansion chamber at the rather low pressure of 50 mm. of oil (3.33 mm. of Hg) and helium was used in the expansion chamber at atmospheric pressure. The model was the 5-degree wedge used in the starting vortex experiment. Two photographs, Figures 100 and 101, were taken with delays differing by about 50 microseconds. The remarkable features of the pictures are that the Mach number is apparently in the neighborhood of 3.5 (if, for lack of a better way, it is deduced from the bow-wave angle with the assumption that this is the Mach angle), that the shock waves are not nicely formed, and that the contact surface is very close to the principal shock. It was also remarkable that after the firings the interior of the tube smelled strongly of chlorine gas and that the familiar odor of carbon tetrachloride was not noticeable. Obviously there was considerable dissociation of the carbon tetrachloride.

For the rest of the experiments one of the wedges used in the detached shock wave study served as the model. Figures 102 and 103 are two photographs in carbon tetrachloride which show excellent contrast. The numerous little shocks starting from the model are caused by slight ridges left in its machining or deliberately scratched onto its surface. The particular contact discontinuity which is part of the Mach shock formation is very well defined. In 103 the shock wave which is about halfway along the model apparently originated at the forward corner and is being swept downstream. Eventually it would form part of the wake.

A set of photographs, Figures 104-106, was made using helium-freon-12. These were made using one value of p_o but different time delays. Qualitatively they are the same as those in carbon tetrachloride. However, the contrast is slightly lower in this case.

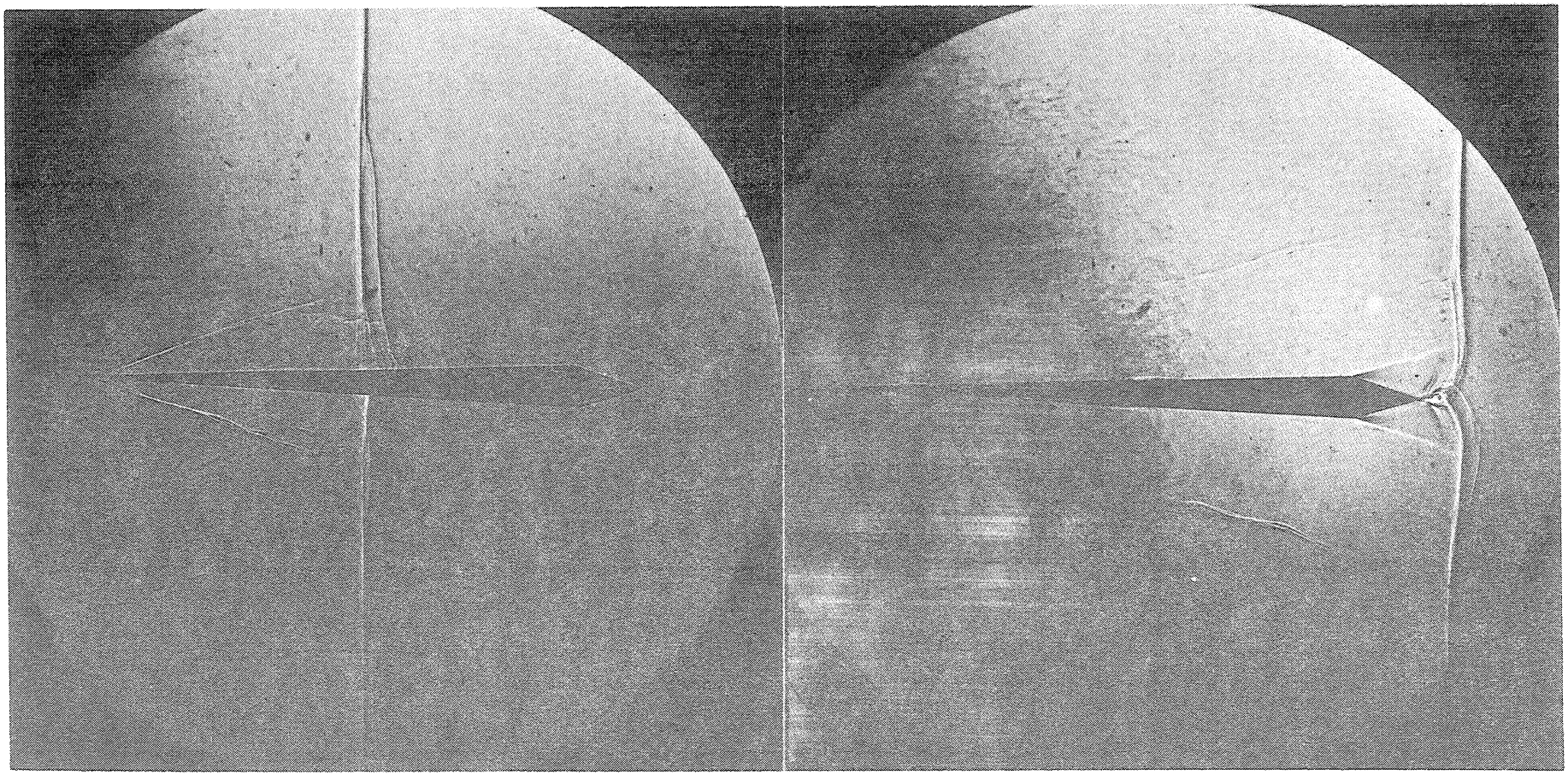

Figure 100

Figure 101

Helium-Carbon Tetrachloride Photographs

These pictures differ in time by 50 microseconds.

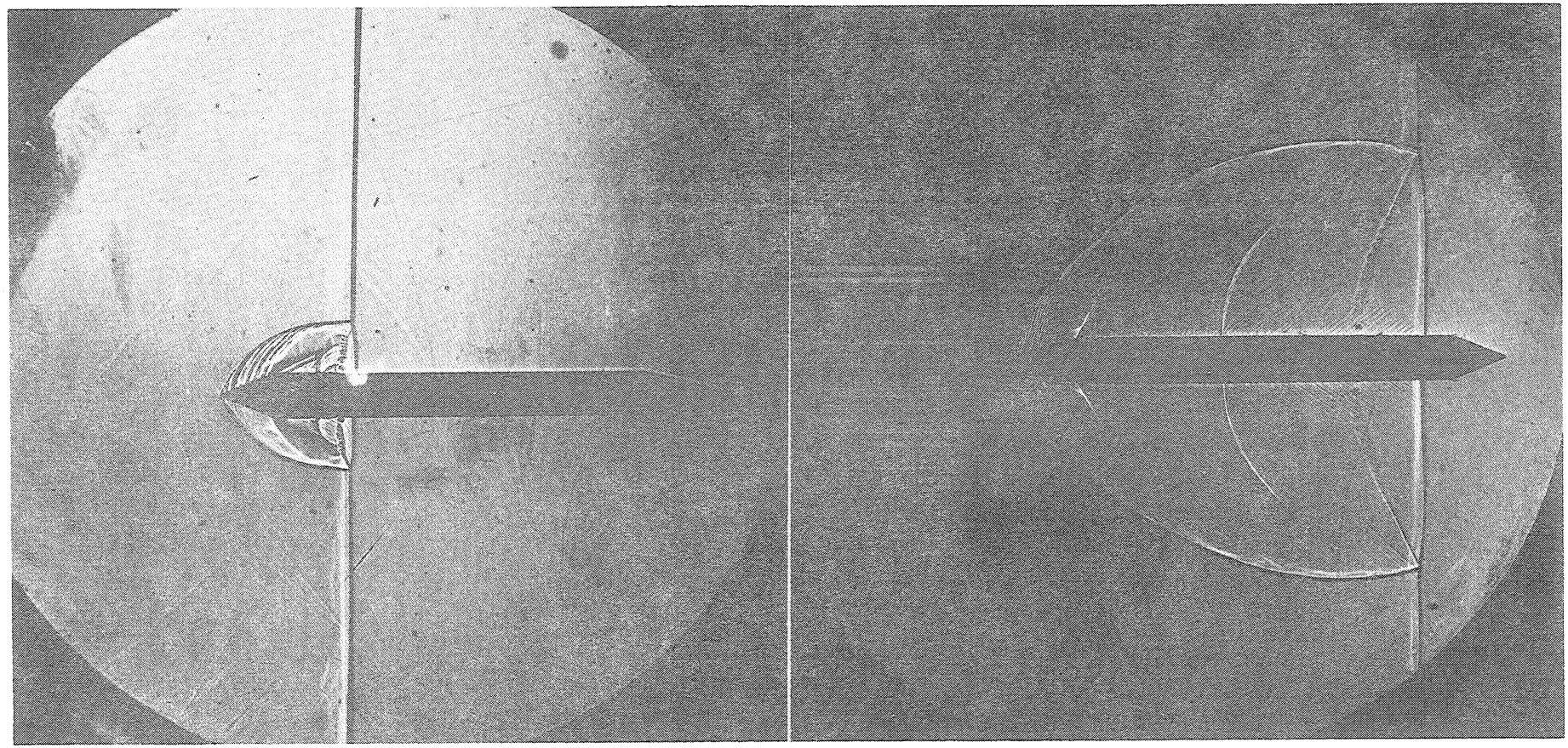

Figure 102

Figure 103

Helium-Carbon Tetrachloride

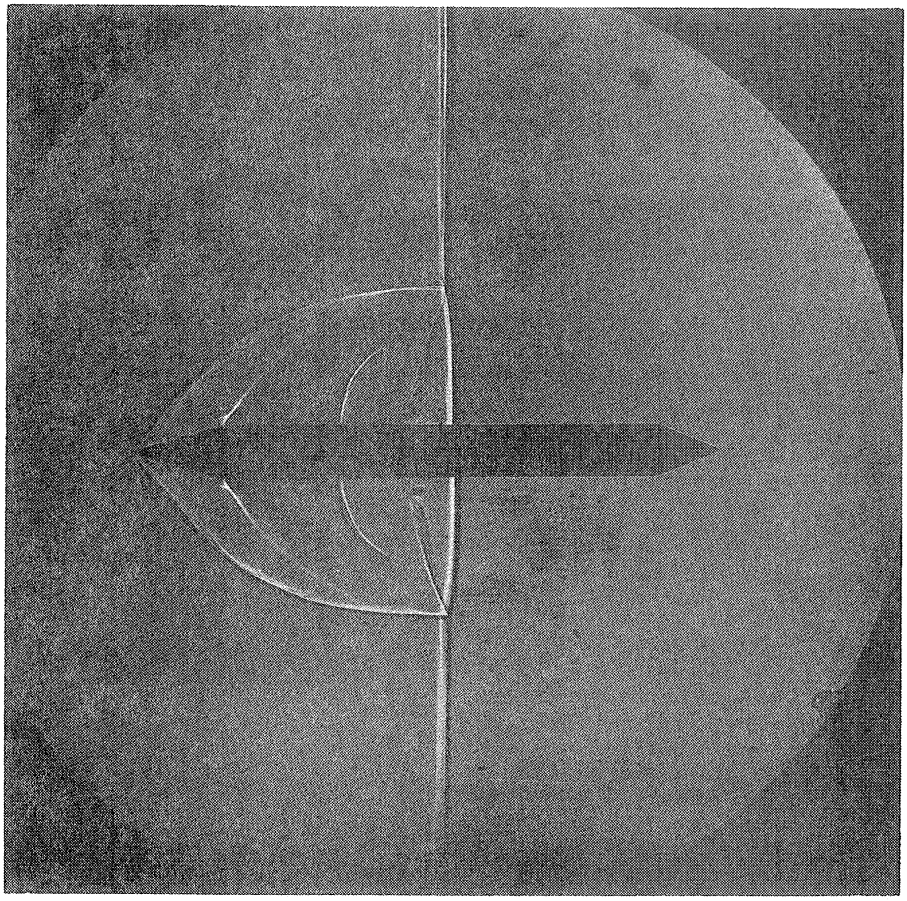

Figure 104

Helium-Freon-12

τ = 80

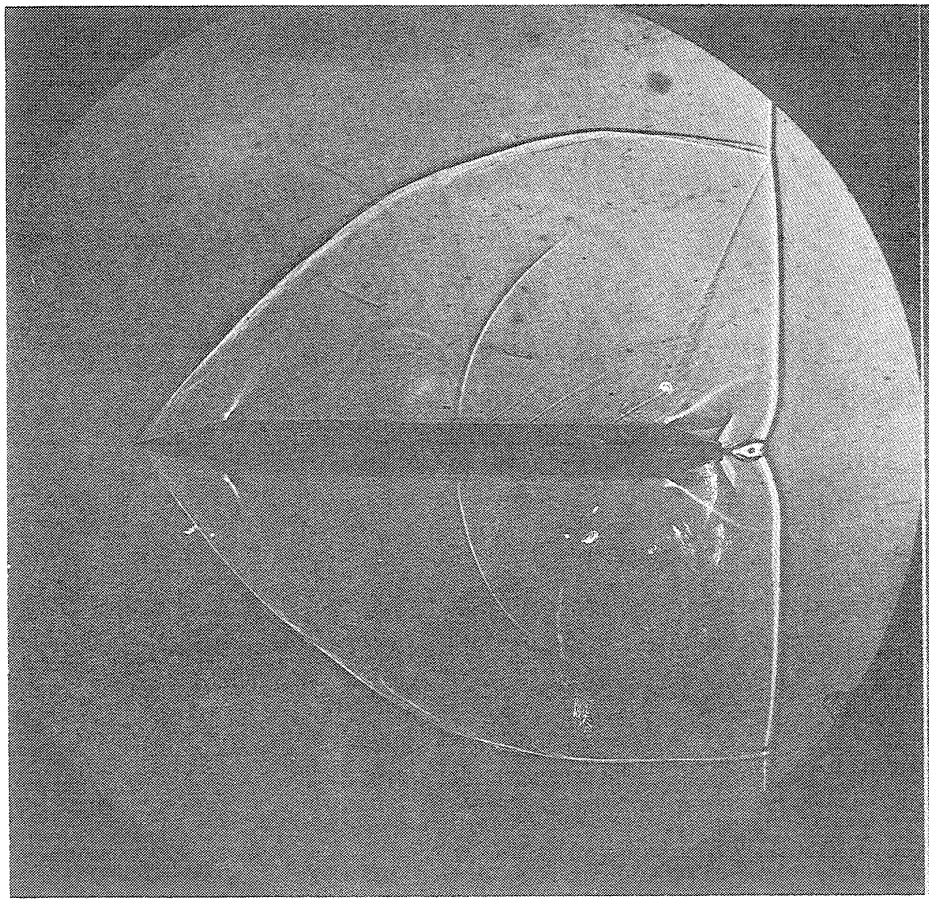

Figure 105

Helium-Freon-12
τ = 186

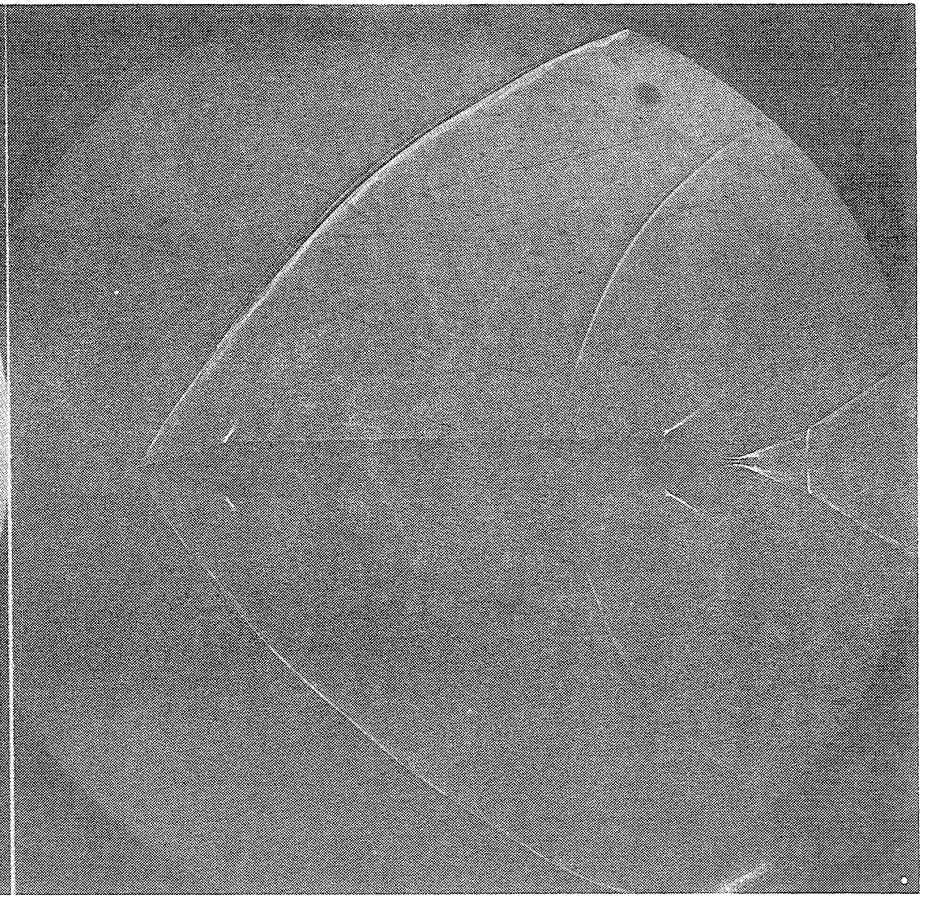

Figure 106

Helium-Freon-12
τ = 286

CONCLUSIONS

Chapter I

The theory of the ideal shock tube (a tube of uniform cross section, divided into two chambers of differing gas pressure by a diaphragm which is assumed to burst instantaneously) predicts that two regions of uniform flow, separated by a temperature discontinuity or contact surface, will follow the shock which is produced when the diaphragm bursts. Either of these regions may be made subsonic, transonic or supersonic, depending on the shock strength employed. The duration of either, as observed at a test section, depends on the length of the tube and on the shock strength.

Chapter IV

The failure of the actual diaphragm to burst instantaneously causes the flow regions to differ from those predicted by the theory of the ideal shock tube; nonetheless, the shock strength is very nearly that predicted, and the flow between the shock and the contact surface is very uniform and is of only slightly smaller duration than that predicted. The flow behind the contact surface, however, is not uniform.

Chapter V

The duration of uniform flow is long enough to provide for the establishment of stationary flow configurations in the neighborhood of

models of convenient size, when the flow is supersonic. The shock tube thus has considerable potentialities for research in this region. One of the valuable features of the shock tube is its ability to show the buildup of stationary flow configurations.

Several phenomena which are familiar in wind tunnel practice are observed in the shock tube: lambda shocks, Mach shocks, boundary layers, and flow separation. Starting vortices in supersonic flow are also easily observed.

Photographs of the choking of a small duct at Mach number 1.16 show that, while the choking process can be investigated in the shock tube, a longer tube than the one used is required to study the process in ducts which are less acutely constricted.

TABLE I. APPARENT MACH NUMBER WITH $M_p = 1.15$

τ micro-seconds	β degrees	M_{ap}		τ micro-seconds	β degrees	M_{ap}
19	62-1/2?	1.201?		416	69-1/4	1.154*
65	70	1.151*		419	detached	
69	65-1/2	1.176		419	61-1/2	1.211
116	70-1/2	1.149*		421	61-1/4	1.213
120	69	1.155		436	64	1.187
165	70-1/2	1.149*		465	curved	*
168	66-1/2	1.169		468	70	1.151
169	68	1.160		469	61	1.216
216	68-1/4	1.159*		511	58	1.250
218	66-1/4	1.171		520	67-1/2	1.163
266	67-1/2	1.163*		570	contact surface	
268	63-1/4	1.194		574	59	1.238
269	64?	1.188?		620	contact surface	
316	66-3/4	1.168*		670	29	2.20
319	67-3/4	1.161?		670	27-1/2	2.31
364	64-1/2	1.184		717	29	2.20
366	65-1/2	1.176*		769	29	2.20
369	68-3/4	1.156		770	27-1/2	2.31
369	60	1.226		818	30-1/4	2.11

TABLE I, CONTINUED

τ micro-seconds	β degrees	M_{ap}		τ micro-seconds	β degrees	M_{ap}
819	27-1/2	2.31		2072	28-3/4	2.21
871	28-1/4	2.25		2564	30	2.13
963	26-1/4	2.42		3066	32	2.00
967	27	2.35		3543	33-3/4	1.91
1173	27	2.35		4066	34-3/4	1.86
1360	27-1/4	2.33		4571	36-1/4	1.91
1567	28	2.27		5061	36-3/4	1.77

*Taken with helium in the compression chamber; others with air in both chambers.

TABLE II. APPARENT MACH NUMBER WITH $M_p = 1.20$

τ micro-seconds	β degrees	M_{ap}		τ micro-seconds	β degrees	M_{ap}
39	66-3/4?	1.162?		244	66-1/2?	1.169?
90	66-3/4	1.180		290	62-1/2	1.201
139	62	1.206		338	61	1.216
194	62	1.206		388	61-1/2	1.210

TABLE III. APPARENT MACH NUMBER WITH M_p = 1.25

τ micro-seconds	β degrees	M_{ap}		τ micro-seconds	β degrees	M_{ap}
61	59-1/4	1.235		262	59	1.237
117	58-3/4	1.240		310	58?	1.250?
162	58-3/4	1.240		316	58	1.250
210	59-1/4	1.235		364	57-1/4?	1.259?
212	58-1/2	1.244				

TABLE IV. APPARENT MACH NUMBER WITH M_p = 1.30

τ micro-seconds	β degrees	M_{ap}		τ micro-seconds	β degrees	M_{ap}
13	52-1/2?	1.330?		233	53-3/4	1.309
36	53-3/4	1.309		237	61-1/2*	1.210*
82	54	1.305		282	53-1/2	1.313
138	53-1/2	1.313		287	53-3/4	1.309
187	53-3/4	1.309		334	55?	1.290?

*It is possible that p_o was inadvertently set to the value required for M_p = 1.20 in this shot.

TABLE V. APPARENT MACH NUMBER WITH $M_p = 1.35$

τ micro-seconds	β degrees	M_{ap}		τ micro-seconds	β degrees	M_{ap}
9	52-1/2?	1.330?		160	51-1/4	1.353
58	50-3/4	1.362		210	50-1/2	1.367
110	50-1/2	1.367		258	50-1/2	1.367

TABLE VI. APPARENT MACH NUMBER WITH $M_p = 1.40$

τ micro-seconds	β degrees	M_{ap}		τ micro-seconds	β degrees	M_{ap}
23	49-3/4	1.380		171	49	1.395
49	48-1/2	1.406		176	49-1/2	1.385
53	49-1/2	1.385		201	49-1/4	1.390
71	48-1/2	1.406		223	49	1.395
128	49	1.395		254	48-3/4	1.400
150	48-1/2	1.406				

TABLE VII. APPARENT MACH NUMBER WITH M_p = 1.45

τ micro-seconds	β degrees	M_{ap}		τ micro-seconds	β degrees	M_{ap}
7	50-1/4?	1.370?		129	46-1/2	1.453
39	46-1/4	1.458		159	46-1/2	1.453
65	46-1/4	1.458		190	46-1/2	1.453
98	46-3/4	1.448		220	46-1/2	1.453

TABLE VIII. APPARENT MACH NUMBER WITH M_p = 1.50

τ micro-seconds	β degrees	M_{ap}		τ micro-seconds	β degrees	M_{ap}
10	45-1/2?	1.477?		101	44-1/2	1.505
40	44-3/4	1.496		133	44-1/2	1.505
70	44-3/4	1.496		162	44	1.518

TABLE IX. DETACHMENT, x, OF BOW-WAVE FROM 1/4-INCH WEDGE WITH 45-DEGREE WEDGE ANGLE

M = 1.10	
τ μ-sec.	x mm.
38	2.4
45	3.0
94	6.3
94	6.3
144	9.2
183	11.5
210	12.5
242	13.9
296	16.2
348	18.0
396	19.0
441	21.7
498	21.5
524	22.5

M = 1.20	
τ μ-sec.	x mm.
28	1.2
46	2.2
82	4.1
96	4.8
143	6.9
211	9.3
246	10.5
283	11.4
324	11.8
346	12.9
400	13.0

M = 1.30	
τ μ-sec.	x mm.
27	1.0
44	1.5
76	2.9
93	3.6
93	3.6
126	4.7
144	5.3
177	6.0
194	6.4
227	7.0
243	7.5
276	8.0
295	7.9
326	8.0

M = 1.40	
τ μ-sec.	x mm.
31	0.7
41	0.9
71	1.8
90	2.3
116	3.0
141	3.3
179	4.1
192	4.1
234	4.4

M = 1.50	
τ μ-sec.	x mm.
20	0.2
51	0.7
82	1.0
112	1.3
135	1.5
142	1.8
170	1.6

TABLE X. DETACHMENT, x, OF BOW-WAVE FROM 1/8-INCH WEDGE WITH 45-DEGREE WEDGE ANGLE

M = 1.10	
τ μ-sec.	x mm.
22	1.7
51	3.3
83	5.3
110	6.7
160	8.7
209	10.5
258	11.6
310	13.0
362	14.0
411	14.8
463	15.3
515	17.6

M = 1.20	
τ μ-sec.	x mm.
31	1.6
57	2.9
81	4.0
107	5.0
144	5.8
181	6.8
230	7.9
251	8.1
306	8.6
346	9.0
383	9.2
430	9.3

M = 1.30	
τ μ-sec.	x mm.
32	1.2
56	2.0
83	2.8
108	3.5
136	3.8
190	4.5
226	4.8
267	4.9
303	4.8

M = 1.40	
τ μ-sec.	x mm.
30	0.7
51	1.3
80	1.8
103	2.0
147	2.5
199	2.5
235	2.5

M = 1.50	
τ μ-sec.	x mm.
27	0.4
28	0.4
46	0.7
68	0.9
84	1.0
107	1.1
130	1.1
149	1.1

TABLE XI. DETACHMENT, x, OF BOW-WAVE FROM 1/16-INCH WEDGE WITH 45-DEGREE WEDGE ANGLE

M = 1.10	
τ μ-sec.	x mm.
6	0.3
20	1.2
54	3.3
84	4.6
116	5.6
155	6.6
214	8.2
251	8.9
314	10.1
358	10.5
414	11.0
464	11.0
508	11.6
509	11.1

M = 1.20	
τ μ-sec.	x mm.
9	0.3
27	1.2
58	2.5
75	3.0
107	3.7
154	4.3
156	4.4
209	5.1
258	5.8
260	5.4
260	5.5
304	5.6
339	5.7
339	5.7
372	5.9

M = 1.30	
τ μ-sec.	x mm.
4	0.1
25	0.8
54	1.5
57	1.9
103	2.3
155	2.6
204	2.9
257	3.0
305	2.5
305	2.8

M = 1.40	
τ μ-sec.	x mm.
26	0.6
50	1.0
50	1.2
76	1.1
101	1.3
152	1.3
201	1.3
248	1.4

TABLE XII. DETACHMENT, x, OF BOW-WAVE FROM 1/4-INCH WEDGE WITH 30-DEGREE WEDGE ANGLE

M = 1.10	
τ μ-sec.	x mm.
29	1.1
48	2.1
98	4.3
124	5.4
150	6.5
198	8.4
247	10.4
300	12.2
351	13.6
397	14.7
433	15.8
449	16.2
483	16.4
498	16.7

M = 1.20	
τ μ-sec.	x mm.
22	0.5
47	1.3
82	2.3
103	3.0
147	4.1
196	5.3
226	6.1
244	6.7
247	6.7
297	7.5
352	8.3
398	9.0
428	9.2

M = 1.30	
τ μ-sec.	x mm.
43	0.7
71	1.1
86	1.3
116	1.8
148	2.3
162	2.5
199	3.1
219	3.3
249	3.6
270	4.1
299	4.1
320	4.0

M = 1.40	
τ μ-sec.	x mm.
31	0.2
44	0.2
95	0.5
147	0.8
195	1.0
230	1.1
244	1.4
246	1.5

TABLE XIII. DETACHMENT, x, OF BOW-WAVE FROM 1/8-INCH WEDGE WITH 30-DEGREE WEDGE ANGLE

M = 1.10	
τ μ-sec.	x mm.
31	1.4
55	2.4
83	3.7
116	5.0
168	6.8
217	8.4
266	9.9
317	10.8
369	11.4
416	12.0
468	12.4
519	12.8

M = 1.20	
τ μ-sec.	x mm.
39	1.0
63	1.8
89	2.7
113	3.1
156	4.0
192	4.8
236	5.6
265	5.9
292	6.0
313	6.0
352	6.4
357	6.5
393	6.4
432	6.5
433	6.1

M = 1.30	
τ μ-sec.	x mm.
36	0.5
59	0.8
111	1.6
151	2.1
194	2.3
229	2.5
272	2.5
308	2.4

M = 1.40	
τ μ-sec.	x mm.
32	0.1
57	0.2
84	0.3
108	0.5
149	0.6
203	0.6

TABLE XIV. DETACHMENT, x, OF BOW-WAVE FROM 1/16-INCH WEDGE WITH 30-DEGREE WEDGE ANGLE

M = 1.10	
τ μ-sec.	x mm.
11	0.4
37	1.6
38	1.6
43	1.9
88	3.7
94	4.0
151	5.5
193	6.5
219	6.9
268	7.6
324	8.5
343	8.9
405	9.3
441	9.5
490	9.0
516	9.5

M = 1.20	
τ μ-sec.	x mm.
34	0.9
37	1.0
43	1.2
85	1.4
95	2.4
134	3.1
142	3.1
189	3.6
244	4.0
268	4.3
323	4.1
324	3.9
344	4.2
385	4.0
386	4.1
447	4.2

M = 1.30	
τ μ-sec.	x mm.
36	0.5
44	0.6
90	1.1
95	1.3
144	1.5
192	1.5
245	1.6
293	1.5

APPENDICES

The following definitions will be used whenever it is convenient:

$\xi \equiv \frac{p_o}{p_1} \leq 1$, where p_o and p_1 are the pressures ahead of and behind a shock front, respectively.

$\mu \equiv \frac{\gamma+1}{\gamma-1}$, where $\gamma = \frac{C_p}{C_v}$.

The numerical values of γ and μ are very nearly 7/5 and 6, respectively, when the gas under consideration is air, and these values will often be substituted into the final formulae.

APPENDIX I

DERIVATION OF THE RANKINE-HUGONIOT RELATION FOR AN IDEAL GAS

The conservation laws of mass, momentum and energy, applied to the gas contained in a cylinder of unit cross section which passes through a plane, stationary shock front are:

mass:
$$\rho_0 v_0 = \rho_1 v_1 \tag{I-1}$$

momentum:
$$p_0 + \rho_0 v_0^2 = p_1 + \rho_1 v_1^2 \tag{I-2}$$

energy:
$$\frac{1}{2} v_0^2 + C_p T_0 = \frac{1}{2} v_1^2 + C_p T_1$$

or

$$v_0^2 + \frac{2\gamma}{\gamma-1} \frac{p_0}{\rho_0} = v_1^2 + \frac{2\gamma}{\gamma-1} \frac{p_1}{\rho_1} , \tag{I-3}$$

where ρ is density, v is velocity, p is pressure, γ is the ratio of specific heats (assumed constant), and the subscripts o and 1 apply to the states on the upstream and downstream sides of the shock, respectively.

Division of the momentum equation by the continuity equation gives

$$\frac{p_0}{\rho_0 V_0} + V_0 = \frac{p_1}{\rho_1 V_1} + V_1$$

or

$$V_0 - V_1 = \frac{p_1}{\rho_1 V_1} - \frac{p_0}{\rho_0 V_0} \quad , \tag{I-4}$$

and multiplication of (I-4) by $v_0 + v_1$ gives

$$V_0^2 - V_1^2 = (V_0 + V_1)\left(\frac{p_1}{\rho_1 V_1} - \frac{p_0}{\rho_0 V_0}\right) . \tag{I-5}$$

Equating this value of $v_0^2 - v_1^2$ to that obtained directly from the energy equation gives

$$(V_0 + V_1)\left(\frac{p_1}{\rho_1 V_1} - \frac{p_0}{\rho_0 V_0}\right) = \frac{2\gamma}{\gamma - 1}\left(\frac{p_1}{\rho_1} - \frac{p_0}{\rho_0}\right) . \tag{I-6}$$

Making use of the continuity equation, this may be written

$$\frac{p_1}{\rho_0} - \frac{p_0}{\rho_0} + \frac{p_1}{\rho_1} - \frac{p_0}{\rho_1} = \frac{2\gamma}{\gamma - 1}\left(\frac{p_1}{\rho_1} - \frac{p_0}{\rho_0}\right) ,$$

or

$$\frac{1}{\rho_0}\left(p_1 - p_0 + \frac{2\gamma}{\gamma-1} p_0\right) = \frac{1}{\rho_1}\left(p_0 - p_1 + \frac{2\gamma}{\gamma-1} p_1\right), \tag{I-7}$$

from which

$$\frac{\rho_1}{\rho_0} = \frac{V_0}{V_1} = \frac{p_0 + \left(\frac{2\gamma}{\gamma-1} - 1\right) p_1}{p_1 + \left(\frac{2\gamma}{\gamma-1} - 1\right) p_0} = \frac{p_0 + \frac{\gamma+1}{\gamma-1} p_1}{p_1 + \frac{\gamma+1}{\gamma-1} p_0} = \frac{\mu + \xi}{1 + \mu\xi},$$

or

$$\frac{\rho_1}{\rho_0} = \frac{V_0}{V_1} = \frac{6 + \xi}{1 + 6\xi}, \tag{I-8}$$

which is the Rankine-Hugoniot relation for air.

v_0 and v_1 are velocities of flow relative to the shock front. For later reference, the transformation to a coordinate system in which the gas ahead of the shock front is stationary is effected by

$$\left.\begin{aligned} V_0 &= U \\ V_1 &= U - u \end{aligned}\right\} \tag{I-9}$$

where U is the velocity of the shock front and u is the velocity of flow behind the shock front. (I-8) is then

$$\frac{U}{U-u} = \frac{\mu+\xi}{1+\mu\xi} = \frac{6+\xi}{1+6\xi} \ , \qquad \text{(I-10)}$$

from which

$$u = U\left(1 - \frac{1+\mu\xi}{\mu+\xi}\right) = U\,\frac{(\mu-1)(1-\xi)}{\mu+\xi} \ . \qquad \text{(I-11)}$$

APPENDIX II

DERIVATION OF PRANDTL'S RELATION $v_o v_1 = a^{*2}$

If a^* is the critical sound speed, defined as the value at which the sound speed and flow speed become equal in an expansion from a reservoir, the energy equation (I-3) may be written

$$\left.\begin{aligned} \frac{\gamma}{\gamma-1}\frac{p_o}{\rho_o} &= \frac{1}{2}\frac{\gamma+1}{\gamma-1}a^{*2} - \frac{1}{2}v_o^2 \\ \frac{\gamma}{\gamma-1}\frac{p_1}{\rho_1} &= \frac{1}{2}\frac{\gamma+1}{\gamma-1}a^{*2} - \frac{1}{2}v_1^2 \end{aligned}\right\} \qquad \text{(II-1)}$$

from which

$$p_o = \rho_o\left(\frac{\gamma+1}{2\gamma}a^{*2} - \frac{\gamma-1}{2\gamma}v_o^2\right),$$

$$p_1 = \rho_1\left(\frac{\gamma+1}{2\gamma}a^{*2} - \frac{\gamma-1}{2\gamma}v_1^2\right).$$

Inserting these values for p_o, p_1 into the momentum equation (I-2),

$$\rho_0 \left(\frac{\gamma+1}{2\gamma} V_0^2 + \frac{\gamma+1}{2\gamma} a^{*2} \right) = \rho_1 \left(\frac{\gamma+1}{2\gamma} V_1^2 + \frac{\gamma+1}{2\gamma} a^{*2} \right) ,$$

$$\rho_0 \left(V_0^2 + a^{*2} \right) = \rho_1 \left(V_1^2 + a^{*2} \right) ,$$

or, using the continuity equation (I-1),

$$V_1 \left(V_0^2 + a^{*2} \right) = V_0 \left(V_1^2 + a^{*2} \right) . \qquad \text{(II-2)}$$

Solving (II-2) for a^{*2} ,

$$a^{*2} = \frac{V_0 V_1^2 - V_0^2 V_1}{V_1 - V_0} = V_0 V_1 . \qquad \text{(II-3)}$$

APPENDIX III

DERIVATION OF THE FORMULAE FOR THE SPEED OF A SHOCK OF PRESSURE RATIO ξ, PROCEEDING INTO A STATIONARY GAS, AND FOR THE FLOW SPEED BEHIND THE SHOCK

The energy equation,

$$\frac{1}{2}V^2 + \frac{1}{\gamma-1}a^2 = \frac{\gamma+1}{2(\gamma-1)}a^{*2},$$

on division by $\frac{1}{2}V^2$, becomes

$$1 + \frac{2}{\gamma-1}\left(\frac{a}{V}\right)^2 = \frac{\gamma+1}{\gamma-1}\left(\frac{a^*}{V}\right)^2. \qquad \text{(III-1)}$$

If v is considered the flow speed upstream of a stationary shock, as in Appendix I, this is

$$1 + \frac{2}{\gamma-1}\left(\frac{a_o}{V_o}\right)^2 = \frac{\gamma+1}{\gamma-1}\left(\frac{a^*}{V_o}\right)^2,$$

or

$$\left(\frac{a^*}{v_0}\right)^2 = \frac{\gamma-1}{\gamma+1}\left[1+\frac{2}{\gamma-1}\left(\frac{a_0}{v_0}\right)^2\right] = \frac{1}{\mu}\left[1+(\mu-1)\left(\frac{a_0}{v_0}\right)^2\right]. \quad \text{(III-2)}$$

An alternate expression for $(a^*/v_0)^2$ is obtained from the Rankine-Hugoniot relation (I-7), and Prandtl's Relation (II-3):

$$\frac{v_1}{v_0} = \frac{v_0 v_1}{v_0^2} = \left(\frac{a^*}{v_0}\right)^2 = \frac{1+\mu\xi}{\mu+\xi}. \quad \text{(III-3)}$$

Setting these expressions for $(a^*/v_0)^2$ equal,

$$\frac{1+\mu\xi}{\mu+\xi} = \frac{1}{\mu}\left[1+(\mu-1)\left(\frac{a_0}{v_0}\right)^2\right], \quad \text{(III-4)}$$

from which

$$\left(\frac{v_0}{a_0}\right)^2 = \frac{\mu+\xi}{(\mu+1)\xi},$$

or, transforming to coordinates in which the medium ahead of the shock front is at rest,

$$U = a_0\sqrt{\frac{\mu+\xi}{(\mu+1)\xi}} = a_0\sqrt{\frac{6+\xi}{7\xi}}. \quad \text{(III-5)}$$

(III-5) with (I-11) gives, for the flow speed behind the shock wave

$$u = a_0 \frac{(\mu-1)(1-\xi)}{\sqrt{(\mu+1)\,\xi\,(\mu+\xi)}} \,. \qquad \text{(III-6)}$$

APPENDIX IV

DERIVATION OF THE EXPRESSION FOR THE MACH NUMBER OF THE FLOW BEHIND A SHOCK WAVE WHICH MOVES INTO A STATIONARY MEDIUM

The ratio of the sound speed ahead of a shock front to that behind it is given by

$$\frac{a_0}{a_1} = \sqrt{\frac{T_0}{T_1}} = \sqrt{\frac{p_0\,\rho_1}{p_1\,\rho_0}} \quad . \tag{IV-1}$$

By means of Equation (I-7) this may be written

$$\frac{a_0}{a_1} = \sqrt{\xi\,\frac{\mu+\xi}{1+\mu\xi}} \quad . \tag{IV-2}$$

With the flow speed given by Equation (III-6), the Mach number is given by

$$M = \frac{u}{a_1} = \frac{u}{a_0}\,\frac{a_0}{a_1} = \frac{(\mu-1)(1-\xi)}{\sqrt{(\mu+1)\,\xi\,(\mu+\xi)}} \cdot \sqrt{\xi\,\frac{\mu+\xi}{1+\mu\xi}}$$

$$= \frac{(\mu-1)(1-\xi)}{\sqrt{(\mu+1)(1+\mu\xi)}} = \frac{5(1-\xi)}{\sqrt{7(1+6\xi)}} \quad . \tag{IV-3}$$

APPENDIX V

DERIVATION OF THE EXPRESSION FOR THE MACH NUMBER IN THE FLOW BEHIND THE CONTACT SURFACE IN THE SHOCK TUBE, WHEN AIR IS USED IN BOTH CHAMBERS

The sound speed in the air behind the contact surface is given by Equation (9):

$$a_{1c} = a_0 \left(\frac{p_1}{p_2}\right)^{\frac{\gamma-1}{2\gamma}} = a_0 \left(\frac{p_1}{p_2}\right)^{\frac{1}{\mu+1}}. \qquad \text{(V-1)}$$

From Equation (16)

$$\frac{p_0}{p_2} = \xi \left[1 - \frac{1-\xi}{\sqrt{(\mu+1)\,\xi\,(\mu+\xi)}}\right]^{\mu+1},$$

or

$$\frac{p_0}{p_2} \cdot \frac{1}{\xi} = \frac{p_0}{p_2} \cdot \frac{p_1}{p_0} = \frac{p_1}{p_2} = \left[1 - \frac{1-\xi}{\sqrt{(\mu+1)\,\xi\,(\mu+\xi)}}\right]^{\mu+1}. \qquad \text{(V-2)}$$

With (V-1), this gives

$$\frac{a_{1c}}{a_o} = 1 - \frac{1-\xi}{\sqrt{(\mu+1)\,\xi(\mu+\xi)}} \quad . \tag{V-3}$$

Therefore the Mach number is given by

$$M_{1c} = \frac{u}{a_{1c}} = \frac{\dfrac{(\mu-1)(1-\xi)}{\sqrt{(\mu+1)\,\xi(\mu+\xi)}}}{1 - \dfrac{1-\xi}{\sqrt{(\mu+1)\,\xi(\mu+\xi)}}}$$

$$= \frac{(\mu-1)(1-\xi)}{\sqrt{(\mu+1)\,\xi(\mu+\xi)} - (1-\xi)} = \frac{5(1-\xi)}{\sqrt{7\,\xi(6+\xi)} - (1-\xi)} \quad . \tag{V-4}$$

APPENDIX VI

DERIVATION OF THE EXPRESSION FOR THE SPEED OF THE REFLECTED SHOCK FRONT

Let

$$\psi = \left[\frac{\text{change in flow speed across shock front}}{\text{sound speed ahead of shock front}}\right]^2.$$

Then if primed quantities refer to the reflected shock,

$$\left.\begin{aligned}\psi &= \frac{u^2}{a_0^2}\\ \psi' &= \frac{u^2}{a_1^2}\end{aligned}\right\} \qquad \text{(VI-1)}$$

since the incident shock accelerates the gas from zero speed to the speed u, and the reflected shock decelerates it back to zero speed. From Equation (III-6),

$$\left.\begin{aligned}\psi &= \frac{(\mu-1)^2(1-\xi)^2}{(\mu+1)\xi(\mu+\xi)}\\ \psi' &= \frac{(\mu-1)^2(1-\xi')^2}{(\mu+1)\xi'(\mu+\xi')}\end{aligned}\right\} \qquad \text{(VI-2)}$$

But $\psi = \psi' \frac{a_1^2}{a_0^2}$, from Equation (VI-1), and from Equation (IV-2) this is

$$\psi = \psi' \frac{1+\mu\xi}{\xi(\mu+\xi)} \tag{VI-3}$$

Combining (VI-2) with (VI-3),

$$\frac{(\mu-1)^2(1-\xi)^2}{(\mu+1)\xi(\mu+\xi)} = \frac{(\mu-1)^2(1-\xi')^2}{(\mu+1)\xi'(\mu+\xi')} \cdot \frac{1+\mu\xi}{\xi(\mu+\xi)}$$

or

$$\frac{(1-\xi)^2}{1+\mu\xi} = \frac{(1-\xi')^2}{\xi'(\mu+\xi')} \cdot \tag{VI-4}$$

This gives the two roots

$$\xi' = \frac{1}{\xi} \, , \quad \frac{1+\mu\xi}{\mu+2-\xi} \tag{VI-5}$$

of which the first must be ruled out, since $\xi, \xi' \leq 1$.

Transformation of the Rankine-Hugoniot relation (I-7) to the frame of reference in which the flow speed behind the shock is at rest gives

$$\frac{U'+u}{U'} = \frac{\mu+\xi'}{1+\mu\xi'} \; ; \qquad U' = u\,\frac{1+\mu\xi'}{(\mu-1)(1-\xi')} \; , \tag{VI-6}$$

where U' is the velocity of the reflected shock front with respect to the wall from which it was reflected.

Insertion of the expression for ξ' from (VI-5) and the expression for u from (III-6) gives

$$U' = a_0\,\frac{(\mu-1)(1-\xi)}{\sqrt{(\mu+1)\,\xi(\mu+\xi)}}\cdot\frac{1+\dfrac{1+\mu\xi}{\mu+2-\xi}}{(\mu-1)\left(1-\dfrac{1+\mu\xi}{\mu+2-\xi}\right)} \; ,$$

which simplifies to

$$U' = a_0\,\frac{2+(\mu-1)\,\xi}{\sqrt{(\mu+1)\,\xi(\mu+\xi)}} = a_0\,\frac{2+5\xi}{\sqrt{7\xi(6+\xi)}} \; . \tag{VI-7}$$

SUBJECT INDEX

A

Airfoil, see Model
Amplifier, 56

B

Boundary layer, interaction in
  supersonic flow, 121, 153
  separated, 124, 131, 137
  subsonic flow, 124

C

Carbon tetrachloride, 154, 155
Choking of a duct, 147-154
Contact surface, arrival of, 87, 89
  and uniform flow, 88
  speed of, 15
Counter, 61

D

Delay circuit, 62
Diaphragm, material, 36
  rupture of, 74, 91-102
  strength of, 37

E

Electronic equipment, 52-66
Expansion, into vacuum, 7-11
  into second gas, 11-18

F

Firing operation, 39
Flow in shock tube, 160
  calibration of, 74-88
  duration of, 24-30, 85, 160
  in cold air, 86, 87
  produced by plane shock, 3-6, 180-5
  uniformity of, 84, 87-8, 91
Freon-12, 155

G

Gate circuit, 58
Glass section, 92

H

Helium, 13-15, 40
Humidity, effect on a_o and ξ, 78

L

Lambda shock, 124, 131, 147

M

Mach, intersection, 152-3
  number in shock tube, 3 (see also Flow)
  number versus T, 69
  number versus ξ, 6
  reflections, 2, 102
  -Zehnder interferometer, 2
Model, 5-degree wedge, 79-80, 118
  10-percent double wedge, 124
  30-degree, 111
  45-degree, 111
  mounting of, 49-51

P

p_o/p_2 versus ξ air-air, 13, 70
p_o/p_2 versus ξ helium-air, 13, 71
Particle path, 17
Photocell, 56

Photography, lens, 48
light source, see Spark Unit
plates, 34
shadowgraph method of, 32, 48
timing of, 32, 54, 81
Plunger, 37
Prandtl's relation, 178
Pressure, measurement of, 39
Pulse source, 61

R

Rankine-Hugoniot relation, 174-176
Rarefaction, reflected, 19-24
time of arrival of reflected, 25

S

Schlieren, 34, 48
Screens, light, 43
amplifier used with, 56-7
lens used with, 46
phototube used with, 56-7
Shadowgraph method of photography, see Photography
Shock tube, description of, 34
Shock wave, detached, 110-116, 137
formation in shock tube, 102-3
lambda, 124-131, 147
oblique, 121, 153
reflected, 18-9, 186-8
"tail", 118, 124
Spark unit, 64-66

T

Temperature, distribution, 19
in compression chamber, 40, 72
effect on ξ, 72
effect on M, 77
effect on T, 78

V

Vacuum connections, 41
Velocity, of contact surface, 15
of foot of rarefaction, 15, 17
of plane shock, 15, 68, 180
of rarefaction, 15
of reflected rarefaction, 20-22
of reflected shock, 18, 186
measurement of, 32, 52
Vortices, starting, 117-8

W

Wedge, see Model
Windows, 49-50

AUTHOR INDEX

Ackeret, J.	128,147	Peterson, J.	124
Barnes, Norman I.	48	Prandtl, L	117,178
Bartlett, G. E.	124	Puckett, A. E.	75
Bellinger, S. L.	48	Rankine, W. J. M.	174
Bleakney, W.	2	Reynolds, G. T.	2,14
Courant, R.	2,94,117	Rott, N.	128,147
Feldman, F.	128,147	Shepherd, W. F. C.	1
Friedrichs, K. O.	2,94,117	Smith, L. G.	2,39,102
Higinbotham, W. A.	62	Stoker, J. J.	18
Hugoniot, H.	174	Tietjens, O. G.	117
Liepmann, H. W.	75	Taub, A. H.	14
von Neumann, John	18,102	Vieille, Paul	1
Payman, W.	1	Wilson, Robert R.	41

DISTRIBUTION LIST

COPIES	GOVERNMENT AGENCIES	COPY NO.
15	Office of Naval Research Department of the Navy Washington 25, D. C. Attn: Fluid Mech. Br. (Code 438)	1 - 15
1	Commanding Officer, Branch Office U. S. Navy Office of Naval Research 495 Summer Street Boston 10, Massachusetts	16
1	Commanding Officer, Branch Office U. S. Navy Office of Naval Research 50 Church Street New York 7, New York	17
2	Commanding Officer, Branch Office U. S. Navy Office of Naval Research 844 North Rush Street Chicago 11, Illinois	18, 19
1	Commanding Officer, Branch Office U. S. Navy Office of Naval Research 801 Donahue Street San Francisco 24, California	20
1	Commanding Officer, Branch Office U. S. Navy Office of Naval Research 1030 East Green Street Pasadena 1, California	21
2	Assistant Naval Attaché for Research U. S. Navy Office of Naval Research American Embassy, London, England Navy 100, F.P.O. New York, New York	22, 23
1	Naval Research Laboratory U. S. Navy Office of Naval Research Washington 20, D. C. Attn: Librarian (Code 2021)	24
1	Bureau of Aeronautics Department of the Navy Washington 25, D. C. Attn: Capt. W. S. Diehl	25

COPIES	GOVERNMENT AGENCIES (con't)	COPY NO.
1	Bureau of Ordnance Department of the Navy Washington 25, D. C. Attn: Code Re9	26
1	Naval Ordnance Laboratory U. S. Navy Bureau of Ordnance White Oak, Silver Spring 19, Md. Attn: Mr. J. M. Kendall	27
1	Directorate of Intelligence Headquarters, U. S. Air Force National Defense Building Washington 25, D. C. Attn: Doc. and Dissem. Br.(AFOIR-DD)	28
1	David Taylor Model Basin Department of the Navy Washington 7, D. C. Attn: Aeromechanics Division	29
1	Air Materiel Command Wright-Patterson Air Force Base Dayton, Ohio Attn: Dr. F.L. Wattendorf (MCREPX)	30
1	Air Materiel Command Wright-Patterson Air Force Base Dayton, Ohio Attn: Air Doc. Div. (MCIDXE)	31
1	Ballistic Research Laboratories Department of the Army Aberdeen Proving Ground, Maryland Attn: Mr. R. H. Kent	32
1	Director of Research National Advisory Committee for Aeronautics 1724 F Street, N.W. Washington 25, D. C.	33
1	Director Langley Aeronautical Laboratory National Advisory Committee for Aeronautics Langley Field, Virginia	34
1	Director Ames Aeronautical Laboratory National Advisory Committee for Aeronautics Moffett Field, California	35

COPIES	GOVERNMENT AGENCIES (cont'd)	COPY NO.
1	Director Lewis Flight Propulsion Laboratory National Advisory Committee for Aeronautics Cleveland 11, Ohio	36

MEMBERS OF O.N.R. ADVISORY COMMITTEE ON BASIC RESEARCH IN AERODYNAMICS

1	Dr. Francis H. Clauser Dept. of Aeronautical Engineering The Johns Hopkins University Baltimore 18, Maryland	37
1	Dr. Arnold Kuethe Dept. of Aeronautical Engineering East Engineering Building University of Michigan Ann Arbor, Michigan	38
1	Dr. Hans W. Liepmann Guggenheim Aeronautical Laboratory California Institute of Technology Pasadena 4, California	39
1	Dr. G. B. Schubauer National Bureau of Standards Department of Commerce Washington 25, D. C.	40
1	Dr. R. J. Seeger Naval Ordnance Laboratory U. S. Naval Bureau of Ordnance White Oak, Silver Spring 19, Md.	41

UNIVERSITIES AND RESEARCH ORGANIZATIONS

1	Dr. William Bollay Post Office Box 89 Downey, California	42
1	Polytechnic Institute of Brooklyn 85-99 Livingston Street Brooklyn 2, New York Attn: Prof. R. P. Harrington	43
1	Brown University Graduate Division, Applied Mathematics Providence 12, Rhode Island Attn: Prof. Willy Prager	44

COPIES	UNIVERSITIES AND RESEARCH ORGANIZATIONS	COPY NO.
1	Brown University Metcalf Research Laboratory Providence 12, Rhode Island Attn: Dr. D. F. Hornig	45
1	California Institute of Technology Guggenheim Aeronautical Laboratory Pasadena 4, California Attn: Dr. Clark B. Millikan	46
1	California Institute of Technology Guggenheim Aeronautical Laboratory Pasadena 4, California Attn: Dr. P. A. Lagerstrom	47
1	University of California Engineering Research Projects Berkeley 4, California Attn: Dr. R. G. Folsom	48
1	University of California Department of Engineering Los Angeles 24, California Attn: Dean L. M. K. Boelter	49
1	University of Colorado Aeronautical Engineering Department Boulder, Colorado Attn: Prof. K. D. Wood	50
1	Cornell Aeronautical Laboratory 4455 Genesee Street Buffalo 21, New York Attn: Dr. J. V. Foa	51
1	Cornell University Graduate School of Aeronautical Engineering Ithaca, New York Attn: Dr. Arthur Kantrowitz	52
1	Cornell University Graduate School of Aeronautical Engineering Ithaca, New York Attn: Dr. W. R. Sears	53
1	Harvard University Dept. of Applied Physica and Engr. Science Cambridge 38, Massachusetts Attn: Prof. H. W. Emmons	54

COPIES	UNIVERSITIES AND RESEARCH ORGANIZATIONS	COPY NO.
1	Indiana University Department of Mathematics Bloomington, Indiana Attn: Prof. T. Y. Thomas	55
1	Applied Physics Laboratory The Johns Hopkins University 8621 Georgia Avenue Silver Spring, Maryland Attn: Supervisor, Tech. Reports	56
1	Guided Missiles Committee Massachusetts Institute of Technology Cambridge 39, Massachusetts Attn: Mr. L. W. Sharpe	57
1	Massachusetts Institute of Technology Mathematics Department Cambridge 39, Massachusetts Attn: Dr. C. C. Lin	58
1	Massachusetts Institute of Technology Aeronautical Engineering Department Cambridge 39, Massachusetts Attn: Dr. J. C. Hunsaker	59
1	University of Michigan Dept. of Aeronautical Engineering East Engineering Building Ann Arbor, Michigan Attn: Prof. E. W. Conlon	60
1	University of Michigan Engineering Research Institute East Engineering Building Ann Arbor, Michigan Attn: Dr. Otto Laporte	61
1	University of Minnesota Dept. of Aeronautical Engineering Minneapolis 14, Minnesota Attn: Prof. J. D. Akerman	62
1	New York University Institute of Mathematics and Mechanics 53 Washington Square South New York 12, New York Attn: Dr. R. W. Courant	63

COPIES	UNIVERSITIES AND RESEARCH ORGANIZATIONS (cont'd)	COPY NO.
1	New York University Department of Aeronautics College of Eng., University Heights New York 53, New York Attn: Prof. F. K. Teichmann	64
1	Princeton University Palmer Physical Laboratory Princeton, New Jersey Attn: Dr. Walker Bleakney	65
1	Princeton University Palmer Physical Laboratory Princeton, New Jersey Attn: Dr. R. Ladenburg	66
1	Princeton University Aeronautical Engineering Department Princeton, New Jersey Attn: Prof. Lester Lees	67
1	Purdue University School of Mechanical Engineering Lafayette, Indiana Attn: Prof. R. C. Binder	68
1	Rensselaer Polytechnic Institute Department of Aeronautical Engineering Troy, New York Attn: Prof. P. E. Hemke	69
1	Stanford University Guggenheim Aeronautical Laboratory Stanford, California Attn: Prof. Elliott G. Reid	70
1	University of Texas Defense Research Laboratory 500 East 24th Street Austin, Texas Attn: Prof. M. J. Thompson	71
1	University of Washington Department of Aeronautical Engineering Seattle 5, Washington Attn: Prof. F. S. Eastman	72
1	University of Wichita Department of Aeronautics Wichita 6, Kansas Attn: Prof. K. Razak	73

COPIES	UNIVERSITIES AND RESEARCH ORGANIZATIONS (Cont'd)	COPY NO.
1	Naval Ordnance Test Station U. S. Navy Bureau of Ordnance Inyokern, China Lake, California Attn: Reports Unit	74 (27-A)